Stress and deformation build-up in

bonded composite patch repair

by

Tomer Maurice Curiel

B.Eng. (Mechanical Engineering), Concordia University, 2002

A THESIS SUBMITTED IN PARTIAL FULFILMENT

OF THE REQUIREMENTS FOR THE DEGREE OF

MASTER OF APPLIED SCIENCE

in

FACULTY OF GRADUATE STUDIES

(Metals and Materials Engineering)

THE UNIVERSITY OF BRITISH COLUMBIA

February 2006

Abstract

Bonded composite patch repairs have many advantages over traditional riveted doubler repairs and have been used successfully in a number of repair programs. A mismatch in the coefficients of thermal expansions of the patch and substrate causes thermally induced residual stresses, which are detrimental to the long-term service life of the repair. A dynamic mechanical thermal analyzer bimaterial beam technique is developed that can be used in a variety of different configurations and loading conditions for innovative and versatile characterization of time, temperature, and cure dependant material properties.

The technique is first used to determine the stress relaxation modulus of a viscoelastic material bonded to an elastic substrate. The relaxation modulus of Lexan specimens are characterized, first as monolithic beams and then bonded to an elastic substrate. Results show that the relaxation modulus of Lexan can be determined from bimaterial beam relaxation tests. The temperature and cure dependant modulus of FM300 adhesive is then characterized by subjecting a bimaterial beam to a dynamic displacement while curing isothermally at a variety of temperatures. The results are fit to a model that defines the instantaneous modulus as a function of two variables - the instantaneous temperature and the instantaneous glass transition temperature. The technique is then extended to quantify the development of process induced residual stresses in beam specimens designed to simulate a bonded composite patch repair. In these beam specimens, residual stresses correspond to an out of plane deflection that can be monitored in-situ throughout a complete cure cycle. Specimens, consisting of a steel shim, an FM300 adhesive layer, and an AS4/3501-6 $[0°]_2$ composite patch, are subjected to a variety of cure cycles to determine the effects of cure time and temperature on the out of plane deflection in single- and multi-hold cycles. The experimental results are then compared to those obtained from a cure hardening instantaneously linear elastic (CHILE) model modified to include thermal softening. Results show that a reduction in thermally induced residual stresses is possible by modifying the cure cycle. Model sensitivities, cycle times, real versus idealized cycles, and the effects of thermal softening are also investigated.

The DMA beam technique is shown to be an effective means of material characterization, as well as monitoring the out of plane deflection of bonded composite patch repair specimens throughout a cure cycle. Insight gained from these measurements can be used to optimize cure cycles so as to reduce the thermally induced residual stresses in real applications of bonded composite patch repairs.

__Table of Contents__

List of Tables

List of Figures

Nomenclature

α	Degree of cure
α_c	Cross-over point between kinetic and diffusion controlled curing
α_{gel}	Degree of cure at which gelation occurs
α_{Tg}	Glass transition temperature model constant
$\dot{\alpha} = \dfrac{d\alpha}{dt}$	Rate of cure
δ	Phase angle
ε	Strain
$\kappa_w, \kappa_\sigma, \kappa_\tau$	Bonded composite patch repair specimen constant for deflection, stress, and shear stress
ν	Poisson's ratio
$\sigma(Ga)$	Thermally induced residual stresses in the patch and substrate layers
$\tau(Ga,x)$	Thermally induced shear in the adhesive layer
χ	Natural coordinate system of a beam
ω	Angular frequency
$A_{Tgi},\ B_{Tgi},\ C_{Tgi}$	Glass transition temperature model constants
A_i	Arrhenius pre-exponential constant
A^*	Modulus model pre-exponential constant
b	Specimen width
C_{DOC}	Diffusion control constant
CTE	Coefficient of thermal expansion
E	Elastic modulus
E'	Storage modulus
E''	Loss modulus
E^*	Complex modulus
$E_{c1},\ E_{c2},\ E_{c3}$	Elastic moduli fit to modulus development model

$(E^* \cdot I)_{Eff}$	Complex bending stiffness of a beam
$(EI)_{eq}$	Equivalent beam stiffness
ΔE_i	Arrhenius activation energy
F	Applied force
$f(G_a), g(G_a), h(G_a)$	Adhesive coupling factor for deflection, stress, and shear stress in a bonded composite patch repair
G_a	Adhesive shear modulus
I	Second moment of inertia
K_i	Kinetic rate constant
K^*	Modulus model constant
L	Specimen length
L_C	Length between the span support and the end of the prepreg material
m_i	Kinetic exponent controlling n^{th} order reaction
n_i	Kinetic exponent controlling autocatalytic reaction
R	Universal gas constant
T	Temperature
T^*	Difference between a specimen temperature and its glass transition temperature
T_{c1}, T_{c2}, T_{c3}	Transition temperatures fitted to modulus development model
T_g	Glass transition temperature
t	Time
t_a	Adhesive thickness
t_p	Patch thickness
t_s	Steel shim thickness
t_T	Total specimen thickness
Δt	Time step
w	Central deflection of a beam specimen
x	Beam coordinate system along the length of the beam

y	Beam coordinate system through the thickness of the beam
y_{eq}	Distance to the neutral axis of a beam

Acknowledgments

I would like to take this opportunity to acknowledge the help of those without whom I could not have finished this work. Firstly, I would like to thank my supervisor Dr. Göran Fernlund for his invaluable advice, expertise, and patience. In addition, Dr. Anoush Poursartip, Dr. Reza Vaziri, and the members of the composites group at UBC (both past and present) have been enormously helpful; Sharing experience and knowledge, as well as a heartfelt laugh and a good time. Many people have passed through the office in Frank Forward 105 and I appreciate the camaraderie. Roger Bennett's technical expertise and help with specimen preparation was especially appreciated. I would also like to thank Dr. Andrew Johnston and Lucy Bordovsky of the Institute for Aerospace Research of the National Research Council of Canada in Ottawa for technical expertise and materials.

I would like to thank all my friends who have helped make my time Vancouver so enjoyable. It has been a wonderful experience and I appreciate their company and support. Many have been ready with an open ear and an outstretched hand whenever I needed help.

Finally, I would like to thank my family. Although they are far away, they have always been a constant source of inspiration. Without their support and fostering I could not have achieved as much.

1. Introduction

1.1 Background

During its service life, an airframe will be subjected to thousands of load cycles in a wide range of environmental conditions involving both temperature and humidity. Although engineers go to great lengths to design and test for fatigue damage, such occurrences are inevitable. Inspection schedules are thus designed to ensure that damage is detected and monitored before it becomes hazardous to the safety of the airframe, passengers, crew, and cargo. Once damage is deemed critical to the structural integrity of the airframe, the damaged part must be retired and replaced or it can be repaired. The high costs associated with retiring components from service, due in part to limited production and availability of replacement parts, and loss of revenue due to downtime, has created the need to develop repair techniques that can extend service life.

Two main repair schemes exist for airframe components: riveted doubler repairs and bonded composite patch repairs. In a riveted doubler repair, shown in *Figure* 1.1-*a*, a metallic doubler is fabricated to the same contour as the original structure. The surface is then prepared, rivet holes are drilled through both the doubler and the original structure and rivets are installed. Rivet patterns are engineered following rules of thumb that define features such as edge distances, pitch, etc.

In a bonded composite patch repair, shown in *Figure* 1.1-*b*, a unidirectional composite patch is designed and fabricated with fibres running perpendicular to the crack direction. The patch is then adhesively bonded to the original structure by applying an aerospace grade adhesive and cured in-situ at an elevated temperature using a heating blanket. The patch is tapered to reduce peel stresses and is designed to restore the strength of the underlying structure without over-stiffening the repaired area.
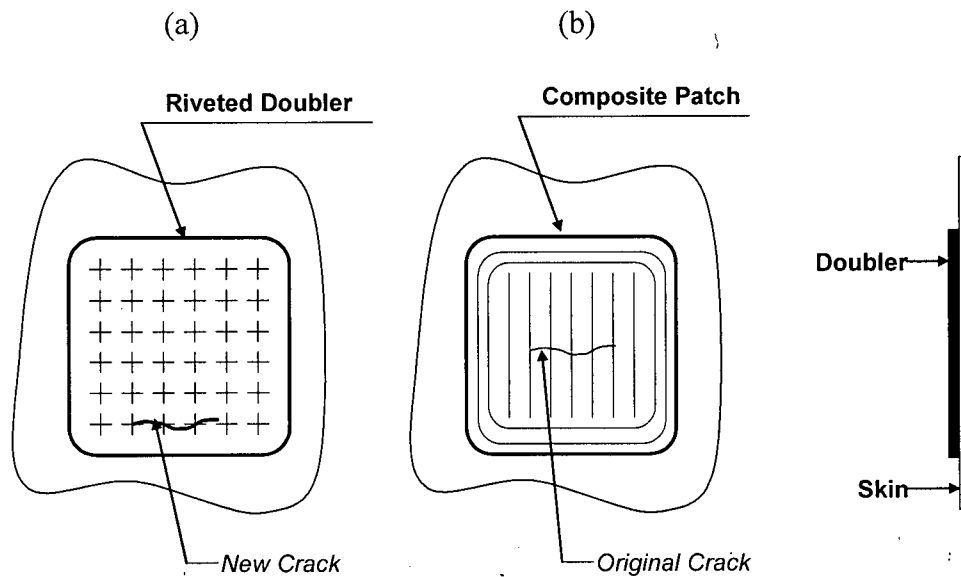
Figure 1.1 – Schematic of (a) a riveted doubler repair and (b) a bonded composite patch repair

Composite reinforcements offer many benefits, such as:

- Stiffening under-designed regions

- Restoring strength or stiffness

- Reducing the stress intensity factor

- Improving damage tolerance

Composite patches also offer a number of advantages when compared to conventional riveted doubler repairs:

- In-situ repair leads to reduced downtime

- Sealed interface eliminates corrosion problems

- Does not cause additional damage to the structure in terms of rivet holes, countersinks, etc.

- Reduces the chances of accidental damage during repair

- Easily contoured to mate with curved surfaces

- Produces a low aerodynamic footprint

Chester *et al.* [1] showed that in a repair to the lower wing skin of an F-111, fatigue life increased from 15.8 flight hours for an unpatched specimen, to over 2000 hours for a boron/epoxy patched specimen. Ong & Shen [2] observed that adhesively bonded repairs could enhance the fatigue life of a cracked aluminium substrate by 60-100 times.

One of the disadvantages of composite repair patches arises from the mismatch in the coefficients of thermal expansion between the repair patch and the underlying metallic repair area. Repair patches are generally designed with the 0° direction perpendicular to the crack growth direction and thus the patch properties are governed by the fibres. Coefficients of thermal expansion for typical fibre materials can range from -1 to 7 μm/m°C [3], while the coefficient of thermal expansion for aluminium is 23 μm/m°C and that of steel is 11.3-17.8 [4]. Thus as the patch is subjected to the adhesive's cure cycle, thermally induced residual stresses are created, shown schematically in *Figure 1.2*, which can limit the effectiveness of the repair in terms of fatigue life.

Heat-up   **Cool-down**

- Patch is applied at room temperature
- Substrate expands
- Adhesive cures
- System couples
- Substrate contracts
- Stresses are produced
- Out of plane deflection in bi-material beam
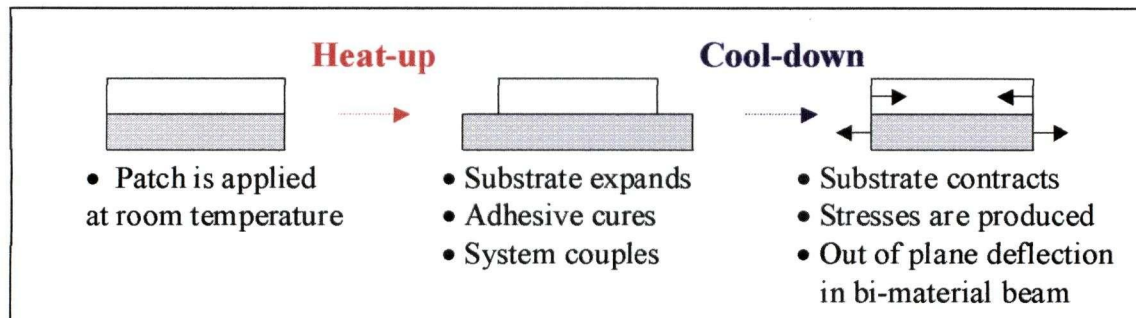
Figure 1.2 - Schematic of thermal residual stress problem

A number of attempts have been made to reduce the detrimental effect produced by this difference in coefficient of thermal expansion. These include prestressing the patch, using materials for the patch, such as boron fibres, whose coefficient of thermal expansion approach that of the underlying structure and, most notably, optimizing the cure cycle to reduce the process induced residual stresses. Cho and Sun showed that by judiciously engineering the cure cycle used to bond a repair patch, an improvement in fatigue life of up to 5 times over the manufacturer's recommended cycle can be achieved [5].

Thus there exists a need to understand the development of thermally induced residual stresses in bonded composite patch repairs: where in the repair process they develop, what factors most influence their development, how systems properties develop as a function of the constituent properties, and how the residual stresses affect the system. Experimental methods are needed that are flexible enough to characterize important material properties throughout a cure cycle. A method is also required to simulate bonded composite patch repairs in a controlled laboratory setting that allows for in-situ measurement of the development of residual stresses throughout a cure cycle. Simultaneously, there is the need to develop simple models to aid in the accurate prediction of the development of residual stresses. Once combined, these tools will help acquire a deeper understanding of the mechanisms through which residual stresses are generated, their effect on the system response, and offer insight into novel methods to reduce the residual stresses produced during the bonding process.

1.2 Objective

The objective of this body of work is to develop and validate a simple and efficient technique for cure cycle optimization of bonded composite patch repair using a Dynamic Mechanical Analyzer (DMA).

2. <u>Literature Review</u>

2.1 Historical Overview

Composites began to see use as repair patches for aerospace applications in the early 70's with the pioneering work of Alan Baker at the Aeronautical and Marine Research Laboratories (AMRL) in Australia [6]. AMRL has since attempted to standardize the repair certification process. Davis and Bond [7] have outlined the principles involved in designing and implementing repairs that should produce durable, reliable bonds. These include design principles for both static and fatigue loadings, fabrication principles including surface preparation and inspection methods, and bonding procedures such as proper thermocouple placement.

A number of military and commercial repair programs have since shown the benefits of bonded composite repairs. These include the repair of a Boeing 727 fuselage lap joint, a Boeing 767 keel beam [8], F-16 FS479 bulkhead vertical attach bosses [9], and an F/A-18 Y470.5 bulkhead crotch area [10]. Baker *et al.* [11] and Chester *et al.* [1] reported on an extensive validation program for the bonded composite repair of a fatigue crack on the lower wing skin of an F-111 aircraft. In conjunction with a detailed FE analysis validated by a strain survey on a full scale wing, three levels of structural testing were conducted: coupon specimens to evaluate the repair under various environmental conditions using double overhead fatigue specimens, panel specimens to simulate the local geometry of the wing skin, and box specimens to simulate the wing structure as a quasi-full scale test. Jones *et al.* [12] found that bonded repairs can extend the service life of fuselage lap joints containing multi-site damage, even when subjected to adverse environmental factors. Their findings were validated on an Airbus A330/340 full-scale fatigue specimen.

2.2 Material Modeling

One of the main differences between a thermoset polymeric material and a simple elastic material is that the polymeric material's properties are highly dependant on its state; during

processing the material undergoes a dramatic change in state, beginning as a viscous liquid and progressing to a viscoelastic solid. A number of models have been developed to account for these effects and are presented herein.

2.2.1   Cure Kinetics

The first step in the material characterization of thermoset polymers is the determination of the cure kinetics of the resin. During cure, the underlying structure of a polymer is altered irreversibly. Single monomer units combine chemically to produce polymers - long chains of repeating units, known as mers - and crosslink.

Generally, cure kinetics models focus on defining the rate of cure. The degree of cure is then found by integrating the rate equation. Two general classes of models are used to describe the rate of cure behaviour. The first class of models, known as mechanistic models, is based on a detailed understanding of the underlying chemical reactions of the system. These models take into account the main chemical reactions and explicitly relate the concentrations of species present in the system to a rate of generation of products in a set of kinetic expressions that describe the overall curing dynamics. While these models are comprehensive, they are difficult and time consuming to create and are generally not of practical use due to the complexity of the system, as well as the proprietary nature of most resin formulations.

The second class of models, known as phenomenological models, captures the main characteristics of the underlying chemical reactions by fitting cure rate equations to experimental data. These are used nearly exclusively and are traditionally reported in the engineering literature. Although several forms of reaction rate equations are used, their general form is

$$\frac{d\alpha}{dt} = Kf(\alpha) \tag{1}$$

where α represents the degree of cure, K is a reaction rate constant and $f(\alpha)$ represent a function of degree of cure. The reaction rate constant is generally taken to be an Arrhenius temperature dependant constant of the form

$$K = A \exp\left(-\frac{\Delta E}{RT}\right) \tag{2}$$

where A is a pre-exponential, ΔE is the activation energy, R is the universal gas constant and T is the temperature (in Kelvin).

2.2.2 Glass Transition Temperature

During cure, as the polymer chains grow in length and cross-links develop, the resin's material properties begin to evolve. The material changes from a viscous-liquid to a viscoelastic solid. The system undergoes two major transitions – gelation and vitrification.

Gelation corresponds to the formation of an infinite network, where the system passes from a liquid to a gel and acquires an equilibrium modulus [13]. Gelation occurs at a characteristic degree of cure, which is dependant on the chemistry of the resin.

Vitrification corresponds to a reversible transition from a rubbery gel to a glassy solid. It relates to the freezing of cooperative motion of the kinetic segment of the main chain, transitioning the system from viscoelastic behaviour to essentially elastic behaviour. A system is said to have vitrified if the system's temperature drops below its glass transition temperature, T_g. The system's glass transition temperature increases with advancing degree of cure; as more bonds form, more input energy is required to shift between the glassy and rubbery regime and thus its onset is retarded [14,15].

Many material properties show a drastic change as the glass transition temperature is approached. A number of experimental techniques have been used to quantify this change. Dynamic scanning calorimetry (DSC) techniques typically determine T_g as a change in specific heat capacity [16], as well as the inflection point of the endotherm [17]. Thermal mechanical analysis (TMA) techniques determine T_g as a change in the coefficient of thermal expansion [18,19,19]. Dynamic mechanical thermal analysis (DMA) techniques determine T_g by monitoring the change in a material's modulus [19]. The glass transition temperature defines the material's useful thermal operating envelop for many applications.

The glass transition temperature as measured in a DMA has been defined in a number of ways [19,20,20]:

1. The temperature at which the storage modulus, E', has fallen below a threshold value. The German standard DIN 53665 sets this threshold at the half height of the step change.

2. The temperature at which the phase angle, $\tan(\delta)$, has its maximum value.

3. The temperature at which the loss modulus, E'', has its maximum value.

Traditionally, the most common definition used for T_g is the temperature at which the phase angle is a maximum. The glass transition temperature has been found to exhibit a one-to-one relationship with degree of cure and is most commonly described using a DeBenedetto type relationship of the form

$$\frac{T_g(\alpha) - T_{g0}}{T_{g\infty} - T_{g0}} = \frac{\lambda\alpha}{1 - (1 - \lambda)\alpha} \qquad (6)$$

where T_{g0} is the glass transition temperature of the uncured resin, $T_{g\infty}$ is the glass transition temperature of the fully cured material, and λ is a material constant. Chern and Poehlein [21] used the DeBenedetto equation to characterize an epoxy resin and Hojjati and Johnston [22] used it to characterize FM73 adhesive. Other models include a piecewise quadratic fit, used by Djokic *et al.* [17] to model FM300 and by Kim and White [23] for the neat resin 3501-6, and a logarithmic fit used by Sourour and Kamal [14] to characterize DGEBPA. Studying the development of glass transition temperature of the prepreg AS4/3501-6, Kim *et al.* [24] noted that the relationship between glass transition temperature and degree of cure was similar to that found by Kim and White [23] for the neat resin 3501-6.

2.2.3   Viscoelasticity

Polymeric materials differ from many other engineering materials as they can exhibit time or temperature dependant response to an applied stimulus and can be modeled using a viscoelastic constitutive model. Viscoelasticity arises as chain segments undergo Brownian motion, moving in discrete diffusional jumps, yet continuing to cohere as a solid. As mobile

molecular segments flow due to the applied stimulus, a back stress is developed that may stop the flow after a long time period and leads to complete recovery when the stimulus is removed [25].

Viscoelastic Constitutive Models

All linear viscoelastic models are governed by a particular case of the following equation.

$$a_0\sigma + a_1\dot{\sigma} + a_2\ddot{\sigma} + a_3\dddot{\sigma} + \ldots + a_n\sigma^{(n)} = b_0\varepsilon + b_1\dot{\varepsilon} + b_2\ddot{\varepsilon} + b_3\dddot{\varepsilon} + \ldots + b_n\varepsilon^{(n)} \qquad (3)$$

where a_i and b_i are constants, and $\sigma^{(n)}$ and $\varepsilon^{(n)}$ represent time derivatives of stress and strain.
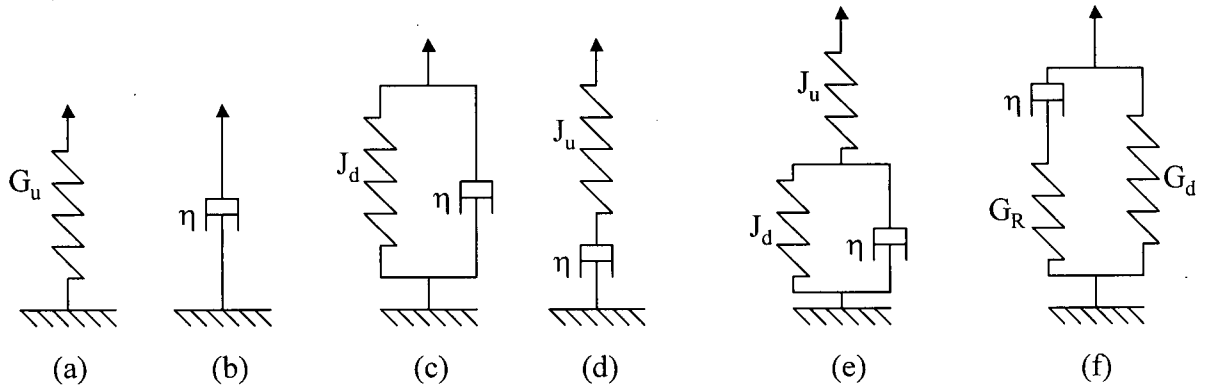
Figure 2.1 - Schematic of material models: elastic (a), viscous (b), Kelvin (c), Maxwell (e), and Zener (e and f)

These models, shown schematically in *Figure 2.1*, include:

- The elastic solid model, consisting of a single spring element
- The simple viscous model, consisting of a single dashpot element
- The Kelvin model, consisting of a spring and dashpot in parallel
- The Maxwell model, consisting of a spring and dashpot in series
- The Zener model, consisting of a spring in series with a Kelvin model, or equivalently, a spring in parallel with a Maxwell model

Stress Relaxation

When a constant strain level is applied to a viscoelastic material, a time-varying stress results [25]. By running relaxation tests at various constant strain levels, a family of stress relaxation curves can be created. Plotting the stresses produced at a given time against the applied strain level and then connecting them with a curve, isochronous stress-strain curves can be produced. For a linearly viscoelastic material, this curve will be linear and the slope is defined as the relaxation modulus. The relaxation modulus can then be plotted versus time and the material's stress relaxation function can be determined. The stress relaxation will generally exhibit three distinct regions:

- An initial maximum plateau, known as the "glassy" modulus, where the material exhibits an initial, essentially elastic response.

- An intermediate, transition zone

- A final minimum plateau, known as the "rubbery" or equilibrium modulus

The point of inflection of the curve is defined as the characteristic relaxation time [26].

Creep Compliance

Similarly, when a constant stress level is applied to a viscoelastic material, a time-varying strain results. By running creep tests at various constant stress levels, a family of creep curves can be created. Plotting creep strains produced at a given time against the applied stress level and then connecting them with a curve once again produces isochronous stress-strain curves. For a linearly viscoelastic material, this curve will be linear and the slope is defined as the creep compliance. Creep compliances can then be plotted versus time and the material's creep compliance function can be determined. The creep compliance will generally exhibit three distinct regions, much like the stress relaxation, beginning with a low plateau and then transitions to a higher plateau.

Dynamic Response

When a viscoelastic material is subjected to a cyclic excitation of the form $\varepsilon(t) = \varepsilon_0 \sin(\omega t)$, the force required to produce this deflection is proportional, but out of phase with the deflection as shown in *Figure 2.2*, and can be defined as $\sigma = \sigma_0 \sin(\omega t + \delta)$.

The stress can then be expressed as

$$\sigma(t) = \sigma_0 \cos(\delta) \cdot \sin(\omega t) + \sigma_0 \sin(\delta) \cdot \cos(\omega t) \tag{4}$$

$$\sigma(t) = \varepsilon_0 \left[E' \sin(\omega t) + E'' \cdot \cos(\omega t) \right] \tag{5}$$

$$E' = \frac{\sigma_0}{\varepsilon_0} \cos(\delta) \tag{6}$$

$$E'' = \frac{\sigma_0}{\varepsilon_0} \sin(\delta) \tag{7}$$
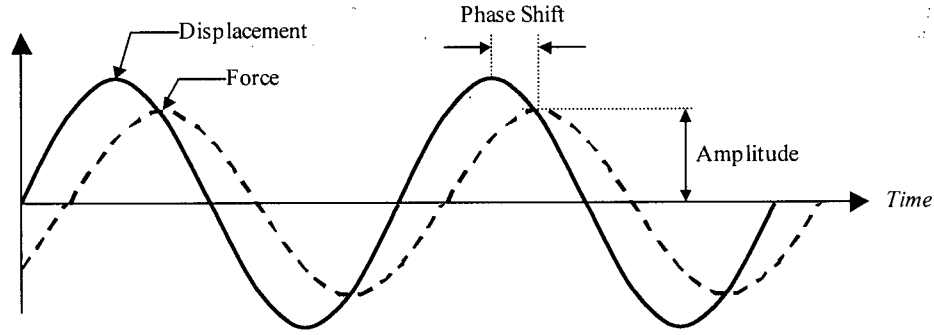
Figure 2.2 - Dynamic response of a viscoelastic material

An electrical analog may be used to replace the time dependant variables with their complex equivalents. Thus the instantaneous modulus can be replaced with an equivalent complex modulus, $E*$. This leads to the definition of an in-phase and an out-of-phase component for the modulus, known respectively as the storage modulus, E', and the loss modulus, E'', as well as a phase angle, δ, where

$$E* = E' + iE'' \tag{8}$$

$$\tan \delta = \frac{E * \sin \delta}{E * \cos \delta} = \frac{E''}{E'} \tag{9}$$

11

Correspondence Principle

In a viscoelastic analysis, the boundary and equilibrium conditions remain similar to those of an elastic analysis. The difference manifests itself through the constitutive equation. The correspondence principle is thus used to transform the solution for an elastic material into one for a viscoelastic material. The correspondence principle states if the elastic solution to a problem is known, the corresponding solution to a viscoelastic problem can be obtained by replacing the elastic modulus with its viscoelastic equivalent [27]. Since viscoelastic functions are generally time-dependant, a transformation into the Laplace domain may also be necessary.

Superposition Principle

Temperature has a very pronounced effect on viscoelastic materials. For thermo-rheologically simple materials, experiments have shown that lowering the temperature has the effect of shifting the response towards longer times, while increasing the temperature has the opposite effect, without affecting the shape of the response. A time-temperature shift factor, a_T, can be used to collapse a series of tests run at varying temperatures into a single master curve. Experimentally this phenomenon can be very useful, as reducing the temperature can slow down transitions that occur too rapidly for the test method, or temperature can be increased to speed up experiments whose duration would be otherwise prohibitive. The shift factor corresponds to a horizontal shift along the time axis, based on a reference temperature. The shift factor can take on a number of forms, including Arrhenius behaviour [25] and W-L-F behaviour [28]. The superposition concept has also been extended to include applied stress [29-32] and degree of cure [22,23,33].

Modulus

The relaxation modulus of polymeric materials has been found to be dependent on factors such as degree of cure, temperature, and time of load application. Using Maxwell elements to model the behaviour of material, the relaxation modulus can be defined as

$$E(\alpha,\zeta)= E_\infty +(E_u - E_\infty)\cdot \sum_{\omega=1}^{N} W_\omega \cdot \exp\left[\frac{-\xi}{\tau_\omega}\right] \qquad (10)$$

where E_u is the unrelaxed or glassy modulus, E_∞ is the rubbery modulus, τ is the stress relaxation time, ζ is the reduced time, and W_ω is a set of weight factors and τ_ω is as set of discrete relaxation times [23,34,35]. With this model, the glassy modulus corresponds to the initial instantaneous response, which then decays over time to the rubbery modulus.

Although this model may be used to accurately represent the relaxation phenomenon encountered, a large number of parameters are required and difficulties arise in the use of curve fittings techniques to determine the parameters. Hojjati and Johnston [22] used a simple, three-parameter stretched exponential model to represent the relaxation modulus as

$$E(\zeta,\alpha) = E_\infty + (E_u - E_\infty) \cdot \exp\left[-\left(\frac{-\xi}{\tau}\right)^b\right] \tag{11}$$

where b is a material constant. This equation can be modified slightly to include cure and temperature effects as

$$E(\zeta,\alpha,T) = E_\infty + (E_u - E_\infty) \cdot \exp\left[-\left(\frac{-\xi(\alpha,T)}{\tau(\alpha)}\right)^b\right] \tag{12}$$

2.2.4   Pseudo-Viscoelastic (PVE) Models

Pseudo-viscoelastic (PVE) models are a class of models where simplifying assumptions are used to disregard the processing or load history of the material. The material is generally characterized using dynamic tests at an arbitrary, but low frequency [36]. Ferry [28] defines the relaxation modulus as a function of the storage and loss moduli at a specified frequency

$$G(t = 1/\omega) = G'(\omega) - 0.40G''(0.40\omega) + 0.014G''(10\omega) \tag{13}$$

O'Brien *et al.* [35] and Cook *et al.* [37] propose similar conversions between dynamic results and relaxation modulus. The constitutive equation can be written in an incremental form as

$$\Delta\sigma = E(T,\alpha) \cdot \Delta\varepsilon \tag{14}$$

where $E(T,\alpha)$ is the instantaneous modulus.

. One such model, known as the cure hardening instantaneously linear elastic, or CHILE model, is essentially an elastic model where the modulus is assumed constant during each time-step, but may be defined as a function of the temperature and the degree of cure [38]. Zobeiry et al. [36] studied the validity of the PVE formulation and discussed the regimes where the CHILE simplifications are valid and the model can be expected to produce accurate results. Johnston *et al.* [38], using a pseudo-viscoelastic constitutive model, defined the resin modulus as a monotonically increasing function of degree of cure.

$$E(T^*) = \begin{cases} E_0 & T^* < T_{c1} \\ E_0 + (E_\infty - E_0)\left(\dfrac{T^* - T_{c1}}{T_{c2} - T_{c1}}\right) & T_{c1} < T^* < T_{c2} \\ E_\infty & T_{c2} < T^* \end{cases} \qquad (15)$$

where $T^* = T - T_g$ is defined as the difference between the current temperature, T, and the instantaneous glass transition temperature, T_g, $E(T^*)$ is the instantaneous modulus of the resin, while E_0, E_∞, T_{c1}, and T_{c2} are material constants. Similarly, Svanberg and Holmerg [39,40] develop a pseudoviscoelasitc model which represents the limiting case of linear-viscoelasticity. In their model, incremental stresses are developed with the material's modulus defined as either the glassy or rubbery modulus, with a softening component implemented above the material's glass transition temperature.

2.3 Bonded Composite Repair Modeling

Full three-dimensional analysis of bonded patch repairs is inherently computationally inefficient, as it involves large aspect ratios, due to the relative size of the thickness with respect to the other two dimensions. Furthermore, single-sided patches develop curvilinear crack fronts and generate a highly non-linear three-dimensional stress response [6]. Thus a number of alternative methods have been developed including analytic models and closed form beam bending models.

2.3.1 Finite Element Modeling

As full three-dimensional finite element modeling is computationally inefficient, a number of simplified FE techniques have been proposed. Sun *et al.* [41] developed a technique whereby the patch and substrate are modeled as plates while the adhesive layer is modeled by three spring elements, representing the in-plane and out-of-plane stiffnesses of the material. This technique was shown to be capable of predicting the stress intensity factor for double-sided repairs, as well as calculating the strain energy release rate along the debond front, but showed appreciable discrepancies for single sided repairs. Modifying the model to account for variation in the stress intensity factor through the thickness of single sided repairs, Klug *et al.* [42] showed that linear and non-linear geometrical analyses produced similar results when thermal effects were superposed on mechanical loading. Their results also indicated that increasing the thickness of single-sided repairs might not significantly affect fatigue life, due to increased thermal residual stresses. Using the same method, Lena *et al.* [43] investigated the use of composite repair patches as crack arrestors. With the aim of hampering crack coalescence, they placed the repair patch between two edge cracks. Monitoring the crack growth, they noted that the patch had no effect until the crack grew into the patched area. They also confirmed that thermal effects during processing could significantly reduce the effectiveness of repairs.

Naboulsi and Mall [44] developed a similar three-layer technique, where the adhesive layer was modeled by an elastic continuum instead of shear-spring elements. Their results showed better agreement to full three-dimensional analysis for both cohesive crack growth and adhesive failure. They proceeded to study the effect of non-linear analysis on damage tolerance of bonded patch repairs [45]. By comparing results with geometric non-linearities (due to out of plane deformation) to those from geometrically linear analysis, they noted that although both exhibited similar trends, non-linear analysis predicted lower stress intensity factors. It did not, however, affect the development of thermal stresses during cure of the adhesive, AF-163-2. No mention was made of the model used to characterize the development of adhesive layer properties. The adhesive was then modeled as an elastic-plastic material to capture debond behaviour. In this case, the difference between

geometrically linear and non-linear analysis disappeared. Comparing different stiffness ratios, they found that higher stiffness ratios tended to reduce the stress intensity factor.

Umamaheswar and Singh [6] compared three different non-linear FE modeling strategies: A two-dimensional plate-beam model where the patch and substrate were modeled with shell elements and the adhesive is modeled as line springs or beams, a two/three-dimensional plate-brick model where the patch and substrate were modeled as shell elements and the adhesive is modeled as a brick element, and a three-dimensional single brick model where each layer was modeled as a single brick element. Results show that the single brick model matched the results obtained from a fully three-dimensional model to within 98%, and could thus be used as a good first order design tool.

Schubbe and Mall [46] investigated the repair of thick panels using bonded composite repairs. They found that for asymmetric repairs, the problem of mismatch of coefficient of thermal expansion caused the crack to open on the patched side and close on the unpatched side, leading to a non-linear crack front that complicates the analysis of thick panel repairs significantly. Simple beam theory was unable to account for thermal effects and

2.3.2   Analytic Modeling

Rose [47] developed an analytic model to determine thermal residual stresses for an infinite isotropic plate reinforced with a circular orthotropic material using an inclusion analogy. Wang *et al.* [48] then proceeded to develop approximate solutions to correct for finite size. Daverschot *et al.* [49] compared the analytic Wang-Rose and Van Barneveld-Fredell models and an FE model. The Van Barneveld-Fredell model is similar to the Rose-Wang model, save that stresses in the plate are calculated using an effective CTE, which is determined by the restraint of the boundary conditions. They distinguished between "test specimens", which are free to contract during cooling, and "in-field specimens", whose thermal response is constrained by the surrounding structure. Experiments were performed on specimens consisting of circular reinforcements applied to two substrates, whose dimensions simulated a test specimen and a much larger in-field specimen, to determine the stresses in the patch and the substrate post adhesive layer curing. Results suggest that while both models were

able to accurately model "test specimens", the Van Barneveld-Fredell model was better able to model "in-field" specimens. The authors also noted that the actual specimen temperatures measured were lower than those predicted by the analytic models, as both models assumed adiabatic conditions.

2.3.3   Closed Form Beam Theory

Hojjati [50] developed a closed form elastic solution for the stresses in a double-sided bonded patch repair, as shown in *Figure 2.3*.
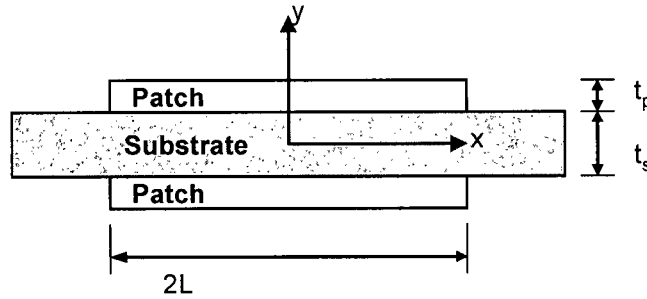
Figure 2.3 - Geometry of double sided bonded composite patch repair

Considering only thermal effects, the equations for adhesive layer shear stress, τ_a, and the normal shear stress in the patch, σ_p, and substrate, σ_s, respectively are:

$$\tau_a = -\frac{(\alpha_s - \alpha_p) \cdot T}{\dfrac{1}{E_p t_p} + \dfrac{2}{E_s t_s}} \cdot \lambda \cdot \frac{\sinh(\lambda x)}{\cosh(\lambda L)} \tag{16}$$

$$\sigma_p(x) = \frac{(\alpha_s - \alpha_p) \cdot T}{t_p \cdot \left(\dfrac{1}{E_p t_p} + \dfrac{2}{E_s t_s}\right)} \cdot \left(1 - \frac{\cosh(\lambda x)}{\cosh(\lambda L)}\right) \tag{17}$$

$$\sigma_s(x) = \frac{-2 \cdot (\alpha_s - \alpha_p) \cdot T}{t_s \cdot \left(\dfrac{1}{E_p t_p} + \dfrac{2}{E_s t_s}\right)} \cdot \left(1 - \frac{\cosh(\lambda x)}{\cosh(\lambda L)}\right) \tag{18}$$

where λ^2 is defined as

$$\lambda^2 = \frac{G_a}{t_a}\left(\frac{1}{E_p t_p} + \frac{2}{E_s t_s}\right)$$ (19)

α_p and α_s are the coefficients of thermal expansion of the patch and substrate respectively, T is the temperature change, L is the half-length, x is the distance along the beam at which the deflection is calculated, and E_p and E_s are the elastic moduli of the patch and substrate respectively, and G_a is the shear modulus of the adhesive.

Hojjati and Johnston [51] presented a closed form solution to the deflection of a one-sided patch caused by mismatch of the coefficient of thermal expansion based on a three-component system, as shown in *Figure 2.4*: an elastic substrate, an elastic adhesive and an elastic substrate. The adhesive is assumed to carry only shear load as its thickness, t_a, is much smaller than that of the patch, t_p, and of the substrate, t_s. Thus the system can be analyzed using a standard shear lag approach that gives the central deflection of a beam subjected strictly to thermal loads.
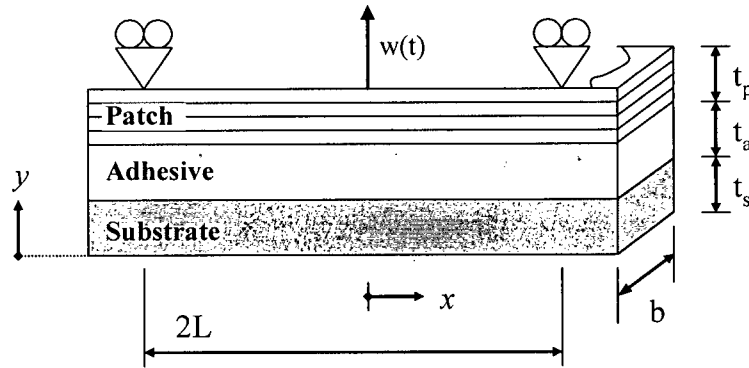
Figure 2.4 - Geometry of single sided bonded composite patch repair

$$w = T \cdot \kappa \cdot f(G_a)$$ (20)

$$\kappa = \frac{(\alpha_p - \alpha_s) \cdot (t_p + 2t_a + t_s) \cdot L^2}{4EI\lambda} \tag{21}$$

$$f(G_a) = 1 - \frac{2 \cdot (\cosh(\lambda L) - 1)}{\lambda^2 \cdot L^2 \cdot \cosh(\lambda L)} \tag{22}$$

$$\lambda = \frac{1}{E_p t_t} + \frac{1}{E_s t_s} + \frac{t_a(t_p + 2t_a + t_s)}{2EI} \tag{23}$$

$$EI = \frac{E_p t_p E_p t_p}{12 \cdot (E_p t_p + E_p t_p)} K \tag{24}$$

$$K = 4 + 6 \cdot \left(\frac{t_p}{t_s}\right) + 4 \cdot \left(\frac{t_p}{t_s}\right)^2 + \frac{E_p}{E_s} \cdot \left(\frac{t_p}{t_s}\right)^3 + \frac{E_x t_x}{E_p t_p} \tag{25}$$

$f(G_a)$ can be conceptualized as the degree of adhesive coupling between the patch and substrate. For an uncured adhesive, $f(G_a) \to 0$, and the constituents acts as two separate beams. As the adhesive's modulus increases $f(G_a) \to 1$ and the system acts as a perfectly bonded beam.

2.4   Optimization

During processing residual stresses are produced by a variety of factors, including mismatch of coefficient of thermal expansion, differential cure shrinkage and moisture desorption. Residual stresses are detrimental for a number of reasons including development of microcracks in the transverse direction and reduction in efficiency of patch repairs. A number of techniques have been developed to determine the residual stresses level of the material. Researchers have mainly focused on reducing the level of process-induced stresses by optimizing the cure cycle. In a similar vein, optimization strategies have been proposed to reduce the thermally induced residual stresses in bonded composite repairs.

2.4.1   Stress Measurement Techniques

Typically, residual stress levels are either quoted as actual stress levels or in terms of a change in temperature, which correlates to a stress level using Laminate Plate Theory. The stress free temperature, T_{sf}, corresponds to the temperature to which the specimen must be raised to eliminate the existing residual stresses, while the effective temperature drop, ΔT_{eff}, corresponds to the temperature drop that would produce thermal stresses in a stress free laminate equivalent to the measured residual stresses.

A number of experimental techniques have been developed to determine process induced residual stresses. The first group of techniques employ strain gauges to measure the surface strains of a specimen and then use laminate plate theory to correlate this strain to residual stresses. White and Hahn [52] measured thermal shrinkage strains by bonding strain gauges to the surface of laminates prior to cure and monitoring the development of strain during intermittent cure. Crasto *et al.* [53] used embedded strain gauges to monitor the development of axial and transverse strains. Crasto and Kim [54] used a peel-ply technique to determine the residual stresses in symmetric angle-ply specimens. In this technique, strain gauges are bonded to the outer ply of a cured laminate and the strains that result when the outer layer is removed are used to determine the residual stresses. Similarly, Cho and Sun [5,55] bonded strain gauges to the substrate of unsymmetric patch repair specimens post-cycle and dissolved the substrates in NaOH.

The second group of techniques, suitable for asymmetric lay-ups, measures the deformation of the specimen due to processing. Kim and Hahn [56] measured the deflection produced during intermittent cure cycles for graphite/epoxy laminates. White and Hahn [57] investigated the effects of cure cycle modification on the development of deflection. Ramani and Zhao [58] bonded a thermoplastic to a steel substrate and measured the deflection during cool-down with a high-resolution camera. Cho and Sun [5,55] measured final deflections in patch repair specimens and found that this technique gave similar results to those obtained through strain gauging. Djokic *et al.* [17] monitored the development of residual stresses during a cure cycle by designing a jig, consisting of an instrumented cantilevered element in

contact with a patch repair specimen spanning two uprights, to measure the out-of-plane deflection in a patch repair specimen in-situ.

Eliminating the need to correlate results with Laminate Plate Theory, Crasto and Kim [54], Findik *et al.* [59], and Djokic *et al.* [17] reheated specimens to produce a stress free condition, thus determining a stress-free temperature. Ochi *et al.* [60] measured the internal strains on an embedded steel ring surrounded by a curing resin, which they used to differentiate between cure shrinkage and thermal shrinkage. Schoch *et al.* [61] used a parallel plate fixture in a DMA to determine the shrinkage stresses of a neat resin in-situ. Similarly, Lange *et al.* [13,62,63] used a parallel plate rheometer to determine the cure shrinkage of epoxy and acrylate systems. Motahhari and Cameron [64] used the relative movement of two guides implanted in a neat resin as a measure of cure shrinkage. They then measured the deflection of a bimaterial specimen, consisting of a layer of the same neat resin and a layer of fibres impregnated with the same resin, to determine the contribution of resin shrinkage to the residual stress of the system.

2.4.2   Process Induced Residual Stresses

Kim and Hahn [56] were one of the first to study the effects of residual stress development during processing. Intermittent curing was used to determine the development of out of plane deflection in T300/301-6 graphite/epoxy $[0_4/90_4]_T$ laminates as a function of degree of cure. They found that although an elastic solution predicted the development of curvature relatively well, the stress free temperature was generally found to be below the cure temperature due to viscoelastic relaxation during cool down.

Crasto and Kim [54] studied the process-induced residual stresses in $[0_4/90_4]_T$ laminates and determined a stress free temperature by reheating specimens. Their results suggested that the stress free temperature was greater than the cure temperature, which they suggest may be caused by cure shrinkage and moisture desorption. Residual stresses in various symmetric angle-ply lay-ups, with 0° outer layers, were also investigated using the peel-ply technique. Stress free temperatures determined by the peel ply technique lay in the vicinity of the cure temperature and were lower than those from the reheat technique. The peel-ply technique

was found to be sensitive to the choice of coefficient of thermal expansion, as an analytical model is used to determine the stress free temperature

Kim and White [65] studied the stress relaxation behaviour of a neat epoxy resin, 3501-6 produced by Hercules Inc., using a parallel arm DMA in stress relaxation mode. This technique eliminated many of the difficulties incurred when transforming creep data in the Laplace domain (or dynamic data in the frequency domain) to stress relaxation data in the time domain. Using samples cured at various degrees of cure, they developed a constitutive model, in the form of a discrete exponential series, incorporating time- and cure-dependant effects. Using this model, they proceeded to extend laminate plate theory to viscoelastic materials and then investigated the cool-down process-induced stresses in terms of interlaminar normal stresses [66]. Comparing their results to the elastic response of Wang and Cross, a reduction of up to 30% in interlaminar stresses is found due to viscoelastic relaxation. They proceeded to run the numerical model for an entire 2-step cure cycle, while neglecting cure shrinkage. Results show that during the ramp to the second hold, compressive interlaminar stresses were developed, which then proceeded to cancel out some of the thermal residual stresses produced during cool-down. The addition of cure shrinkage to the model was found to increase the process-induced residual stresses. This effect is magnified if cure shrinkage is assumed to occur later in the cure process.

White and Hahn [52,67] developed a comprehensive model to predict the development of residual stresses during cure by modifying Laminate Plate Theory to account for time and cure varying parameters and viscoelastic relaxation. The residual stresses produced in interrupted cure cycles were shown to compare favourably to model results, except for the over prediction of creep response at high degrees of cure. They note that further investigation into the development of some of the material parameters was necessary. They concluded that cure shrinkage appears to account for approximately 5% of the final process-induced residual stresses and that elastic models cannot properly predict the development of residual stresses when viscoelastic effects are significant. They proceeded to study the effect of varying the cure cycle on the process induced residual stresses in cross-ply $[0_4/90_4]_T$ graphite/BMI specimens [57], by investigating the sensitivity of the curvature to cure cycle parameters

including dwell times and temperatures, cool down rates, cool down pressure, and the effects of post-curing. Results showed that reducing the cure temperature and dwell times had the most profound effect on the curvature, however one must be conscientious in ensuring full cure as a reduction in degree of cure correlates to a reduction in the mechanical properties. Slower cool down rates were shown to reduce final residual stresses, as relaxation processes were permitted longer times at higher temperatures. Post curing was shown to negate much of the perceived benefit of low temperature one-step cycles, while varying pressure during cool-down did not affect the residual stresses. Finally, three step cycles, mimicking a two-step cycle immediately followed by a post-cure, without an intermediate cool-down, were investigated. These cycles showed a marked improvement over the one-step cycles. They did, however, highlight the need for a judicious selection of the cycle and a matching of the dwell times to the dwell temperatures. They also compared their results to those of a simple elastic model and found that such models over-predict the curvature. This was attributed to the inability of the elastic model to capture relaxation phenomena, which tend to reduce the curvature.

Gopal *et al.* [68], using the model developed by White and Hahn, performed a numerical study to determine the effects of heating/cooling rates on the process-induced stresses. Their results suggest that the optimum cure cycle requires an almost instantaneous temperature jump to the fist dwell as well as the second, while for cool-down, an optimum, cool down rate can be determined, which does not necessarily correspond to the minimum cool-down rate.

Crasto *et al.* [53] endeavoured to reduce process-induced stresses in unidirectional AS4/3501-6 laminates by matching thermal residual stresses to cure shrinkage stresses during heat up. Using an embedded strain gauge technique, they monitored the development of axial and transverse stresses in the laminates and found that the final process-induced residual strains could be significantly reduced by using a feedback-controlled heating rate that allowed matrix thermal expansion to compensate for cure shrinkage.

Bogetti and Gillespie [69] studied the evolution of residual stresses in thick thermoset laminates. They developed an elastic process model based on Laminate Plate Theory that calculated the lamina stresses based on a curing model for the resin that included cure kinetics, modulus development, cure shrinkage, and thermal effects. They found that the progression of cure occurred very differently in thick section composites, when compared to thin composites. In thin composites, curing begins in the interior and progresses to the outside, while in thick section composites show a cure front that travels from the outside to the centre of the material [70]. This cure front causes a reversal in the through thickness stress distribution. Due to the cure front, trends observed in thin section composites may not be applicable to thick composites. As an example, slower ramp rates promote an inside to outside cure history, developing internal compressive stresses. They also note that the definition of a stress-free temperature isn't representative of thick composites, as the stresses show a large variation through the thickness.

2.4.3 Patch Repair Optimization

Cho and Sun [5,55] studied the effects of modifying the cure cycle on the residual stresses produced in patch repairs consisting of a Carbon(IM7)/Epoxy(954-2A) patch bonded to an aluminium substrate, using the aerospace grade adhesive Cytec FM73. A number of their conclusions were instrumental in the further development of this area of research. First they studied the effect of modifying the cure temperature and hold time in 1-step cycles on the lap shear strength of the adhesive at room temperature and at elevated temperatures (82°C and 110°C). Room temperature mechanical properties were found to be a required, but not sufficient, measure of the extent of cure, as evidenced by determination of the glass transition temperatures of the same cycle using ASTM E1824. Conversely, if a specimen exhibits fully developed mechanical properties at elevated temperatures, they premise that it has reached full cure.

Table 2.1 - Summary of Cho & Sun patch repair tests [5]

Test	T_{cure} [°C]	t_{hold} [min]	Heating Rate [°C/min]	Cooling Rate [°C/min]	ΔT_{eff} [°C]	Percent reduction in ΔT_{eff}
1	121	60			-90	-
2	77/104	300/60			-61	32
3	77/104	360/60			-51	43
4	82/104	210/60	3.3	1.1	-57	37
5	82/104	240/60			-53	41
6	82/104	300/60			-53	41
7	88/104	210/60			-62	31
8	88/104	240/60			-62	31

They then proceeded to modify both cure temperature and dwell times for 2-step cycles, as summarized in *Table 2.1*. Cycles were selected such that the first dwell temperature allowed for sufficient development of mechanical properties without requiring inordinate dwell times. Their second dwell temperatures were chosen to ensure full cure as determined by their tests on 1-step cycles. Their results can be summarized by noting that "ΔT_{eff} decreases as degree of cure increases and cure temperature deceases in the first-step cure," resulting in a maximum reduction of 40% in ΔT_{eff}. Cho and Sun [71] then proceeded to develop a model to predict the behaviour of FM73 when subjected to a multi-temperature bonding cycle. The viscoelastic response of the adhesive was described by a Maxwell model and the effective temperature drop, ΔT_{eff}, was found to compare favourably with previously determined experimental results.

Table 2.2 - Summary of Djokic *et al.* FM73 patch repair tests [72]

Test	T_{cure} [°C]	t_{hold} [min]	DOC Model	DOC Exp.	T_g Model [°C]	T_g Exp. [°C]	T_{sf} Model [°C]	T_{sf} Exp. [°C]
1	121	60	0.989	0.985	93.8	106	99.6	102.0
2	104	60	0.972	0.976	88.5	104	91.3	101.4
3	82	240	0.970	0.896	88.1	97	82	78.8
4	82	210	0.966	N/A	86.9	N/A	82	68.1
5	77	360	0.963	0.876	86	96	77	76.6
6	82/104	210/60	0.989	0.966	94	108	98	100
7	82/104	240/60	0.990	0.976	94	109	98	98
8	82/104	480/60	0.991	0.975	94	109	98	95
9	82/104	360/60	0.994	0.975	95	112	91	94
10	82/96	480/60	0.992	0.942	95	108	89	89

Djokic [73] extended the work of Cho and Sun by designing a jig to monitor the development of residual stresses in a patch repair specimen in-situ. Specimens consisted of 10 plies of AS4/3501-6 carbon fibre/epoxy unidirectional laminate bonded to an aluminium substrate by FM73 adhesive. Simultaneously, Djokic *et al.* [72] developed a viscoelastic model to describe the development of warpage. The cure kinetics [73,74], glass transition temperature [22], and the development of mechanical properties as a function time, temperature, and degree of cure for FM73 adhesive were characterized. The Boltzmann superposition principle was then used to model the development of stresses throughout a cure cycle. Experimental results showed that the model accurately predicted the warpage produced in patch repair. Experimentally, T_{sf} was determined using the reheat technique, while numerically, an elastic model was used. The results are summarized in *Table 2.2*. Heating rates were 5 °C/min in all cases and cooling rates were 2.5 °C/min for tests 1 through 8 and for tests 9 and 10 a cooling rate of 0.2 °C/min was used to 75 °C followed by a cooling rate of 2.5 °C/min.

A number of important observations can be drawn from the results. Focusing on one-step cure cycles (1-5), a reduction in T_{sf} with reduced cure temperature is evident. One must however be careful to ensure a sufficient degree of cure. For two-step cycles (6-10), reductions in residual stresses over those found for a 1-step, 104°C cycle were observed. The reduction was not as pronounced as that found by Cho and Sun, as substantial reduction in residual stresses was only achieved by significantly extending the cure times at lower temperature. This was due to relaxation occurring during the ramp between first and second dwell temperatures as well as during the second hold, essentially negating the assumed benefit of an initial, low temperature dwell. The results also suggest that although E_∞ is small, it is non-zero. The findings of Findik *et al.* [59,75] support the results of Djokic over those of Cho and Sun. Using an implanted strain gauge method on similar specimens, they found that using a 2-step cure cycle resulted in a maximum reduction of thermal residual stresses of approximately 20%.

Using the same experimental set-up previously described, Djokic *et al.* [17] studied the effect of modifying the manufacturer's recommended cure cycle on the aerospace grade adhesive Cytec FM300 (1 hour at 177°C) by:

- Changing the cure temperature, cure time, and cool down rate for 1-step processes
- Investigating the effects of post-curing
- Changing the first hold temperature for 2-step processes
- Introducing 3-step process to reduce processing times

Although they did not develop a viscoelastic model for FM300, they did characterize the cure kinetics and development of glass transition temperature to guide their cycle design. From the results, summarized in *Table 2.3*, a number of the conclusions drawn from the study performed on FM73 can be reiterated. First, a reduction in T_{sf} occurs with reduced cure temperature. Second, 2-step cycles can be used to reduce T_{sf} considerably. A number of novel observations can also be made. First, post curing at 177°C to ensure full development of mechanical properties eliminated the benefits of reducing the cure temperature. Second, cooling rate had little effect on the results, paralleling the results of White and Kim [66]. Finally, their results suggest that it may be possible to develop a 3-step cure cycle that

minimizes residual stresses as well as cure time. This 3-step cycle would be comprised of an initial high temperature hold to promote initial cure, followed by a cool-down to a lower hold temperature at which vitrification occurs, before ramping to the final hold temperature to complete cure. The design of such a 3-step cure cycle is, however, very dependent on accurate cure kinetics and glass transition development models. Conversely, it would seem apparent that good temperature control is an absolute necessity to derive full benefits from such a cycle, and may thus be impractical in actual application.

Table 2.3 - Summary of Djokic *et al.* FM300 patch repair tests [17]

Test	T_{cure} [°C]	t_{hold} [min]	Heating Rate [°C/min]	Cooling Rate [°C/min]	ΔT_{eff} [°C]
1	177	60			178
2	150	160	2.5	2.5	150
3	120	480			122
4	177	60			178
5	150	160	2.5	0.5	152
6	120	480			123
7	177 / 177	60 / 5			178
8	150 / 177	160 / 5	2.5	2.5	172
9	120 / 177	480 / 5			169
10	150 / 177	60 / 30	2.5 to 1st hold	2.5	165
11	120 / 177	330 / 30	1.0 to 2nd hold		167
12	150 / 130 / 177	28 / 40 / 38			168
13	150 / 130 / 177	28 / 40 / 38	2.5 to 1st hold	2.0 to 2nd hold	158
14	150 / 130 / 177	28 / 55 / 38	0.5 to 3rd hold	2.5 to RT	153
15	150 / 130 / 177	28 / 55 / 38			151

3. <u>Models and Analysis</u>

3.1   Introduction

This chapter describes the theory behind the DMA beam technique that was developed to characterize material properties as a function of cure, time, and temperature, as well as to monitor the development of thermally induced warpage in-situ in bonded composite patch repair specimens.

First, equations are developed that describe the behaviour of a composite beam when subjected to external mechanical loads. The behaviour is shown to be a function of the geometry of the beam and constituents and the mechanical properties of the constituents. The equations are then modified in order to determine the instantaneous modulus of a curing adhesive on a steel substrate.

A model for the modulus of a curing resin as a function of two variables - the instantaneous temperature and the instantaneous glass transition temperature is developed. Cure kinetics and glass transition temperature models for FM300 adhesive are also presented.

The deflection of bonded composite patch repair specimens when subjected to a variety of cure cycles was then explored. A shear-lag model was used to describe the response of an elastic specimen to thermal loads. A cure hardening instantaneously linear elastic (CHILE) constitutive model, modified to account for thermal softening, was then developed to predict warpage, thermal stresses, and shear stresses in the adhesive layer in a non-linear elastic system.

3.2   Bimaterial beam stress relaxation

The relationship between force, F, and displacement, w, for an elastic beam in three-point bending is

$$w = \frac{FL^3}{48EI} \tag{26}$$

where E is the elastic modulus and I the moment of inertia [76].
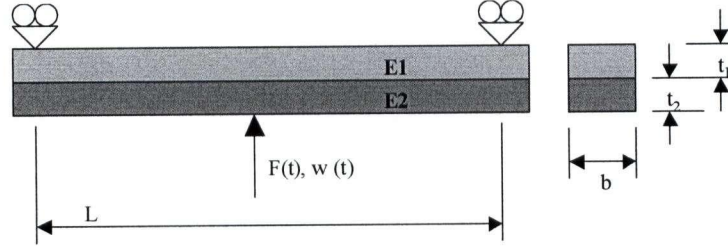
Figure 3.1 - Schematic of bimaterial beam specimen

For a bimaterial beam consisting of two elastic materials as shown in *Figure 3.1*, *Equation (26)* is still valid if the product EI is replaced with the equivalent beam bending stiffness $(EI)_{eq}$. Assuming perfect bonding and that the adhesive layer can be neglected (due to its small thickness and low modulus), the system's bending stiffness, $(EI)_{eq}$, can be expressed as a function of the modulus of the constituent materials and the specimen geometry as

$$(EI)_{eq} = E_1 \cdot I_1 + E_2 \cdot I_2 = E_1\left(I_{1o} + r_1^2 \cdot A_1\right) + E_2\left(I_{2o} + r_2^2 \cdot A_2\right)$$

$$(EI)_{eq} = E_1\left[\frac{b \cdot t_1}{12} + \left(t_2 + \frac{t_1}{2} - y_{eq}\right)^2 (b \cdot t_1)\right] + E_2\left[\frac{b \cdot t_2}{12} + \left(\frac{t_2}{2} - y_{eq}\right)^2 (b \cdot t_2)\right] \tag{27}$$

$$y_{eq} = \frac{t_1 \cdot t_2 + \dfrac{t_1^2}{2} + \dfrac{E_2}{E_1}\dfrac{t_2^2}{2}}{t_1 + \dfrac{E_2}{E_1}t_2} \tag{28}$$

In the case where the modulus of one of the constituents is unknown, *Equation (26)* can be used to determine $(EI)_{eq}$ from experimental force and displacement data. *Equations (27)* and *(28)* can then be used to solve for the unknown modulus (either E_1 or E_2).

In the case where one of the constituents is viscoelastic, the system will exhibit a time dependent response. In a time dependent mechanical test, either a load $F(t)$ is applied to the

specimen and the displacement $w(t)$ is recorded, or vice-versa. For tests where a constant displacement is applied, *Equations (26)-(28)* are still valid but the Young's modulus, E, is replaced by the time dependant relaxation modulus, $E(t)$.

3.3   FM300 Cure Kinetics Model

Rogers and Lee-Sullivan developed a cure kinetics model for FM300 incorporating autocatalytic/n^{th} order mechanisms as well as a diffusion-controlled denominator [7].

$$\frac{d\alpha}{dt} = \frac{K_1 \alpha^{m_1}(1-\alpha)^{n_1} + K_2 \alpha^{m_2}(1-\alpha)^{n_2}}{1+\exp[-C_{DOC}(\alpha - \alpha_c)]} \tag{29}$$

where α represents the degree of cure, m_i and n_i are exponents which control the nth order and autocatalytic reactions respectively, C_{DOC} is a diffusion control constant, α_c is the cross-over point between kinetic and diffusion controlled curing for a given cure temperature, and K_i is an Arrhenius form reaction rate constant.

$$K_i = A_i \exp\left(-\frac{\Delta E_i}{RT}\right) \tag{30}$$

where A_i is a pre-exponential, ΔE_i is the activation energy, R is the universal gas constant (J/mol·K) and T is the temperature (in Kelvin). *Table 3.1* lists the constants that were used in this model [77].

Table 3.1 - Cure kinetics model constants

$A_1 = 447.89 \times 10^9$ min^{-1}	$A_2 = 72.450$ min^{-1}	
$\Delta E_1 = 105.56 \times 10^3$ J/mol	$\Delta E_2 = 18.352 \times 10^3$ J/mol	
$m_1 = 0.3$	$m_2 = 9.4259 - 0.04853 \times T$	$C_{DOC} = 40$
$n_1 = 1.5$	$n_2 = 4.9416 - 0.01791 \times T$	$\alpha_c = 0.003495 + 0.3934 \times T$

3.4   FM300 Glass Transition Temperature Development Model

Development of FM300's glass transition temperature, T_g, was modelled as a quadratic function of degree of cure by Djokic *et al.* [17].

$$T_g(\alpha) = \begin{cases} A_{Tg1} + B_{Tg1}\alpha + C_{Tg1}\alpha^2 & \alpha < \alpha_{Tg} \\ A_{Tg2} + B_{Tg2}(\alpha - \alpha_{Tg})\alpha + C_{Tg2}(\alpha - \alpha_{Tg})^2 & \alpha > \alpha_{Tg} \end{cases} \tag{31}$$

where A_{Tgi}, B_{Tgi}, C_{Tgi}, and α_{Tg} are fitting constants. The model constants, presented in *Table 3.2*, were modified slightly from those used by Djokic *et al.* to more appropriately model the development of modulus. *Figure 3.2* shows the resulting development of the glass transition temperature of FM300 with cure.

Table 3.2 - FM300 Glass transition temperature model constants

$A_{Tg1} = 1.40 \times 10^1 \,^\circ C$	$B_{Tg1} = 5.46 \times 10^1 \,^\circ C$	$C_{Tg1} = 8.38 \times 10^1 \,^\circ C$
$A_{Tg2} = 1.21 \times 10^2 \,^\circ C$	$B_{Tg2} = 3.50 \times 10^2 \,^\circ C$	$C_{Tg2} = 8.38 \times 10^1 \,^\circ C$
	$\alpha_{Tg} = 0.844$	
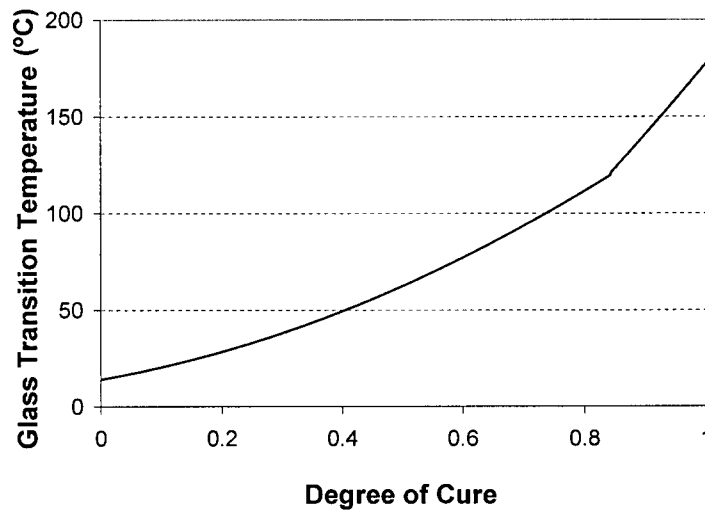
Figure 3.2 - Development of the glass transition temperature of FM300 with cure

3.5   FM300 Modulus Development Analysis

The general relationship between force, F, and the midspan deflection, w, for an elastic beam in three-point bending as shown in *Figure 3.1* is given by *Equation (26)*. When a dynamic deflection of the form $w(t) = w_0 \sin(\omega t)$ is applied, the force required to produce the deflection is proportional to, but out of phase with, the deflection and can be defined as $F(t) = F_0 \sin(\omega t + \delta)$. For a viscoelastic beam subjected to this dynamic load, the correspondence principle states that the solution is equivalent to the elastic solution if the instantaneous modulus, $E(t)$, is substituted for the elastic modulus [27].

$$E(t) = \frac{L^3}{48 \cdot I} \frac{F(t)}{w(t)}$$

(32)

In order to determine the storage modulus of a neat resin from a system consisting of a steel shim and an initially uncured resin in the RSI DMTA V, a slight modification to the specimen geometry was necessary. To reduce the effect of the supports resting on the soft, low viscosity resin, the film adhesive was trimmed so as to only cover the metallic substrate between the supports, as shown in *Figure 3.3.*
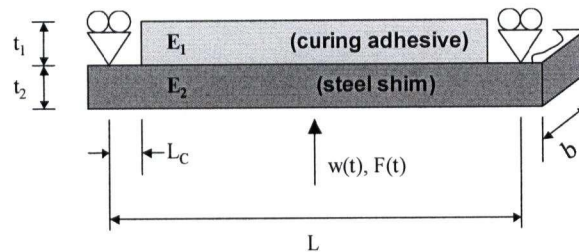
Figure 3.3 - Modulus development specimen geometry and loading conditions

To account for the change in geometry, Twigg [78] developed a modified beam equation

$$(E^* I)_{Eff} = \frac{F \cdot L^3 \cdot (EI)_{Steel} + 8 \cdot F \cdot L_C^3 \cdot (EI)_{Steel}}{48 \cdot b \cdot (EI)_{Steel} - 8 \cdot F \cdot L_C^3}$$

(33)

33

where $(E^* I)_{Eff}$ is the bending stiffness of the beam, F and L are defined as previous, b is the specimen thickness, $(EI)_{Steel}$ is the product of the steel shim modulus and moment of inertia, and L_C is the length between the span support and the end of the prepreg material. Noting that the complex modulus and the storage modulus are related through the phase angle and that for slow test frequencies $E \approx E'$ [78], *Equation (33)* can be rewritten to represent the effective bending stiffness of the bimaterial portion of the beam as

$$(E \cdot I)_{Eff} \approx (E' \cdot I)_{Eff} = \frac{F \cdot L^3 \cdot (EI)_{Steel} + 8 \cdot F \cdot L_C^3 \cdot (EI)_{Steel}}{48 \cdot w \cdot (EI)_{Steel} - 8 \cdot F \cdot L_C^3} \cdot \cos\delta \qquad (34)$$

Using test data for force and displacement, *Equation (34)* can be equated to the classical solution of *Equation (28)* to determine the modulus of the resin, E_1, as a function of time. In parallel, the degree of cure of the adhesive, and subsequently the glass transition temperature, can be calculated as functions of the cure cycle using *Equations (29)* and *(31)*.

Classically, a viscoelastic constitutive model is used to define the modulus of a time, temperature, and cure dependant material. These models generally define a rubbery modulus, a glassy modulus and a time, temperature, and cure dependant transition [23,34,35,79]. An alternate material model defines an instantaneous modulus for the resin as a function of the difference between the resin's temperature and its instantaneous glass transition temperature [38]. This model incorporates a relaxed and unrelaxed modulus and a piecewise defined transition regime,

$$E(T^*) = \begin{cases} 0 & \alpha < \alpha_{gel} \\ E_{c1} & T^* < T_{c1} \\ A^* \cdot \exp(-K^* \cdot T^*) & T_{c1} < T^* < T_{c2} \\ E_{c2} + (E_{c3} - E_{c2})\left(\dfrac{T^* - T_{c2}}{T_{c3} - T_{c2}}\right) & T_{c2} < T^* < T_{c3} \\ E_{c3} & T_{c3} < T^* \end{cases} \qquad (35)$$

where $T^* = T - T_g$ is defined as the difference between the current temperature, T, and the instantaneous glass transition temperature, T_g. α is the instantaneous degree of cure, α_{gel} is the degree of cure at which gelation occurs (assumed as 0.5 for FM300), $E(T^*)$ is the instantaneous modulus of the resin, and E_{c1}, E_{c2}, E_{c3}, T_{c1}, T_{c2}, T_{c3}, A^*, and K^* are constants fit to the data as shown in *Figure 3.4*.

The adhesive's instantaneous shear modulus is then determined using Hooke's law for an isotropic material. The Poisson's ratio was assigned a constant value of 0.4 following Hojjati *et al.* [22], such that

$$G_a = \frac{E_a}{2(1+v)} = \frac{E_a}{2.8} \tag{36}$$
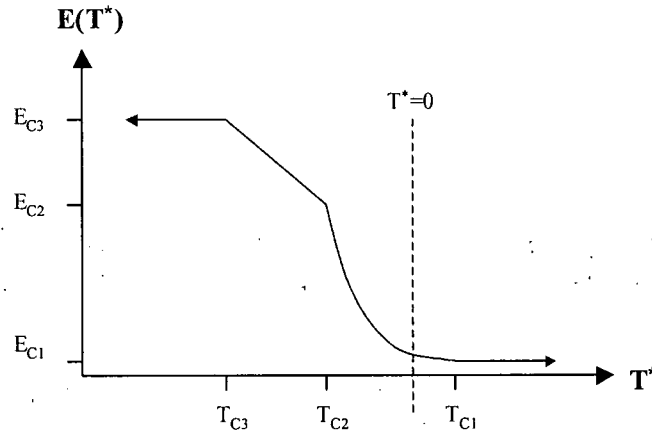
Figure 3.4 - Modulus versus T-Tg model

3.6   Bonded Composite Patch Repair Specimen

3.6.1   Thermo-elastic Deflection

Hojjati and Johnston [51] developed a closed form solution for the thermo-elastic deflection of a one-sided bonded composite patch repair geometry based on a three-component system as shown in *Figure 3.5*.
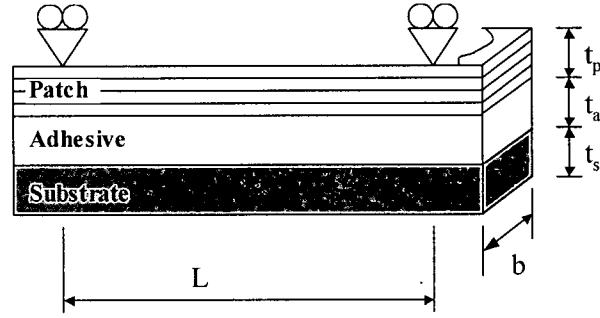
Figure 3.5 - Schematic of bonded composite patch repair specimen

The system was modelled using an elastic shear lag approach by assuming that the adhesive layer carries only shear load. Modifying the definition of beam bending stiffness, EI, to account for the adhesive layer thickness, the central deflection, w, of an elastic beam subjected strictly to a thermal load, T, can be expressed as

$$w = T \cdot \kappa_w \cdot f(G_a) \tag{37}$$

$$\kappa_w = \frac{(CTE_p - CTE_s) \cdot (t_p + 2t_a + t_s) \cdot (L/2)^2}{4EI\lambda} \tag{38}$$

$$\lambda = \frac{1}{E_p t_p} + \frac{1}{E_s t_s} + \frac{t_a(t_p + 2t_a + t_s)}{2EI} \tag{39}$$

$$EI = E_p \cdot \left[\frac{t_p^3}{12} + t_p \cdot \left(t_s + t_a + \frac{t_p}{2} - y_{eq} \right)^2 \right] + E_s \cdot \left[\frac{t_s^3}{12} + t_s \cdot \left(y_{eq} - \frac{t_s}{2} \right)^2 \right] \tag{40}$$

$$y_{eq} = \frac{\dfrac{t_p^2}{2} + t_p t_a + t_p t_s + \dfrac{E_s}{E_p} \dfrac{t_s^2}{2}}{t_p + \dfrac{E_s}{E_p} t_s} \tag{41}$$

$$f(G_a) = 1 - \frac{2}{\lambda(G_a)^2}\left(1 - \frac{1}{\cosh(\lambda(G_a))}\right) \qquad (42)$$

$$\lambda(G_a) = \frac{L}{2} \cdot \sqrt{G_a \cdot \frac{\lambda'}{t_a}} \qquad (43)$$

where CTE_p and CTE_s are the coefficients of thermal expansion of the patch and substrate respectively, T is the temperature change, L is the length of the specimen, G_a is the instantaneous shear modulus of the adhesive, and E_p and E_s are the elastic moduli of the patch and substrate respectively.
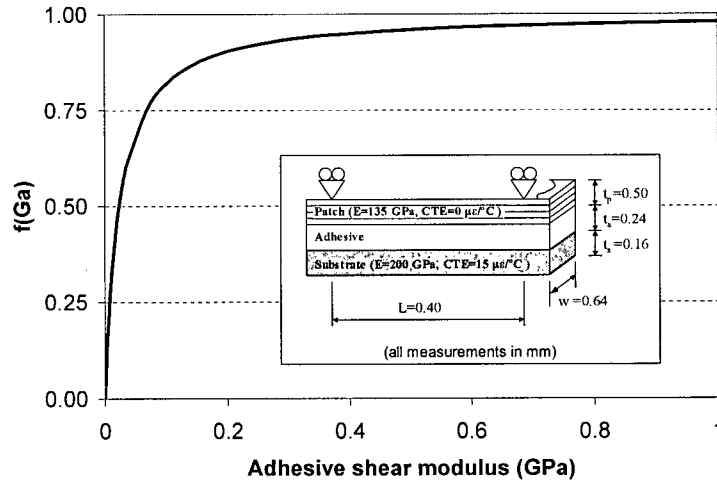
Figure 3.6 - Effect of the adhesive's shear modulus, G_a, on the coupling factor, $f(G_a)$, for the geometry shown in the insert

$f(G_a)$ in *Equation (37)* can be conceptualized as the degree of adhesive coupling between the patch and substrate and is dependant on both the specimen geometry and the adhesive layer's shear modulus. As can be seen in *Figure 3.6*, for an uncured adhesive $f(G_a) \to 0$ and the constituents act as two separate beams. As the adhesive's modulus increases, $f(G_a) \to 1$ and the system acts as a perfectly bonded beam.

3.6.2 Constitutive Model

The closed-form solution presented for thermal deflection, *Equation (37)*, is only valid for linear elastic systems. A linear elastic constitutive model is path independent and defines increments in deflection as a function of increments in temperature and a constant that accounts for the geometry of the specimen and the thermo-mechanical properties of the constituents as

$$\Delta w = K \cdot \Delta T \qquad (44)$$

Linear elastic constitutive models have generally been shown to be inadequate in describing the behaviour of cure hardening materials [52,57,80]. A cure hardening, instantaneously linear elastic (CHILE) constitutive model was thus investigated to describe the development of deflection observed during a cure cycle [36,38]. CHILE models are path dependant and define a thermo-elastic component due to a step change in temperature occurring at an instantaneously defined modulus, which is assumed constant during each time-step, but may be defined as a function of temperature and the degree of cure, such that

$$dw_i = \left.\frac{\partial w}{\partial T}\right|_i \cdot dT = \kappa \cdot f(G_a)_i \cdot dT \qquad (45)$$

where dw_i is an incremental deflection due to the temperature change dT.

The CHILE constitutive model was found to be incapable of completely describing the experimentally observed behaviour of bonded composite patch repair specimens, as tested in a DMA with the adhesive FM300. The model was thus modified to include a thermal softening component, so that the deflection, w, is affected both by changes in temperature and by softening of the adhesive. Changes in temperature are treated as a thermo-elastic deflection occurring with an instantaneously defined modulus. Softening of the adhesive layer affects accumulated deflection, resulting in a relaxation of accumulated thermally induced stresses. The difference in these behaviours is shown schematically in *Figure 3.7*.
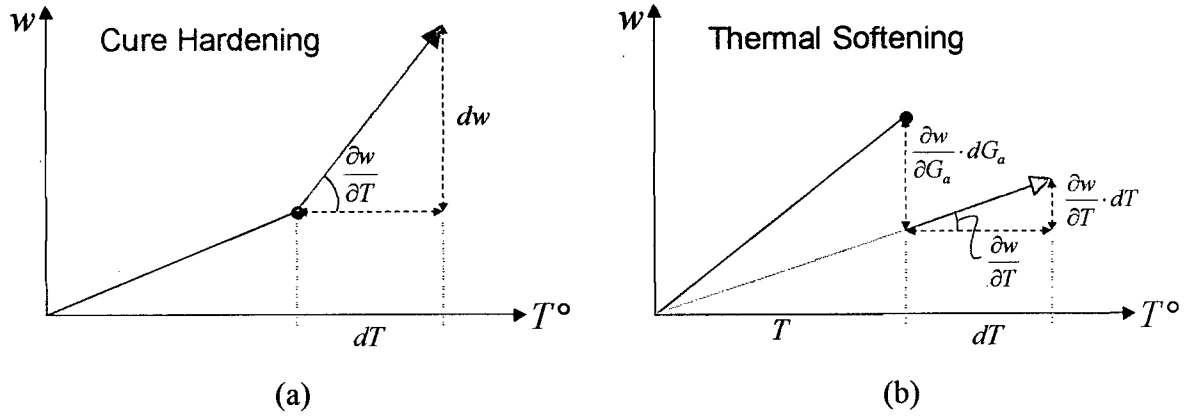
Figure 3.7 - Schematic illustrating the difference between cure hardening (a) and thermal softening (b)

As the adhesive's modulus is a function of the difference between the temperature and the instantaneous glass transition temperature of the material, the deflection is a function of two independent variables, T and T_g, and *Equation (37)* can be written in differential form as

$$dw_i = \frac{\partial w}{\partial T} \cdot dT + \frac{\partial w}{\partial (G_a)} \cdot d(G_a) \tag{46}$$

$$dw_i = \frac{\partial w}{\partial T} \cdot dT + \frac{\partial w}{\partial (G_a)} \cdot \frac{\partial (G_a)}{\partial (T - T_g)} d(T - T_g) \tag{47}$$

$$dw_i = \kappa \cdot f(G_a)_i \cdot dT + \kappa \cdot T \cdot \frac{\partial [f(G_a)]}{\partial (G_a)} \frac{\partial (G_a)}{\partial (T - T_g)} d(T - T_g) \tag{48}$$

$$dw_i = \kappa \cdot f(G_a)_i \cdot dT + \frac{w_{i-1}}{f(G_a)_{i-1}} \cdot \frac{\partial [f(G_a)]}{\partial (G_a)} \frac{\partial (G_a)}{\partial (T - T_g)} d(T - T_g) \tag{49}$$

A number of conditions must be imposed on *Equation (46)*. First, during a temperature hold, no changes in deflection occur. Cure is assumed to advance by the creation of new, unstrained bonds and cross-links in the material. Thus advancement of cure should not affect deflection until a further stimulus is applied. This marks one of the major differences between CHILE type models and viscoelastic models used to predict thermal residual stresses in patch repair systems. Second, thermal softening only occurs during a heat up if the temperature increases at a faster rate than the development of glass transition temperature. Thus the second term of *Equation (47)* is only incorporated if $dT > 0$ and $d(T - T_g) > 0$.

Thermal softening results in a reduction in the built-up deformation due to a drop in the modulus of the adhesive. This can be inferred by noting that from *Figure 3.6*

$$\frac{\partial[f(G_a)]}{\partial(G_a)} > 0 \tag{50}$$

and from *Figure 3.4*

$$\frac{\partial(G_a)}{\partial(T - T_g)} < 0 \tag{51}$$

Since $dT > 0$ and $d(T - T_g) > 0$, the second term in *Equation (47)* is opposite in sign to the first term and the net result is that the deflection during that time step is less than that predicted by an instantaneously elastic model.

3.6.3 Thermal Residual Stresses

In a real structure, a bonded composite patch repair is applied to a localized region of a much larger structure. As such the repair area's out-of-plane deflection is constrained, producing thermally induced residual stresses. An expression for the thermo-elastic residual normal stresses of a one-sided bonded composite patch repair geometry based on the three-component system shown in *Figure 3.5*, can be derived from the elastic shear lag model of Hojjati and Johnston [51] as

$$\sigma(y) = E(y) \cdot \varepsilon_{mech} = E(y) \cdot \left[\varepsilon_{bending} + \varepsilon_{tensile}\right] \tag{52}$$

$$\sigma(y) = \frac{P}{t(y)} + \frac{M \cdot E(y)}{EI} \cdot (y_{eq} - y) \tag{53}$$

$$P = -P_p = P_s$$

$$P = \frac{(CTE_p - CTE_s) \cdot \Delta T}{\lambda} \cdot \left(1 - \frac{1}{\cosh(\lambda(G_a))}\right) \tag{54}$$

$$M = \frac{(CTE_p - CTE_s) \cdot (t_p + 2t_a + t_s) \cdot \Delta T}{2\lambda} \cdot \left(1 - \frac{1}{\cosh(\lambda(G_a))}\right) \qquad (55)$$

where $\sigma(y)$ is the stress at the centreline of the specimen at a height of y, $E(y)$ is the modulus of the constituent material at a height of y, $t(y)$ is the thickness of the constituent located at the height y, P is the thermally induced force in the x-axis direction, M is the thermally induced moment. *Equation (53)* can be simplified as

$$\sigma(y) = T \cdot \kappa_\sigma(y) \cdot g(G_a) \qquad (56)$$

$$\kappa_\sigma(y) = \frac{(CTE_p - CTE_s)}{\lambda} \cdot \left[\frac{1}{t_y} - E_y \cdot \frac{(t_p + 2t_a + t_s)}{2EI} \cdot (y_{eq} - y)\right] \qquad (57)$$

$$g(G_a) = 1 - \frac{1}{\cosh(\lambda(G_a))} \qquad (58)$$

In *Equation (56)*, $g(G_a)$ can be conceptualized as the degree of adhesive coupling between the patch and substrate. As can be seen in *Figure 3.8*, for an uncured adhesive $g(G_a) \to 0$. The constituents act as separate beams and no stresses are developed. As the adhesive's modulus increases, $g(G_a) \to 1$ and the system acts as a perfectly bonded beam resulting in thermally induced residual stresses.

Figure 3.8 - Effect of the adhesive's shear modulus, G_a, on the coupling factor, $g(G_a)$, for the geometry shown in the insert

Similarly, an expression for the thermo-elastic shear stresses in the adhesive can also be derived from the elastic shear lag model of Hojjati and Johnston [51] as

$$\tau(x) = T \cdot \kappa_\tau \cdot h(G_a, \chi) \tag{59}$$

$$\kappa_\tau = \frac{2 \cdot (CTE_S - CTE_P)}{\lambda \cdot L} \tag{60}$$

$$h(G_a, \chi) = \frac{\lambda(G_a) \cdot \sinh(\lambda(G_a) \cdot \chi(x))}{\cosh(\lambda(G_a))} \tag{61}$$

$$\chi(x) = 2\frac{x}{L} - 1 \tag{62}$$

In *Equation (59)*, $h(G_a, \chi)$ can be conceptualized as the degree of adhesive coupling between the patch and substrate. As can be seen in *Figure 3.9 and Figure 3.10*, the shear stress in the adhesive layer is zero at the centre of the specimen and increases to a maximum at the edges. For an uncured adhesive, $h(G_a) \to 0$, the constituents act as separate beams and no stresses

are developed. As the adhesive's modulus increases, $g(G_a) \to 1$ and the system acts as a bonded beam resulting in thermally induced shear stresses in the adhesive layer.
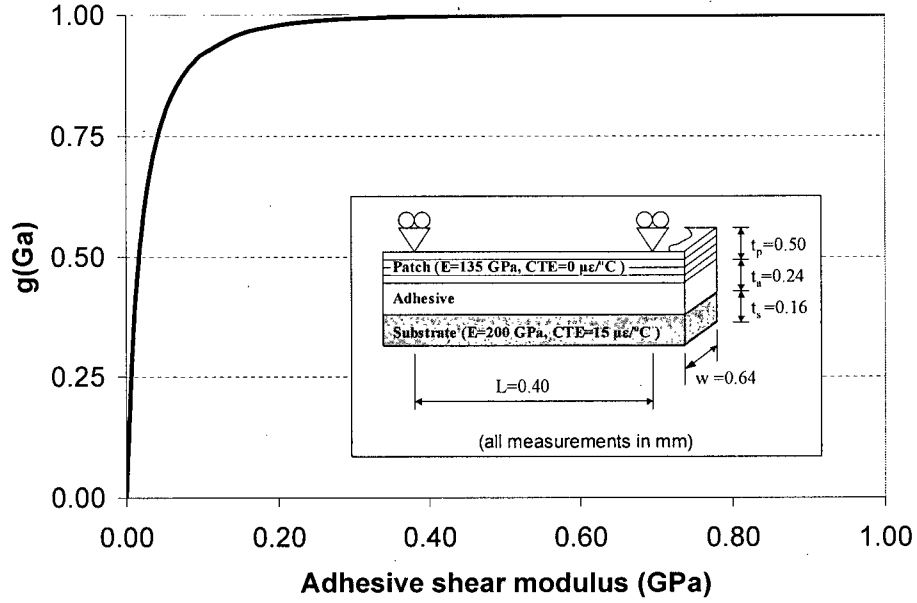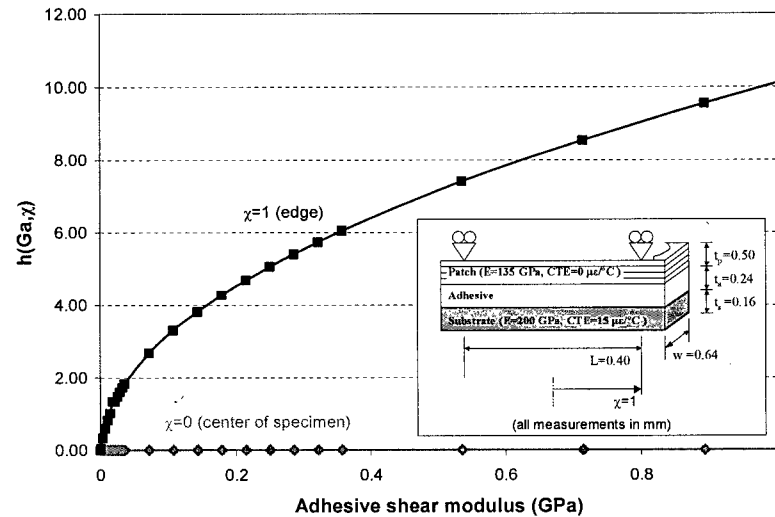

Figure 3.9 - Effect of the adhesive's shear modulus, G_a, on the coupling factor, $h(G_a, \chi)$, for the geometry shown in the insert
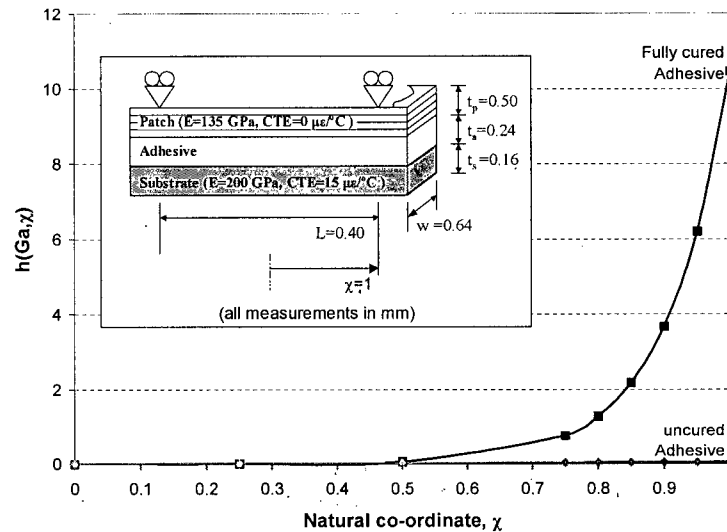
Figure 3.10 - Coupling factor, $h(G_a, \chi)$, as a function of natural coordinate system of the beam, for the geometry shown in the insert

As shown for deflection, a CHILE constitutive model modified to include thermal softening can be used to describe the experimentally observed behaviour of bonded composite patch repair specimens as tested in a DMA with the adhesive FM300. The stresses are once again a function of two independent variables, T and T_g, and *Equations (56)* and *(57)* can be written in differential form as

$$d\sigma(y)_i = \frac{\partial \sigma(y)}{\partial T} \cdot dT + \frac{\partial \sigma(y)}{\partial (G_a)} \cdot d(G_a) \tag{63}$$

$$d\sigma(y)_i = \kappa_\sigma(y) \cdot g(G_a)_i \cdot dT + \frac{\sigma(y)_{i-1}}{g(G_a)_{i-1}} \cdot \frac{\partial [g(G_a)]}{\partial (G_a)} \frac{\partial (G_a)}{\partial (T - T_g)} \cdot d(T - T_g) \tag{64}$$

$$d\tau(x)_i = \frac{\partial \tau(x)}{\partial T} \cdot dT + \frac{\partial \tau(x)}{\partial (G_a)} \cdot d(G_a) \tag{65}$$

$$d\tau(x)_i = \kappa_\tau(y) \cdot h(G_a, x)_i \cdot dT + \frac{\tau(x)_{i-1}}{h(G_a, \chi)_{i-1}} \cdot \frac{\partial [h(G_a, \chi)]}{\partial (G_a)} \frac{\partial (G_a)}{\partial (T - T_g)} \cdot d(T - T_g) \tag{66}$$

The same conditions as those imposed on the deflection model, detailed in *section 3.6.2*, are valid for the development of thermally induced residual stresses in the patch and substrate, as well as the thermally induced shear stresses in the adhesive layer. First, during a temperature hold, no changes in residual stresses occur. Second, thermal softening only occurs during a heat up if the temperature increases at a faster rate than the development of glass transition temperature. Thus the second terms in *Equation (63)* and *Equation (65)* are only incorporated if $dT > 0$ and $d(T - T_g) > 0$.

4. <u>Methods</u>

4.1 Introduction

This chapter describes the experimental DMA beam technique that is used for material characterization and for the determination of thermally induced residual stresses in a bonded composite patch repair specimen. The DMA beam technique is used in three different modes. First, the stress relaxation moduli of monolithic and adhesively bonded bimaterial beam specimens are determined by applying a constant displacement and monitoring the time varying force at various temperatures. Second, the cure and temperature dependant modulus of a curing adhesive is determined by subjecting bimaterial (steel/adhesive) specimens to an offset fully reversing cyclic displacement while monitoring the required force under various thermal cycles. Finally, the DMA is used to measure the deflection of bonded composite patch repair specimens in-situ throughout a variety of cure cycles.

4.2 Rheometric Scientific Inc. DMTA V

The Rheometric Scientific Inc. DMTA V (DMA) is a mechanical spectrometer that controls and measures force and displacement of a load head in a temperature-controlled environment. A variety of fixtures can be installed in the DMA to facilitate tensile/compressive, shear, or three-point bend testing of rigid specimens. A DMA can be used to perform a number of mechanical tests to determine a wide range of mechanical material properties and examine how they vary with time, frequency, and temperature:

- Static, constant displacement: Stress relaxation
- Static, constant force: Creep compliance
- Dynamic tests: Storage modulus, loss modulus, phase angle, glass transition temperature
- Thermal ramp tests: Coefficient of thermal expansion, thermally induced warpage
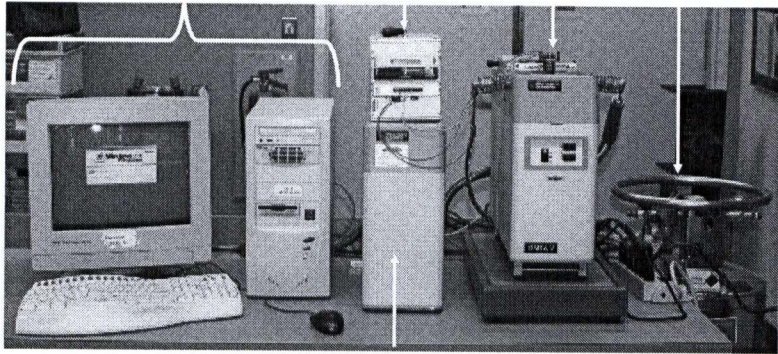
Figure 4.1 - RSI DMTA V

The DMA offers a number of advantages over other mechanical test methodologies:

- Small sample size reduces material costs, preparation times, and thermal lag

- Accurate, precise measurement of force and displacement

- Versatility allows for development of novel test methods

- Potential for rapid material characterization
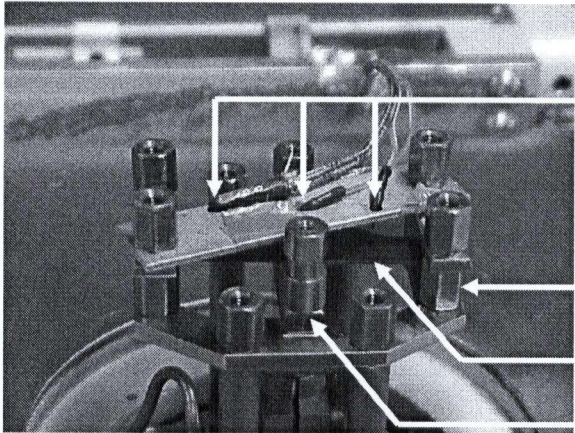
Figure 4.2 - DMTA three-point bend set-up

The RSI DMTA V's specifications allow for a maximum 125 micron deflection at an applied force of 15 N [1]. The three-point bend fixture used required specimens having a 40 mm span

length (L) and a nominal 6.4 mm width (b), as shown in *Figure 4.2*. A schematic of a generic DMA beam specimen used is shown in *Figure 4.3*.
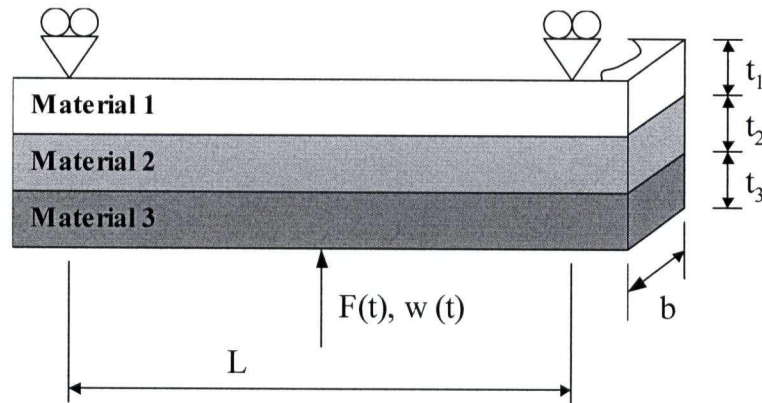
Figure 4.3 - Generic Schematic of DMA beam specimen

The inherent flexibility of the DMA beam technique allows for a variety of tests to be conducted using a simple three-point bend specimen. These tests can be used to both assess a system's response to external stimulus and to characterize material properties. In this work, the DMA beam technique is used for three different tests, summarized in *Table 4.1*. First, stress relaxation tests are conducted on monolithic and bimaterial beam specimens. During these tests, temperature is held constant while a constant displacement is applied. The force required to produce the displacement can then be correlated to the time-dependant stress relaxation modulus of the specimen. Second, modulus development tests are conducted on bimaterial beam specimens with a curing resin layer. In these test a dynamic displacement is applied to the specimen while temperature follows a pre-programmed cure cycle. The force required to produce the displacement can then be correlated to the cure and temperature dependant instantaneous modulus of the specimen. Thirdly, bonded composite patch repairs are simulated using a trimaterial beam specimen. A nominal force is applied to ensure contact of the load head, while a pre-programmed temperature cycle is applied. The resulting out of plane deflection is measured by the load head and can be correlated to the thermal residual stresses generated in the specimen.

Table 4.1 - Summary of DMA beam techniques

| | Bimaterial Stress Relaxation | | Modulus Development | Bonded Composite Patch Repair |
	Set-up 1	Set-up 2		
Material 1	-	Steel, Lexan	-	AS4/3501-6 [0]$_2$
Material 2	-	Hysol EA9392	FM300	FM300
Material 3	Steel, Lexan	Steel	Steel	Steel
Test Type	Stress relaxation	Stress relaxation	Dynamic	Thermal
Temperature Condition	Step	Step	Cure cycle	Cure cycle
Loading Condition	Static applied strain	Static applied strain	Cyclic applied strain	None
Result	Relaxation modulus	Relaxation modulus	Instantaneous modulus	Deflection

4.3   Temperature Control

Previous work on the RSI DMTA V by Graham Twigg [78] led to the discovery of a large temperature gradient through the DMA's environmental chamber. As the DMA's controlling platinum resistance thermometer device (P-RTD) is located approximately 25 mm from the specimen, three J-type thermocouples were placed at a distance of approximately 2 mm from the specimen and logged externally using a data acquisition (DAQ) system and a LabVIEW software applet. Temperature differences of up to 20°C between the P-RTD and externally logged thermocouples were measured. Control temperatures were determined by calibrating DAQ temperature readings to DMA temperature readings. The DAQ readings of the three thermocouples were averaged and linearly interpolated to match the DMA's sampling rate. Throughout this work temperature measurements from the DAQ were used instead of the DMA's temperature readings.

4.4 Bimaterial beam stress relaxation

4.4.1 Objective

The objective of these tests was to ascertain whether it is possible to accurately determine the viscoelastic response of a polymeric material from the system response of bimaterial beams consisting of an elastic substrate adhesively bonded to the viscoelastic polymeric material. To validate the approach, relaxation tests were performed on steel shims, Lexan beams, and bimaterial specimens of Lexan adhesively bonded to a steel shim. Adhesively bonded steel-steel shims were also tested to ensure the test regime was below the glass transition temperature of the adhesive and to show that the adhesive layer did not significantly affect the results.

4.4.2 Specimen Preparation

Steel shims were nominally 45 mm long, 0.16 mm thick, and 6.4 mm wide, while the polymeric material used, GE Lexan (polycarbonate), was nominally 45 mm long, 1.8575 mm (1/16") thick, and 6.4 mm wide. Monolithic steel and Lexan specimens were prepared by the Materials Engineering machine shop and by the Composites group technician, Roger Bennett. For each specimen, thicknesses and widths were measured at three locations along the beam and averaged.

Bimaterial specimens were created by adhesively bonding Lexan specimens to steel substrates. Steel shims were prepared by sanding the surface with 320-grit sandpaper and then wiping them clean with acetone. The adhesive used was Hysol EA9392, a two-part room temperature cure epoxy paste adhesive with good mechanical strength at high temperatures [81]. The adhesive was mixed as per the manufacturer's recommended ratio (100:32 by weight) and applied to the surface of the steel shim. The Lexan specimens were then placed over the adhesive, pressure was applied, and excess adhesive was cleaned off. The specimen was then allowed to cure for a minimum of 7 days at room temperature with a constant pressure applied to the top surface. Thicknesses and widths of both steel and Lexan beams were measured at three locations along the beam prior to being adhered. After the

adhesive cured, the total system thickness was measured at three locations along the beam. The adhesive layer thickness was found as the difference between the total specimen thickness and the thicknesses of the steel and Lexan. Adhesive thicknesses were of the order of 0.10 mm. The system width was taken as the average of the Lexan and steel widths.

4.4.3   Experimental Details

Specimens were heated to the initial test temperature of 30°C and held for 10 minutes to equilibrate thermally. A stress relaxation test was then run for 30 minutes by applying a constant strain to the specimen and monitoring the force required to maintain the strain. Specimens were heated to 40°C at a ramp rate of 10°C/min and held at a constant temperature for 1 hour. This dwell period allowed for temperature equilibration and relaxation of any residual stress from the previous test, which was performed at a lower temperature hold. Specimens were then subjected to a stress relaxation test before being heated by 10°C increments up to the final temperature of 110°C, repeating the temperature hold and stress relaxation test at each increment. This final temperature was chosen to be below the glass transition temperature of the adhesive. During temperature ramps and holds only a nominal force of 0.05 N was applied to the specimen to maintain contact between the load head and the specimen.

Specimens were designed to deflect 50 microns at their maximum stiffness under an applied force of approximately 1 N to maximize measurement resolution. This resulted in the selection of a specimen substrate thickness of 0.16 mm and a patch thickness of 1/16" or 1.8575 mm. The applied strain was approximately 375 µε, as calculated using *Equation (67)*

$$\varepsilon = K * w = \left(\frac{6t_T}{L^2} \right) * w \qquad (67)$$

where t_T is the total specimen thickness and w is the deflection [82].

4.5 FM300 Modulus Development

4.5.1 Objective

The objective of these tests was to determine the instantaneous modulus of FM300 as a function of the instantaneous temperature and the material's instantaneous glass transition temperature. Bimaterial beams consisting of FM300 film adhesive adhered to a steel shim were dynamically tested in a Rheometric Scientific Inc. DMTA V at different cure temperatures. Test data was then used in conjunction with a cure kinetics model and glass transition temperature model to plot the relation between modulus and T-Tg. A piecewise defined model was then fit to the resulting data.

4.5.2 Specimen Preparation

Bimaterial beam specimens were prepared by adhering FM300 to a metallic substrate. The substrate consisted of steel shims, nominally 45 mm long, 0.16 mm thick, and 6.4 mm wide. Preparation consisted of sanding the shims with 320-grit sandpaper, cleaning with acetone and wiping dry. The dimensions of the shims (thickness and width) were then measured at three locations along the shim with a digital micrometer and recorded. The shims were then wiped clean with acetone once more to remove any contaminants that may have been deposited on the shims during measurement. One layer of FM300 film adhesive was then applied and excess adhesive was trimmed. The peel ply was then carefully removed on half the specimens, while the other half retained the peel ply throughout the experiment. The specimens were then wrapped lightly in FEP before being loaded into the DMTA.

4.5.3 Experimental Details

In order to determine FM300's modulus development as a function of degree of cure, three-point bend specimens were tested in *Dynamic Temperature Ramp Mode*. Specimens were subjected to a cure cycle that consisted of a 2.5°C/min ramp to a specified cure temperature and then a prescribed hold, before being allowed to cool to room temperature.

During the cure cycle a controlled cyclic displacement, $w(t)$, was applied as an offset fully reversing cycle, as shown in *Figure 4.4*, with a frequency of 0.1 Hz and an amplitude of 100 µm. This corresponded to a strain amplitude (ε) of $2.0*10^{-4}$ as found using *Equation (67)*. An offset of 125% of the amplitude was used.
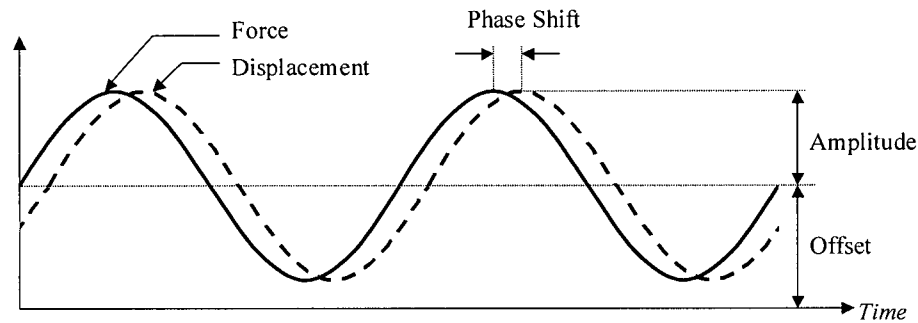
Figure 4.4 - DMA multi-frequency - strain mode

Tests were conducted at four isothermal cure temperatures. Each test was run until the cure kinetics model predicted a cessation of the cure process. Two specimens were tested at each cure temperature: One specimen with the peel-ply removed and another with the peel ply on the adhesive. Test temperatures, durations, and maximum degrees of cure are listed in *Table 4.2*.

Table 4.2 - Test Temperatures, Durations, and Maximum Degree of Cure

Test	Specimen Temperature (°C)	Control Temperature (°C)	Hold Time (min)	Final DOC*
1	120	101.0	404	0.86
2	140	119.4	168	0.92
3	160	137.0	127	0.98
4	180	152.0	60	1.00

* as predicted by cure kinetics model

4.6   Bonded Composite Patch Repair

4.6.1   Objective

The objective of this set of experiments was to develop and validate a simple and effective technique for cure cycle optimization of bonded composite patch repairs. A Rheometric Scientific Inc. DMTA V was used to measure the deflection of a bonded composite patch repair specimen in-situ during the entire cure cycle. The experimental data was then compared to the results of a modified CHILE model, which incorporates both cure and temperature dependant behaviour for the adhesive.

4.6.2   Specimen Preparation

Bonded composite patch repair specimens were created by adhesively bonding a unidirectional composite patch to a metallic substrate using FM300 adhesive. A $[0]_2$ panel of AS4/3501-6 was prepared at NRC-IAR according the manufacturer's recommended cure cycle and cut with a slow-speed diamond saw into specimens nominally 45 mm long, 6.4 mm wide, and approximately 0.5 mm thick. Steel shims nominally 45 mm long, 0.16 mm thick, and 6.4 mm wide were prepared by sanding the surface with 360-grit sand paper and then wiping them with acetone. One layer of FM300 was then applied to the steel shim and trimmed to size. The AS4/3501-6 patch was then laid on the adhesive and pressed in place. Thicknesses and widths of both the steel substrate and the AS4/3501-6 patch were measured at three locations along the beam. After cure, the total system thickness was measured at three locations. The adhesive layer thickness, on the order of 0.20-0.30 mm, was found as the difference between the total specimen thickness and the sum of the patch and substrate thicknesses. The system width was taken as the average of the steel and patch widths.

4.6.3   Experimental Details

A schematic of the bonded composite patch repair specimen is shown in *Figure 4.5*. The specimen was placed in the three-point bend fixture of the DMA, where the deflection generated by the thermal expansion mismatch between the patch and the substrate throughout a complete cure cycle was measured. To ensure that the load head maintained contact with

the specimen throughout the cure cycle, a constant nominal force of 0.05 N was applied to the specimen.
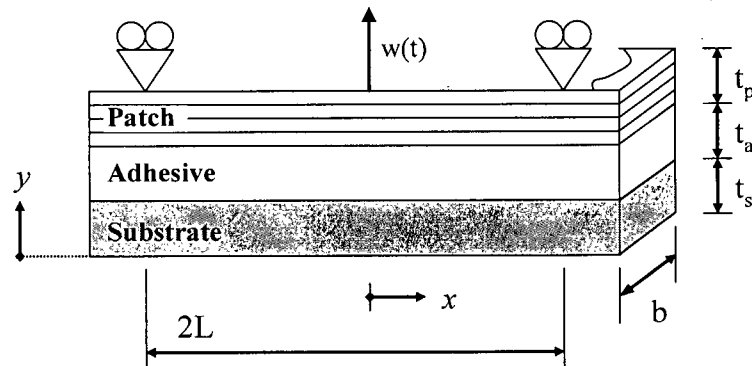
Figure 4.5 - Schematic of Specimen Geometry and Loading Conditions

A series of cure cycles were investigated, which fit broadly into three categories: one-step cycles, post-cure cycles, and two-step cycles. Three different one-step cycles were investigated, consisting of a heat-up ramp to the dwell temperature and then a cool-down to room temperature. Similarly, three post-cure cycles were investigated. These consisted of a one-step cycle followed by a heat up to 177°C, a 5 minute hold and another cool-down to room temperature. Two different two-step cycles were investigated, consisting of a heat-up ramp to a first dwell temperature followed by a heat-up ramp to a second dwell temperature and then a cool-down to room temperature. These cycles were run with three different ramp rates between the first and second dwell, resulting in a total of six permutations. The cure cycles investigated are summarized in *Table 4.3*.

Table 4.3 - Cycles specifications

	Description	Temp (°C)	Dwell Time (min)	Heating Rate (°C/min)	Cooling Rate (°C/min)
			Cycle		
[1]	1 step - 177°C	177	60	2.50	2.50
[2]	1 step - 150°C	150	160	2.50	2.50
[3]	1 step - 120°C	120	480	2.50	2.50
[4]	177°C + Post Cure	177	60	2.50	2.50
		177	5	2.50	2.50
[5]	150°C + Post Cure	150	160	2.50	2.50
		177	5	2.50	2.50
[6]	120°C + Post Cure	120	480	2.50	2.50
		177	5	2.50	2.50
[7]	2 step - 155°C /177°C (2.5°C/min)	155	60	2.50	
		177	30	2.50	2.50
[8]	2 step - 120°C /177°C (2.50°C/min)	120	330	2.50	
		177	30	2.50	2.50
[9]	2 step - 155°C /177°C (1.00°C/min)	155	60	2.50	
		177	30	1.00	2.50
[10]	2 step - 120°C /177°C (1.00°C/min)	120	330	2.50	
		177	30	1.00	2.50
[11]	2 step - 155°C /177°C (0.10°C/min)	155	60	2.50	
		177	30	0.10	2.50
[12]	2 step - 120°C /177°C (0.10°C/min)	120	330	2.50	
		177	30	0.10	2.50

5. <u>Results and Discussion</u>

This chapter presents the results and discussion of the experimental program that was undertaken to validate the DMA beam technique. In the first section, results of bimaterial beam stress relaxation tests conducted on monolithic steel and Lexan specimens, as well as bimaterial steel/Lexan specimens are presented. Test results show that the stress relaxation behaviour of Lexan can be extracted from the stress relaxation behaviour of a bimaterial beam. The second section presents modulus characterization tests conducted on bimaterial steel/FM300 specimens. Test results show that the instantaneous elastic modulus of FM300 can be modeled as a function of the difference between the material's instantaneous temperature and its instantaneous glass transition temperature. The third section presents results of bonded composite patch repair specimens cured using a variety of cure cycles and shows that the DMA can be used to obtain an in-depth look at the development of warpage throughout a cure cycle. Model results show that a modified CHILE model can accurately predict the warpage. Model Sensitivities, cycle times, real versus idealized cycles, and the effects of thermal softening are also investigated.

5.1   Bimaterial beam stress relaxation

5.1.1   Effect of the Adhesive layer

In order to ensure that the use of a thin adhesive layer does not affect the behaviour of bimaterial beam specimens, results of steel/adhesive/steel samples were compared to those of monolithic steel samples. Temperature ramp dynamic tests were conducted to ensure the system modulus corresponded to the monolithic steel modulus throughout the temperature range of interest. Relaxation tests were also conducted to ensure that the adhesive layer did not cause time-dependant effects.

Figure 5.1 shows results of 30 minute relaxation tests performed on monolithic steel specimens in 10 °C increments from 30 °C to 110 °C, which correspond to expected values of 185-195 GPa. This modulus value can be compared to the results of dynamic tests

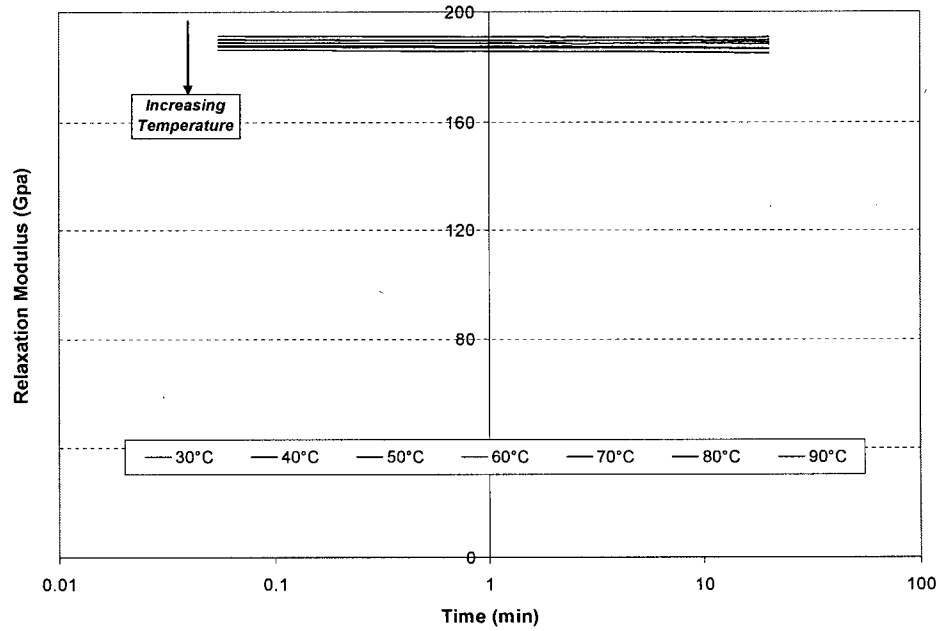performed on Steel/Adhesive/Steel samples with a temperature ramp to 110 °C, as shown in *Figure 5.2.*

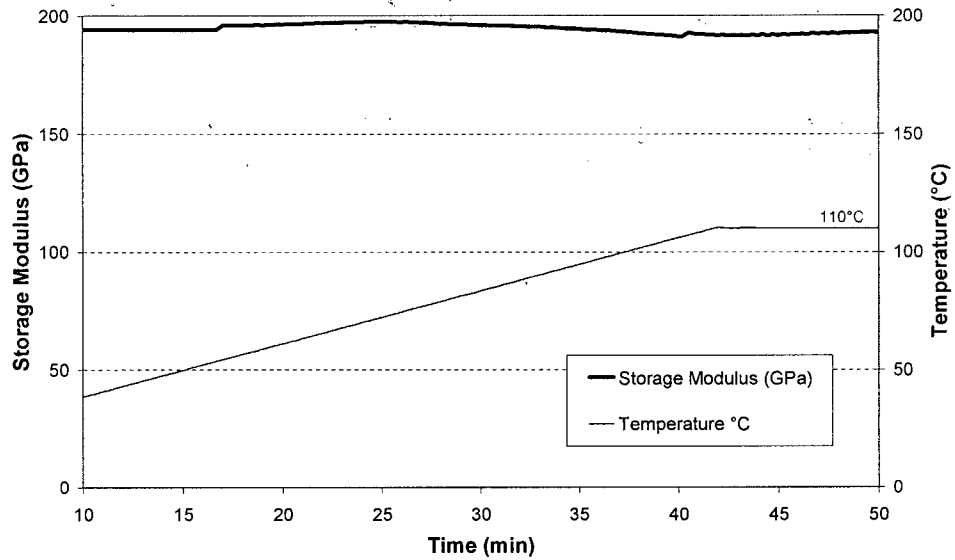**Figure 5.1 - Steel Specimen - Relaxation Modulus**

Figure 5.2 - Dynamic testing for Steel/EA9392/Steel (Frequency = 0.1 Hz)

The system's response throughout the temperature range shows a modulus whose magnitude is equivalent to that of the stress relaxation tests of monolithic steel specimens. From this we can also conclude that the system response is insensitive to the adhesive layer properties in this temperature range. Since the system's response remains relatively constant throughout the temperature range, we can also conclude that the adhesive's glass transition temperature is above 110°C, which agrees with the adhesive's recommended maximum operating temperature of 177°C [81].

Thirty minute stress relaxation tests were then performed on steel/EA9392/steel specimens in 10°C increments from 30°C to 110°C. The results in *Figure 5.3* show a near constant modulus throughout the temperature range with no time effects. As the system modulus is once again consistent with that obtained for monolithic steel specimens, these tests confirm that under these conditions, the adhesive layer does not have a marked effect on the system results.
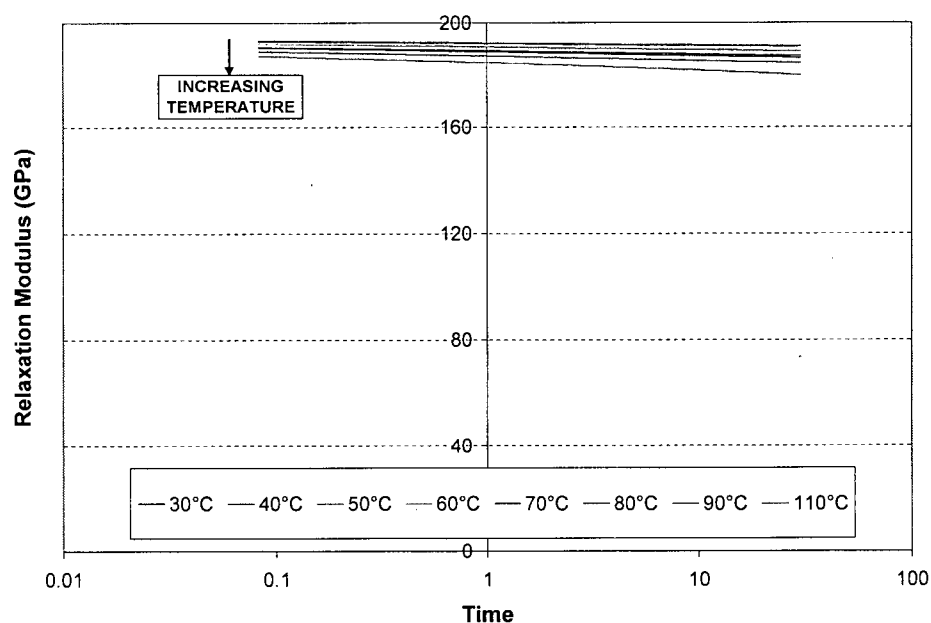

Figure 5.3 - Steel/EA9392/Steel Average System Relaxation Modulus

5.1.2   Bimaterial beam stress relaxation results

In order to validate the bimaterial beam technique for the characterization of the time-dependent properties of a viscoelastic material, three sets of tests were performed. First, 30 minute stress relaxation tests on monolithic steel and Lexan specimens were performed in 10 °C increments from 30 °C to 110 °C. Averaged results for steel were previously shown in *Figure 5.1*, and the averaged results for Lexan are shown in *Figure 5.4*. While the results for steel show insensitivity to both temperature and time, Lexan results show the classic viscoelastic response, where the modulus decays with time and the rate of decay accelerates as the temperature is increased. Bimaterial specimens consisting of steel, Hysol EA9392 adhesive, and Lexan were then prepared and similar stress relaxation tests were performed. The system response, shown in *Figure 5.5*, also shows a viscoelastic response. The viscoelastic properties of Lexan were then determined from the system response using *Equations (26)-(28)* and are shown in *Figure 5.6*.
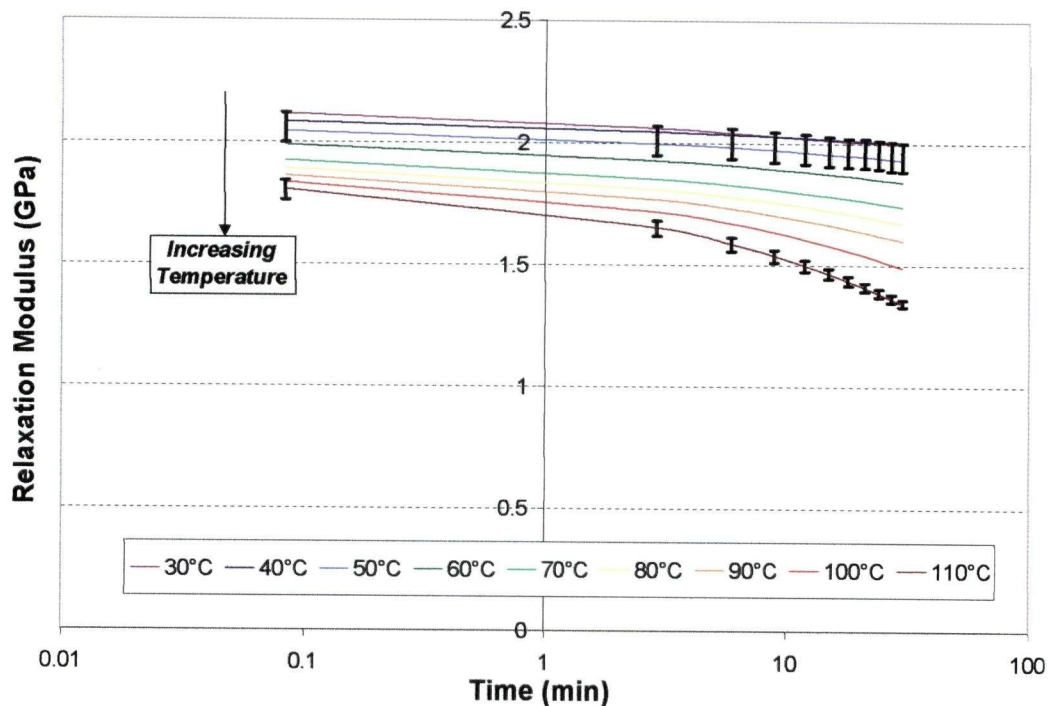

Figure 5.4 - Lexan Specimens - Average Relaxation Modulus
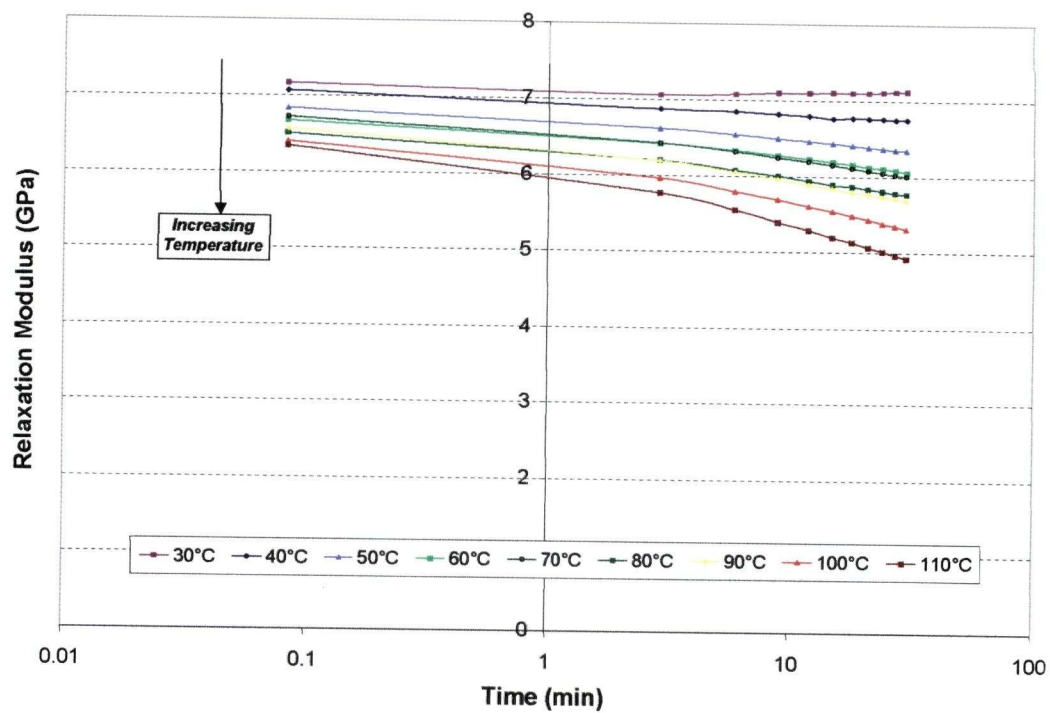
(based on 3 tests)

Figure 5.5 - Steel/EA9392/Lexan Specimens - Average *System* Relaxation Modulus
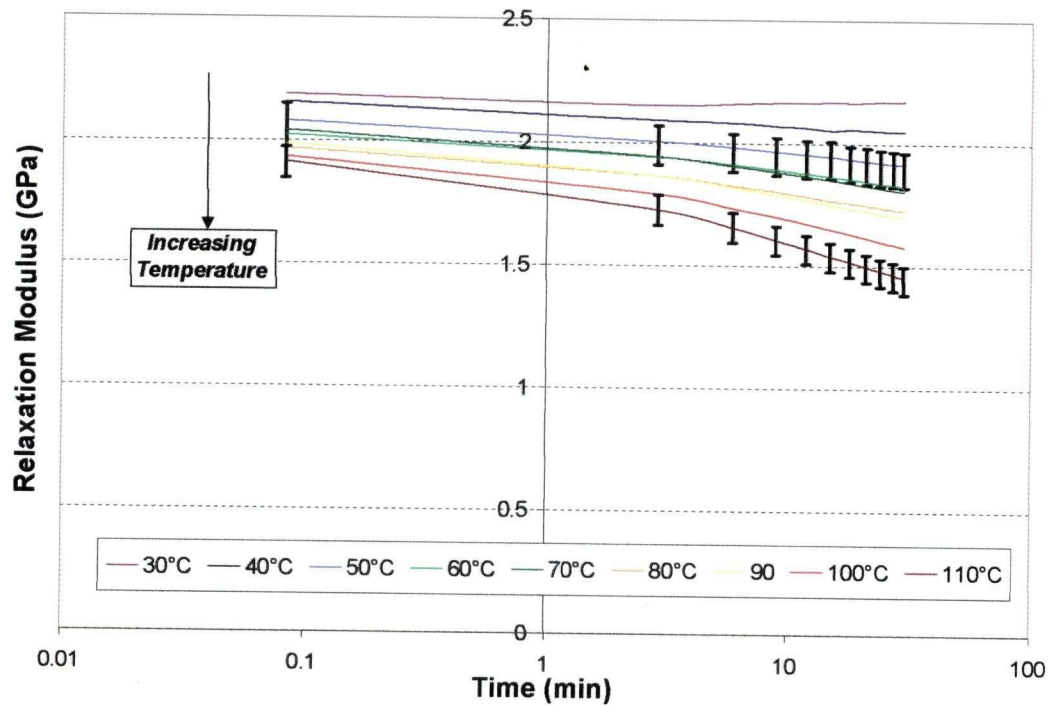
(based on 3 tests)

Figure 5.6 - Steel/EA9392/Lexan Specimens - Average *Lexan* Relaxation Modulus

(based on 3 test)

Table 5.1 –Stress relaxation of Lexan – monolithic versus system response

TIME (min)	Lexan Modulus (GPa)								
	50°C			**80°C**			**110°C**		
	Monolithic	System	%	Monolithic	System	%	Monolithic	System	%
0.08	2.04	2.08	*1.77*	1.93	2.01	*4.15*	1.81	1.92	*5.98*
2.91	2.00	2.01	*0.54*	1.85	1.94	*4.97*	1.65	1.73	*4.47*
5.91	1.98	1.98	*0.02*	1.83	1.91	*4.35*	1.59	1.65	*4.32*
8.91	1.97	1.97	*0.26*	1.81	1.88	*4.08*	1.54	1.60	*4.26*
11.91	1.96	1.95	*0.44*	1.79	1.87	*4.09*	1.50	1.57	*4.77*
14.91	1.96	1.95	*0.45*	1.78	1.85	*3.83*	1.47	1.54	*5.07*
17.91	1.95	1.94	*0.68*	1.77	1.84	*3.84*	1.43	1.52	*5.88*
20.91	1.95	1.93	*0.83*	1.76	1.83	*3.70*	1.41	1.50	*6.42*
23.91	1.94	1.92	*0.93*	1.75	1.82	*3.77*	1.38	1.48	*7.16*
26.91	1.94	1.92	*0.83*	1.75	1.81	*3.69*	1.36	1.47	*7.73*
29.91	1.93	1.92	*0.86*	1.74	1.81	*3.86*	1.34	1.45	*8.43*

From the data presented in *Table 5.1*, we see good correlation between the stress relaxation data for the monolithic Lexan specimen (*Figure 5.4*) and the reduced data for Lexan when tested bonded to the steel substrate (*Figure 5.6*). Error bars for both the monolithic Lexan and the reduced Lexan data from the bi-material system were included in the figures for data at 50°C and for 110°C. The data shows a scatter of less than ±5%. The error bars are representative of the scatter seen at all temperatures. An anomaly appears at the lowest test temperature (30°C) for the system response, where the modulus is seen to increase slightly with time. No explanation for this is given, however we note that this increase represents less than a 1% increase over the minimum modulus value for this temperature.

5.1.3   Sources of error

The major source of error in this experiment is machine compliance. Although many newer DMA models (such as the TA DMA Q800) include a machine compliance calibration, the calibration procedure used for the RSI DMTA V does not include a calibration to determine

the stiffness of the fixtures. Thus the force/displacement data collected by the DMA is result of a fixture response superposed on the specimen response. No attempt was made to characterize the stiffness response of the fixtures.

A second source of error is the unknown initial state of the material. The Lexan specimens were not pre-conditioned and so any residual stresses present in the specimen before testing may affect the relaxation response slightly and may account for some of the observed variability.

5.2 Modulus Development

5.2.1 FM300 Modulus Development

The bimaterial beam method can be used to explore the relationship between the development of mechanical properties and the advancement of chemical cure. The development of the system storage modulus of a bimaterial beam specimen is monitored as samples are cured with a series of different temperature cycles. The modulus of the curing resin layer can then be extracted from the system response using the bimaterial beam analysis presented in *Section 3.5*.

Results obtained with this method, while agreeing qualitatively with expected trends, did not correspond quantitatively to values in the literature. Cytec lists the room temperature shear modulus of FM300 as 908 MPa [83]. Using Hooke's law for an isotropic material, *Equation (36)* with a Poisson's ratio of 0.4 yields an unrelaxed modulus of 2.54GPa. LaPlante and Lee-Sullivan [84], investigating fully cured neat FM300 adhesive specimens, found the unrelaxed modulus, E_u, to be 2.69 GPa and the fully relaxed modulus, E_∞, to be 18 kPa. Experimentally determined values for the unrelaxed modulus in the current study were, however, found to be nearly twice the value quoted in the literature. This is believed to be an experimental artefact, as the experimental method offers no means of controlling the thickness of the resin layer, to which the calculation of the modulus is very sensitive. The experimentally determined instantaneous modulus, E_{uncal}, was thus calibrated by scaling the

experimentally determined moduli between the known limits. The experimental unrelaxed modulus, E_{max}, was defined as the maximum E_{uncal} and the experimental fully relaxed modulus, $E_{\alpha=0.5}$, was defined as E_{uncal} at gelation (degree of cure of 0.5). The calibrated instantaneous modulus, E_{cal}, was then found as

$$E_{cal} = E_\infty + \left(E_u - E_\infty\right)\frac{\left(E_{\alpha=0.5} - E_{uncal}\right)}{E_{\alpha=0.5} - E_{max}} \tag{68}$$

Figure 5.7 shows representative results for a cure cycle of 160°C for 127 minutes. The cure cycle temperature, system storage modulus, uncalibrated and calibrated resin modulus are shown.
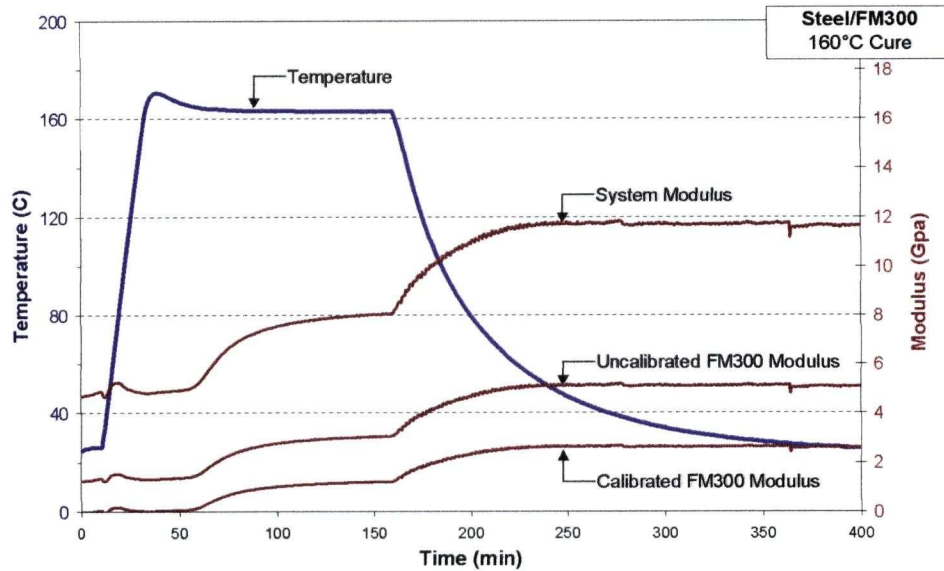

Figure 5.7 - Typical Modulus development as a function of time

Simultaneously, using the cure kinetics model of *section 3.3* and the glass transition temperature model of *section 3.4*, the development of glass transition temperature through the same temperature cycle can be calculated. *Figure 5.8* shows the development of glass transition temperature for the same 160°C cycle.
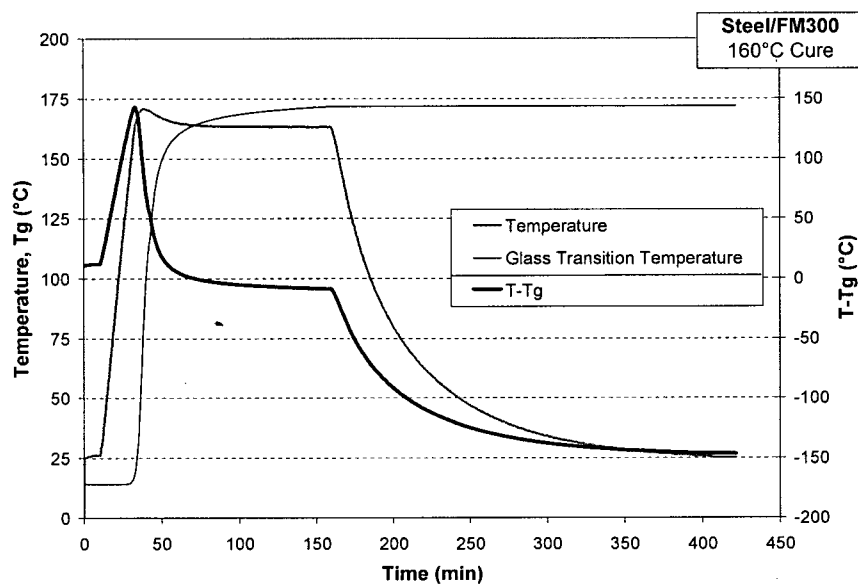
Figure 5.8 - Typical Tg development versus time

As both modulus and glass transition temperatures are functions of the cure cycle, the resin's modulus can then be plotted against $T - T_g$. *Figure 5.9* shows a typical resin instantaneous modulus versus $T - T_g$ curve for the 160°C cycle.
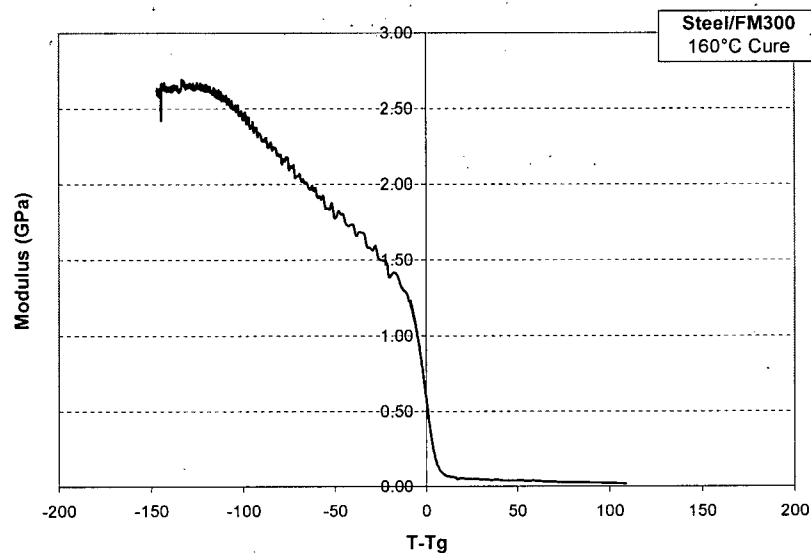

Figure 5.9 - Typical FM300 modulus versus T-Tg

The results of a series of cure cycles can then be plotted on the same graph. *Figure 5.10* shows results obtained for the adhesive FM300. All four cycles studied show a similar response. For the purposes of this analysis, all data collected pre-gelation is ignored and is not shown in the graphs. In the pre-gelation regime, the resin's viscosity drops and the resin may flow. As this method offers no dimensional control, any data collected in this regime is unreliable due to variations in the system's geometry.
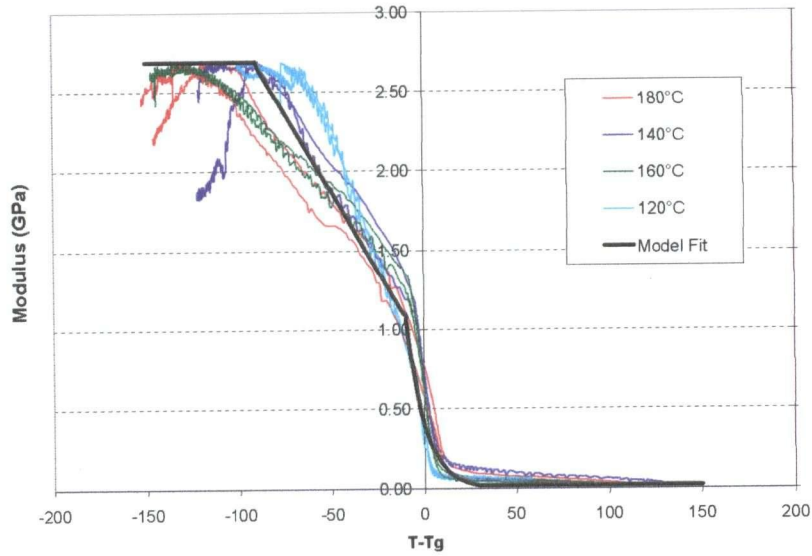

Figure 5.10 - Modulus versus T-Tg for FM300

Superimposed over the test data, *Figure 5.10* also shows the modulus model for FM300 as presented in *Section 3.5*. The model constants of *Equation (35)*, which were selected to provide a best fit to the experimental data, are summarized in *Table 5.2*.

Table 5.2 - Modulus model constants

$T_{c1} = 30\,°C$	$T_{c2} = -10\,°C$	$T_{c3} = -90\,°C$
$E_{c1} = 0.02\,GPa$	$E_{c2} = 1.1\,GPa$	$E_{c3} = 2.69\,GPa$
$\alpha_{gel} = 0.5$	$A^* = 0.40393\,GPa$	$K^* = -0.10018\,°C$

5.2.2   Sources of Error

The major source of error in this test methodology relates to dimensional stability. Initially the adhesive is uncured and very soft, and accurate pre-test measurement of the thickness is not feasible. During the experiment, the adhesive is unconstrained and changes to the thickness may occur. As the neat adhesive cures and the viscosity drops, the adhesive may flow causing an uneven, cratered surface, as seen in *Figure 5.11*, which shows a typical specimen post-test. Since vacuum bagging cannot be used in this method, out gassing adds to the creation of a pockmarked, uneven surface. In an effort to reduce flow, half the specimens were tested without removing the peel-ply. Visual inspection shows that while this attempt did improve the surface, experimental results were comparable to specimens that were tested without the peel ply.
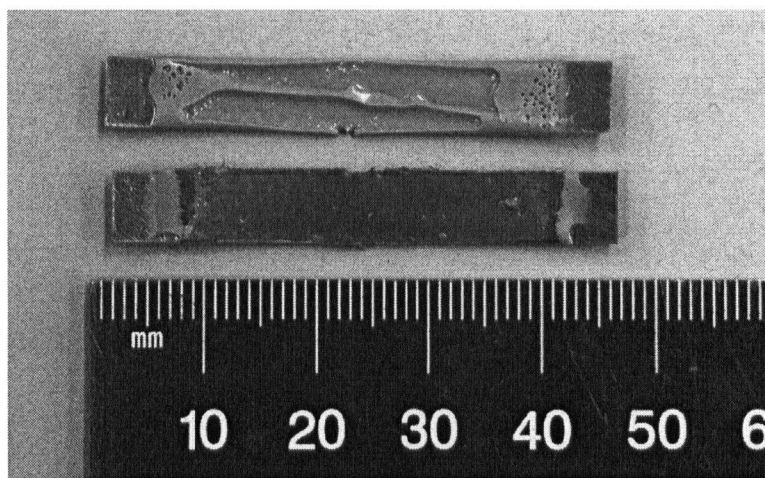

Figure 5.11 – Modulus development specimens – with and without peel-ply

Another thickness related issue is that the model does not take cure shrinkage into account, nor does it incorporate thermal expansion. As neat resins have relatively high coefficients of thermal expansion and may shrink by as much as 2-6% during cure [57,64,69] these phenomena may have an effect on the results.

These errors justify the need to calibrate the modulus values between known relaxed and unrelaxed moduli from monolithic resin specimens, which can be determined with much better accuracy.

5.3   Bonded Composite Patch Repair

5.3.1   Presentation of Results

Throughout this work, results from representative cycles of bonded composite patch repair specimens cured under a variety of cure cycles are presented. Results show experimental deflections, model predictions and the difference between them. The development of glass transition temperature and the instantaneous shear modulus are also shown, to aid in obtaining a better understanding of the factors that affect the development of thermal residual stresses and warpage.

Although results of thermal residual deflection tests can be displayed in the classical time domain, a number of important phenomena are more apparent when viewed in the temperature domain. Firstly, the temperature domain linearizes temperature ramps, eliminating artefacts in the time domain response caused by loose control of ramp rates, overshoots, etc. Thus it allows one to easily distinguish between linear elastic and non-linear elastic temperature-deflection response. Second, the temperature domain contracts temperature dwells, magnifying phenomena occurring at a constant temperature; Phenomena such as creep and relaxation are displayed as vertical lines occurring at a constant temperature instead of slow drifts. Throughout this chapter, results are presented in both the time and temperature domain.

Figure 5.12 shows a representative profile for a one-step cycle in the time domain, while *Figure 5.13* shows the profile in the temperature domain. A number of characteristic features can be observed. First, during heat up to the first hold, no warpage is measured. This is expected, as during this stage, the adhesive is uncured and the system is uncoupled. Second, during the first isothermal hold, no response is noted; the system is held isothermally and no stresses have been introduced. Third, during cool down, the resulting warpage for non-linear elastic materials differs from that of linear elastic materials. While linear elastic materials show warpage that is linearly proportional to the change in temperature, non-linear elastic materials may show different results.
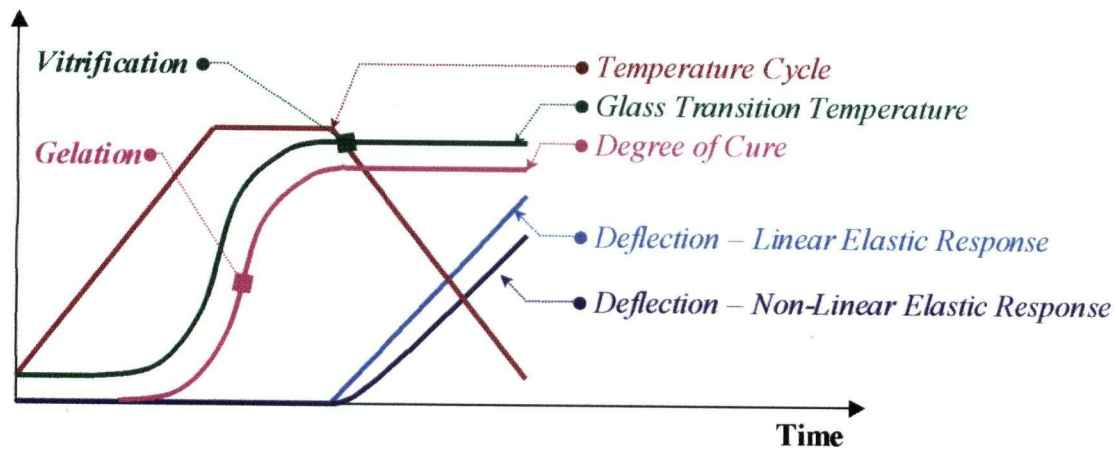
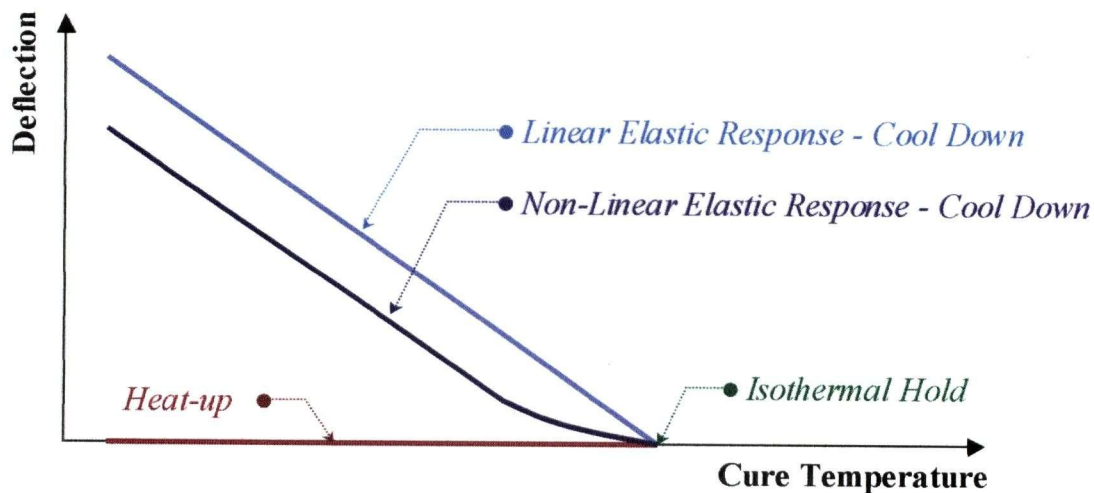**Figure 5.12 - Characteristic time domain 1-step cure cycle response**

Figure 5.13 - Characteristic temperature domain 1-step cure cycle response

Two-step cycles show distinctly different characteristics, as shown in *Figure 5.14* (time domain) and *Figure 5.15* (temperature domain).   The response during the ramp to the first hold and during the first hold is similar to that of the one-step cycles. During the second heat up, linear elastic and non-linear elastic materials once again show differing responses. Elastic materials show a "negative" warpage that is linearly proportional to the change in temperature. They show no response during the second hold and then follow the same slope during cool down in the "positive" warpage direction until the specimen has cooled to room temperature.

Non-linear elastic materials, on the other hand, show a more complex response. Although during heat up to the second hold they also exhibit a "negative" warpage that increases with temperature, the magnitude of the warpage may be less than that of a linear elastic material due to thermal softening. Proper characterization of the material's intrinsic properties (degree of cure, glass transition temperature, etc.) in this region is vital to accurately capture the response of the specimens. The development of T_g up to this point is limited by the temperature of the first hold, which retards the cure process due to diffusion. This region thus corresponds to a state where the material's behaviour is highly dependant on these properties.

During the second temperature hold no change in deflection is seen. Finally, during cool-down, the system exhibits behaviour similar to that seen in the one-step cycles.
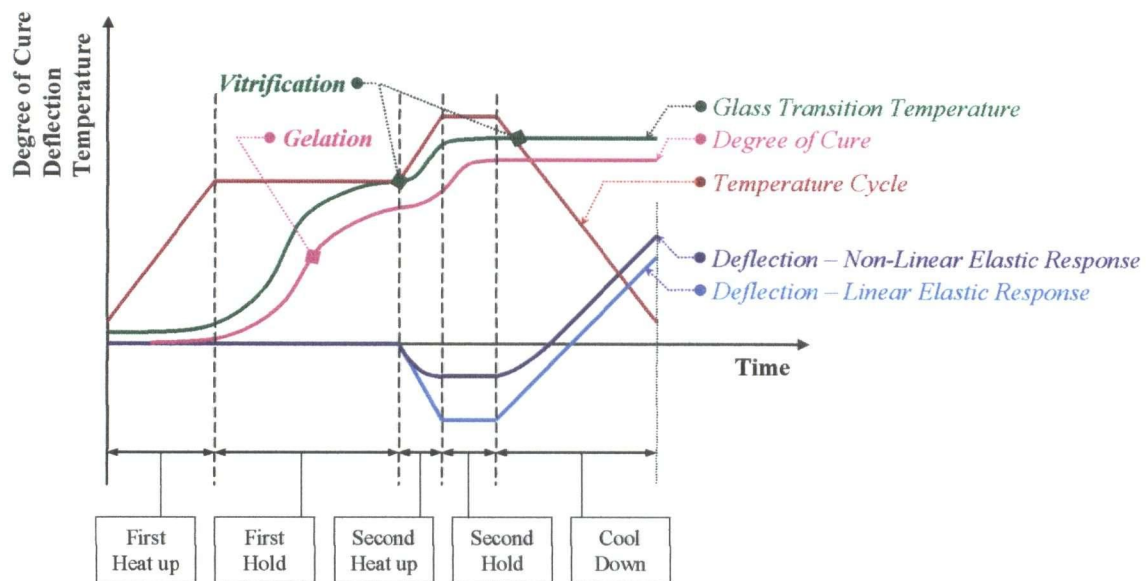

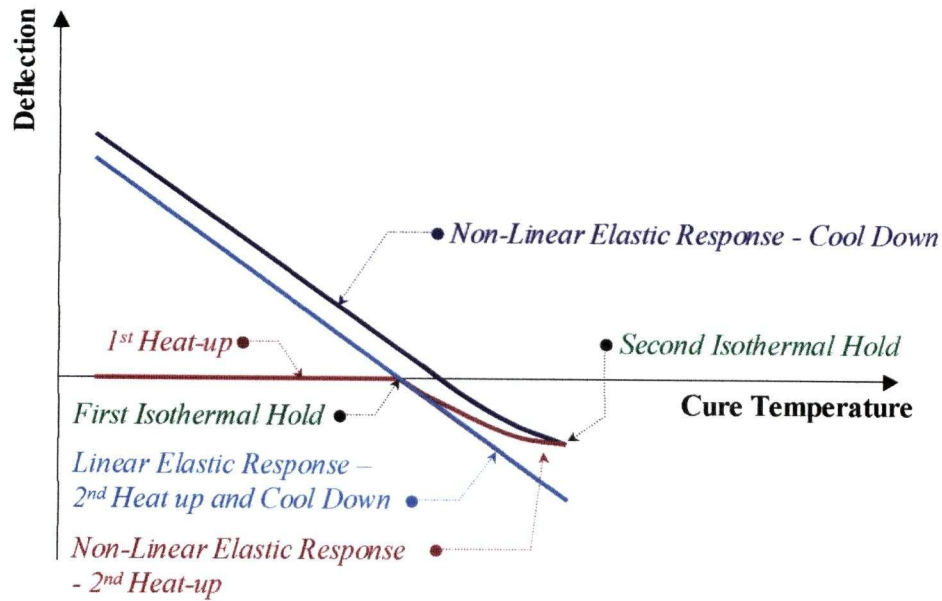**Figure 5.14 - Characteristic time domain 2-step cure cycle response**

Figure 5.15 – Characteristic temperature domain 2-step cure cycle response

5.3.2   Model Implementation

Material Constants

The material constants for the patch and substrate where taken from the literature, as no characterization tests were performed. A modulus of 200 GPa and a coefficient of thermal expansion of 11-17 $\mu\varepsilon$/°C are listed for the steel substrate [4], while a modulus of 140 GPa and a coefficient of thermal expansion of –0.5 $\mu\varepsilon$/°C are listed for the AS4/3501-6 patch in the 0° direction [85]. Characterization tests were performed on the adhesive to determine its instantaneous modulus and the results are presented in *section 5.2*. The modulus is shown to be a function of the adhesive's instantaneous temperature and glass transition temperature.

Geometry

The specimen length of 40 mm is based on the manufacturer specified distance between the supports of the three-point bend fixture used in the experimental technique. The patch and substrate thicknesses are measured before the specimen is assembled. The adhesive thickness

is determined as the difference between the total specimen thickness (as measured post-test) and the sum of the patch and substrate thicknesses. A slight non-uniform thickness was found, with the adhesive layer being thicker at the ends and thinner in the middle of the specimen. The adhesive layer thickness used in the model was thus taken to be slightly less than the average thickness, as the deflection is a strong function of the thickness and the average is not a true representation of the specimen thickness.

Warpage Prediction

Using the DAQ temperature profile, the cure cycle is stepped through using a spreadsheet application and an associated macro language. For each time-step, the degree of cure is calculated using the cure kinetics model of Rogers and Lee-Sullivan presented in *section 3.3*. The glass transition temperature is then calculated using the glass transition temperature development model presented in *section 3.4*. The instantaneous modulus can then be determined using the temperature and glass transition temperature corresponding to that time-step and the modulus development model presented in *section 3.5*.

The warpage model presented in *section 3.6* is used to predict the out of plane deflection of the bonded composite patch repair specimens. The deflection is assumed to be zero until the end of the first temperature hold: during the ramp to the first temperature hold the adhesive is a viscous liquid that cannot develop stresses and during the first isothermal hold no thermally induced effects occur. As the cycle progresses, the adhesive's instantaneous modulus is compared to that of the previous time-step. If the modulus has dropped, then thermal softening is assumed to have occurred. *Equation (46)* is then used to predict the warpage at that time-step. Since the modulus history of the specimen is known, $\frac{\partial (G_a)}{\partial (T-T_g)} d(T-T_g)$ is treated as $\Delta G_a = (G_a)_i - (G_a)_{i-1}$. If the modulus increases or remains the same, thermal softening does not occur, *Equation (46)* simplifies to *Equation (45)*, and basic CHILE is used to predict the warpage at that time-step.

Two model calibrations were performed due to some uncertainty in the model input. First, coefficients of thermal expansion were chosen that matched the experimentally determined

slope of deflection versus temperature during cool down. This resulted in the selection of a ΔCTE of 15 ± 1 µε/°C, which agrees well with literature values for the coefficient of thermal expansion of steel and AS4/3501-6. Second, the average adhesive layer thickness was reduced by 10% to account for the non-uniform adhesive layer exhibited by the specimens (thinner at the middle of the specimen and thicker at the ends). While this allowed for better predictions of the experimental deflections during post-cure or at the second hold temperature, it did not have a considerable effect on final deflections. The sensitivity of the model to adhesive layer thickness is discussed further in *section 5.8.1*.

5.3.3   One-step cycle

The first method of cure cycle optimization investigated was reduction of the cure temperature. Three one-step cycles were examined (177°C, 150°C, and 120°C) as summarized in *Table 5.3*. The 177°C cycle is used as the baseline, standard cycle for warpage comparisons.

Table 5.3 - One-step cure cycles

Description	Cycle			
	Temp (°C)	Dwell Time (min)	Heating Rate (°C/min)	Cooling Rate (°C/min)
[1] 1 step - 177°C	177	60	2.50	2.50
[2] 1 step - 150°C	150	160	2.50	2.50
[3] 1 step - 120°C	120	480	2.50	2.50

The results of a representative 177°C cycle are shown in *Figure 5.16* (in the time domain) and *Figure 5.17* (in the temperature domain). The time domain graph shows the cure cycle temperature, the deflection measured by the DMA, the predicted degree of cure, and the predicted glass transition temperature. The temperature domain graph shows the deflection measured by the DMA, the degree of cure, and the glass transition temperature.
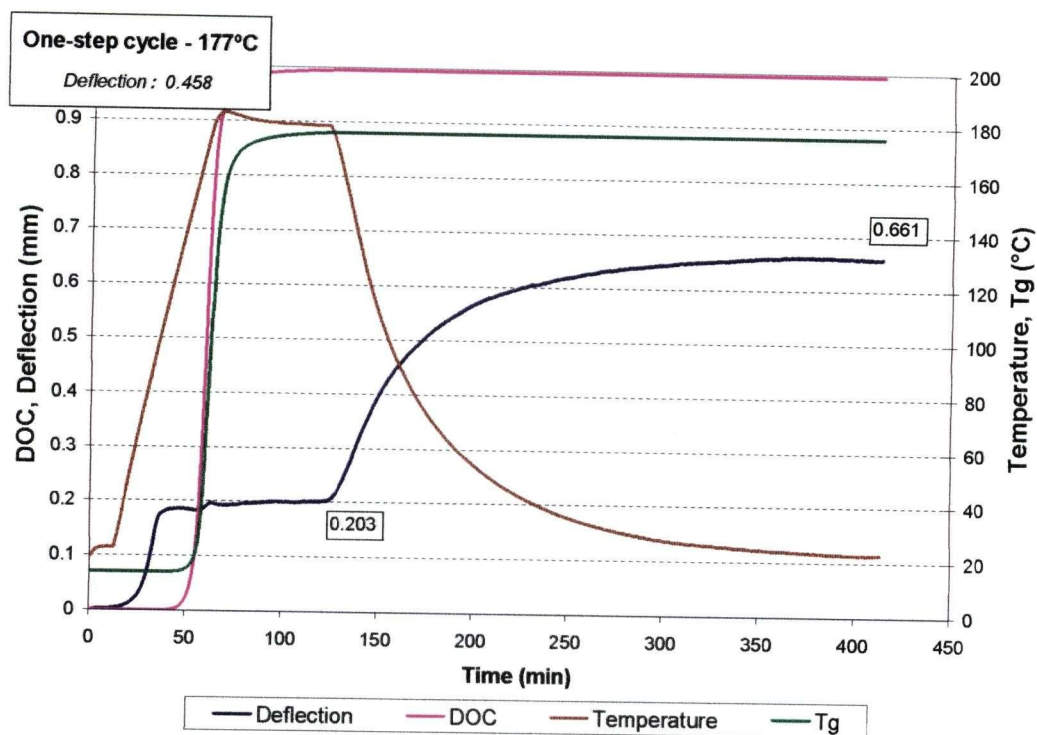
Figure 5.16 - Representative time domain experimental results for one-step cycles
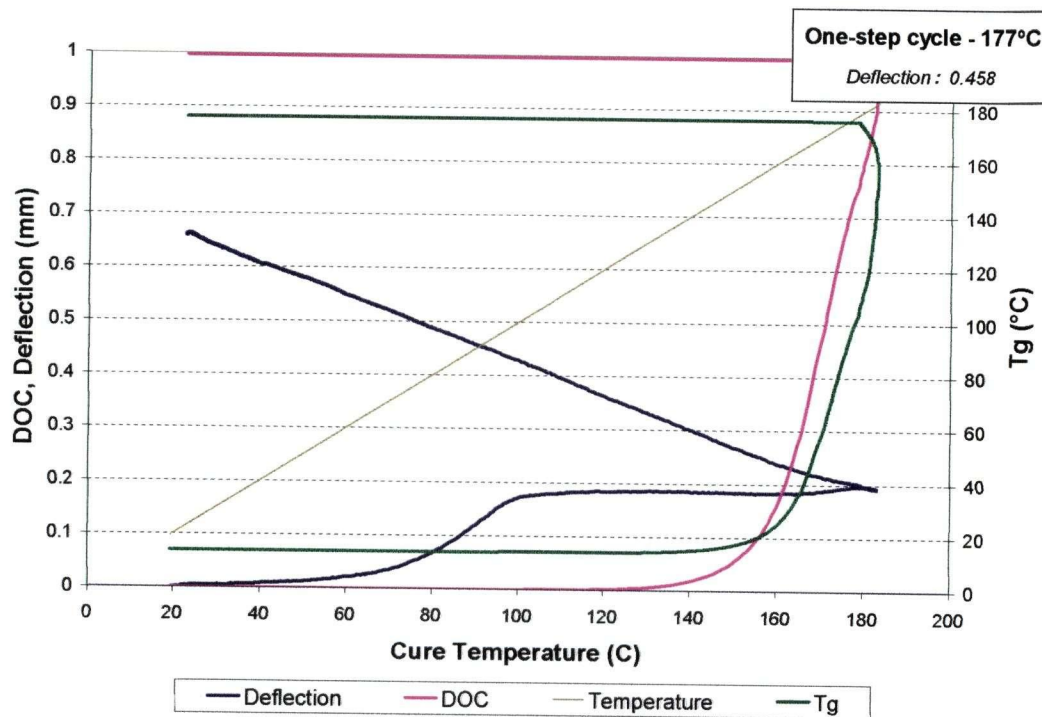

Figure 5.17 - Representative temperature domain experimental results for one-step cycles

These graphs illustrate a number of important observations. First, an initial deflection is observed during heat up with a magnitude of approximately 0.20 mm. Post-test thickness measurements show a reduction in the adhesive layer thickness of approximately the same magnitude. Post-test visual inspections of the test specimens shows that some of the adhesive squeezed out of the samples during the test, as can be seen in *Figure 5.18*. The initial displacement of the load head is thus assumed to be due to a thinning of the adhesive layer caused by an initial drop in the adhesive's viscosity during heat-up. As this initial displacement is an experimental artefact due to the sample size and geometry, the deflections are zeroed at the end of the first hold. The zeroed results for this cycle, along with the model deflections and the difference between the experimental and model deflection, are shown again in *Figure 5.19* (in the time domain) and *Figure 5.20* (in the temperature domain). Second, the deflection increases monotonically with temperature drop during cool-down. When viewed in the temperature domain, a linear relationship between deflection and temperature is easily observed at low temperatures, while a slightly non-linear relationship is seen at high temperatures.
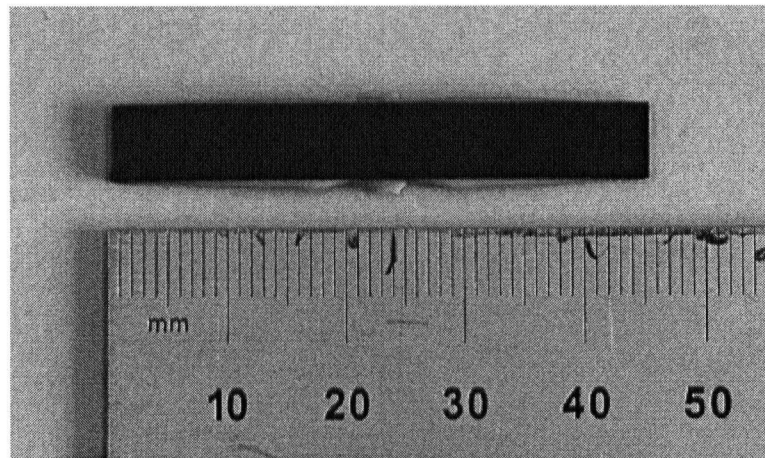

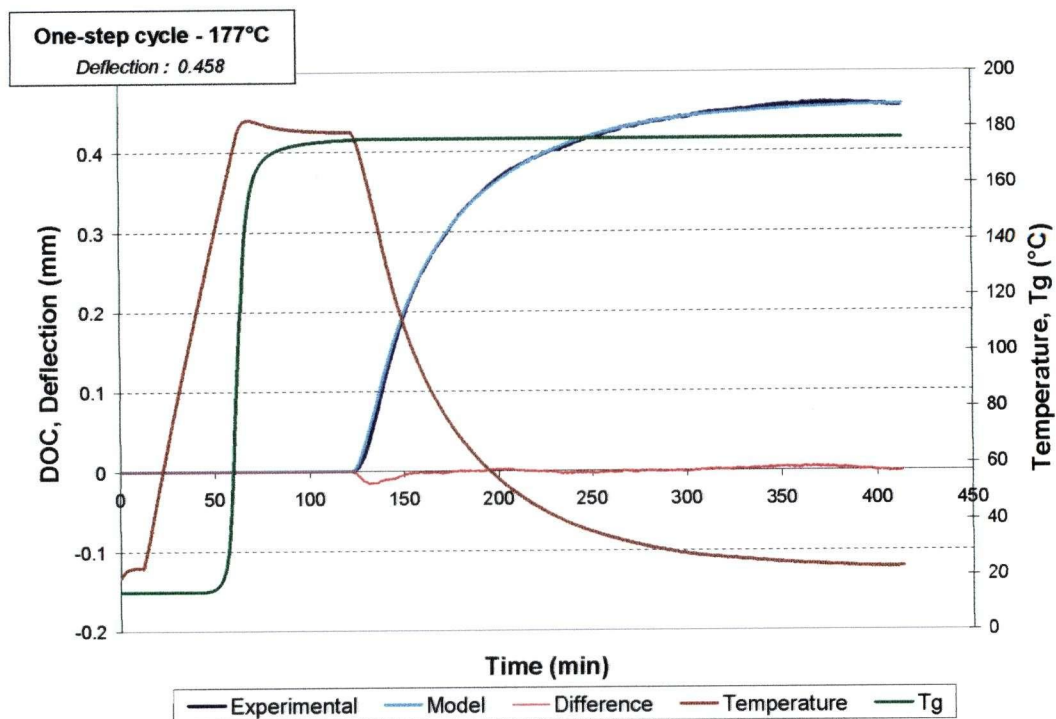**Figure 5.18 - Bonded composite patch repair specimen - post-cure, showing adhesive layer squeeze out**

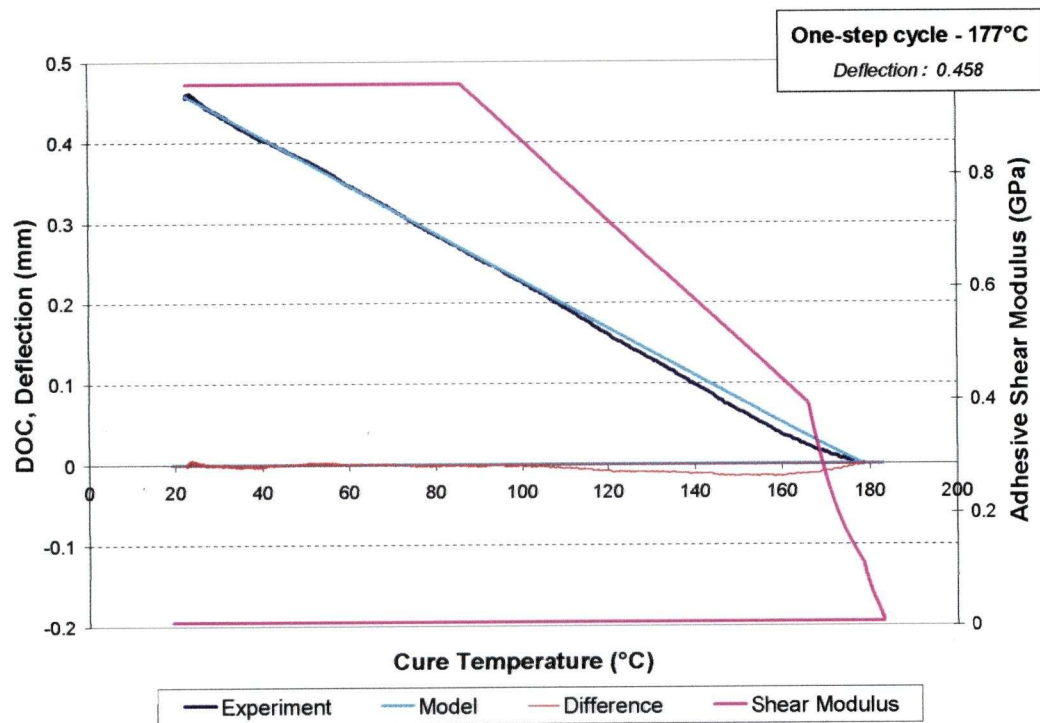**Figure 5.19 - Representative time domain results for one-step cycles**

Figure 5.20 - Representative temperature domain results for one-step cycles

The results for the one-step cure cycles examined are listed in *Table 5.4*. For each specimen, the experimental deflection at the end of the cycle, the model deflection at the end of the cycle, the relative difference, and the degree of cure as predicted by the model are listed. The deflections and degrees of cure are then averaged for all specimens cured using the same cycle. The standard deviations are also shown for deflection values. Results show very good agreement between experiments and the model.

The experimental deflection results are also shown graphically in *Figure 5.21*, along with the calculated degrees of cure. Results show that a considerable reduction in deflection can be achieved by curing at a lower temperature, however this results in a lower final degree of cure. As mechanical properties at elevated temperatures have been shown to be directly affected by degree of cure, the drop in degree of cure is unacceptable for most applications. This illustrates the competing requirements placed on an optimized cure cycle: reduce the final thermally induced stresses, but ensure complete cure. This trend is consistent with that found by Cho and Sun [5] and Djokic *et al.* for FM73 and FM300 [17,72].

Table 5.4 - Experimental Results - One-step cure cycles

| Cycle	Deflection			Model DOC
	Experiment (mm)	Model (mm)	Difference (%)	
[1] 1 step - 177°C *(a)*	0.458	0.458	0.13	0.996
(b)	0.502	0.510	-1.53	0.998
(c)	0.486	0.506	-4.20	0.997
(d)	0.469	0.480	-2.43	0.997
(e)	0.416	0.414	0.62	0.998
Average	0.466	0.473	-1.56	0.997
Standard Deviation	0.029 (6.26%)	0.035 (7.48%)	1.75	
[2] 1 step - 150°C *(a)*	0.406	0.405	0.37	0.966
[3] 1 step - 120°C *(a)*	0.335	0.337	-0.63	0.861
(b)	0.338	0.338	-0.03	0.868
Average	0.336	0.337	-0.33	0.865
Standard Deviation	0.002 (0.52%)	0.001 (0.22%)	0.30	
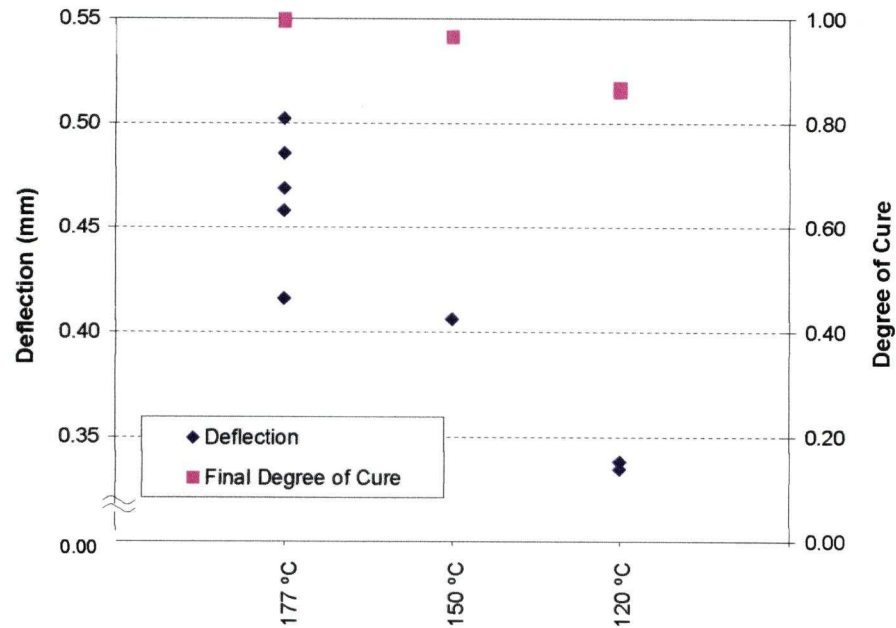
Figure 5.21 - Experimental results - One-step cycles

The scatter in the experimental data can largely be explained by variations in the actual specimen geometries. *Table 5.5* lists the geometries for the specimens used in the one-step 177°C cycles.

Table 5.5 - Specimen geometries - One-step 177 °C cycles

Cycle		Substrate (mm)	Patch (mm)	Adhesive (mm)	Total (mm)
[1] 1 step – 177°C	*(a)*	0.154	0.508	0.266	0.928
	(b)	0.155	0.526	0.192	0.873
	(c)	0.154	0.522	0.207	0.883
	(d)	0.152	0.535	0.229	0.916
	(e)	0.150	0.523	0.287	0.960

Figure 5.22 shows the deflection values, both experiment and model, for the 1 step 177°C cure cycles plotted versus adhesive layer thickness. Using the geometry and the cure temperature history of the 1 step – 177°C (d) specimen, the model was run with adhesive layer thickness of 0.200, 0.225, 0.250, 0.275, and 0.300 mm. These results are also plotted in

Figure 5.22 to show the effect of the adhesive layer thickness. All the experimentally determined deflection for this cycle fall very close to this line, highlighting the sensitivity of the experiment to the adhesive layer thickness. Thus the variability in measured deflection for the 1-step 177°C cured specimens, as shown in *Figure 5.21* and *Table 5.4*, is found to be due to variability in the thickness of the adhesive layer of the specimens. The model shows that the results are sensitive to the thickness of the adhesive layer and is discussed further in *section 5.8.1*.
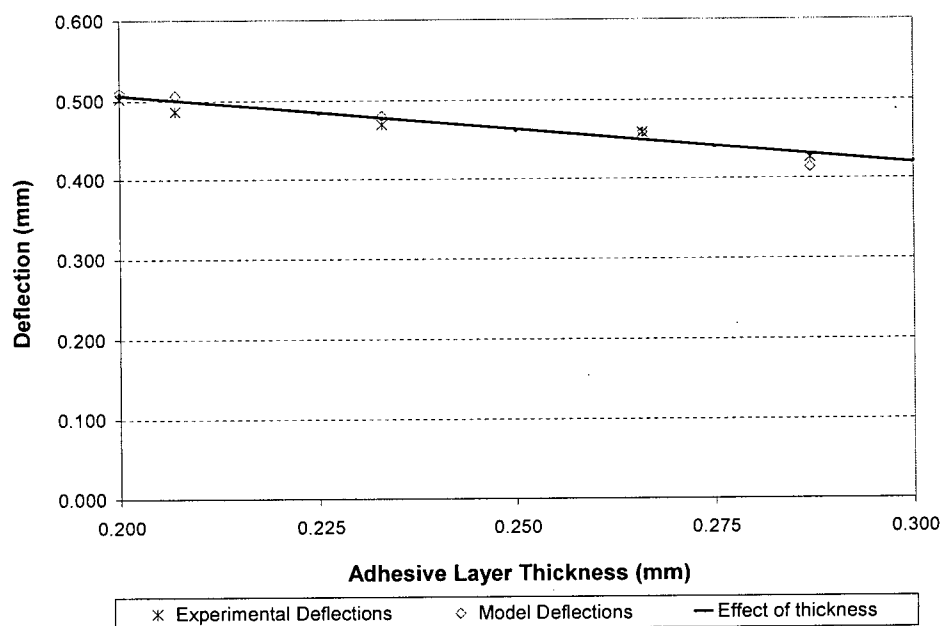

Figure 5.22 - Scaled results for 177°C cycle

5.3.4   Post-cure cycles

Post-curing following low temperature cure cycles was examined as a method of attaining complete cure while reducing the process induced residual stresses. Three post-cure cycles were studied, as summarized in *Table 5.6*. These cycles consisted of the one-step cycles previously investigated followed by a five-minute post-cure at 177 °C.

The results of a representative 120°C post-cure cycle are shown in *Figure 5.23* (in the time domain) and *Figure 5.24* (in the temperature domain). The model agrees with experimental

78

results at key points in the cycle: the end of the cool-down from the cure temperature, the end of the post cure hold, and the end of the cool-down from the post-cure temperature. In the time domain, the model results track the experimental results well. When viewed in the temperature domain, however, the model is seen to deviate from the experimental results during ramps. This is likely caused by small differences between measured temperature and actual temperature in the specimen during temperature ramps, which eventually equilibrate during holds. These types of effects are magnified in the temperature domain.

Table 5.6 - Post-cure cycles

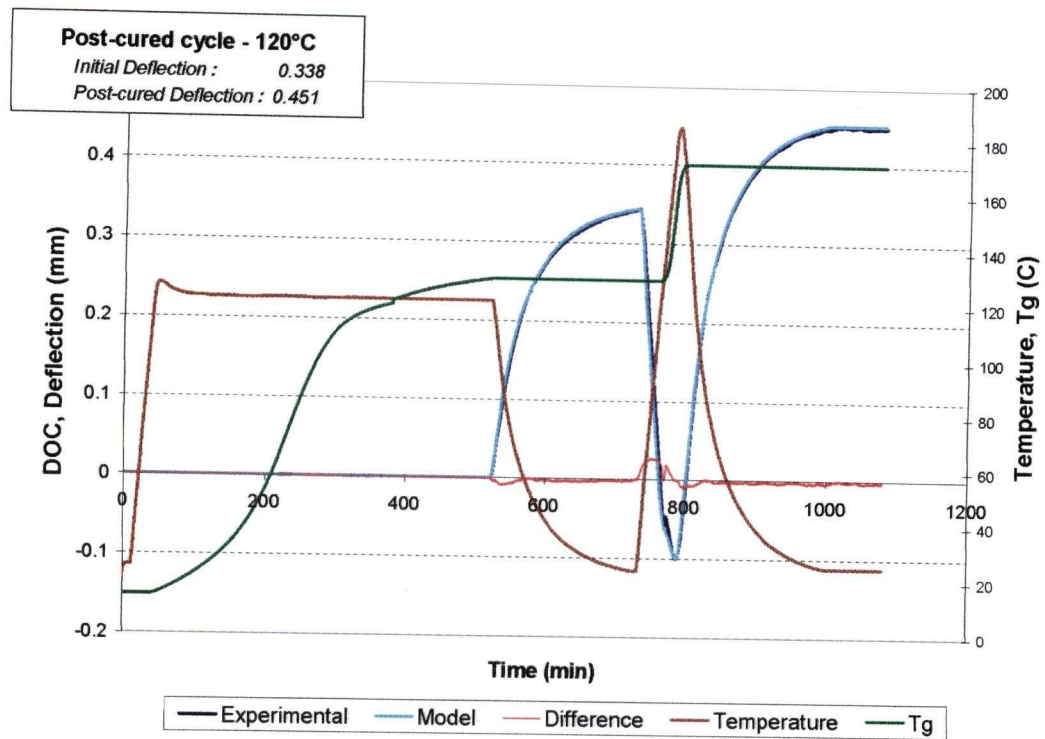| Description	Cycle			
	Temp (°C)	**Dwell Time (min)**	**Heating Rate (°C/min)**	**Cooling Rate (°C/min)**
[4] 177°C + Post Cure	177	60	2.50	2.50
	177	5	2.50	2.50
[5] 150°C + Post Cure	150	160	2.50	2.50
	177	5	2.50	2.50
[6] 120°C + Post Cure	120	480	2.50	2.50
	177	5	2.50	2.50

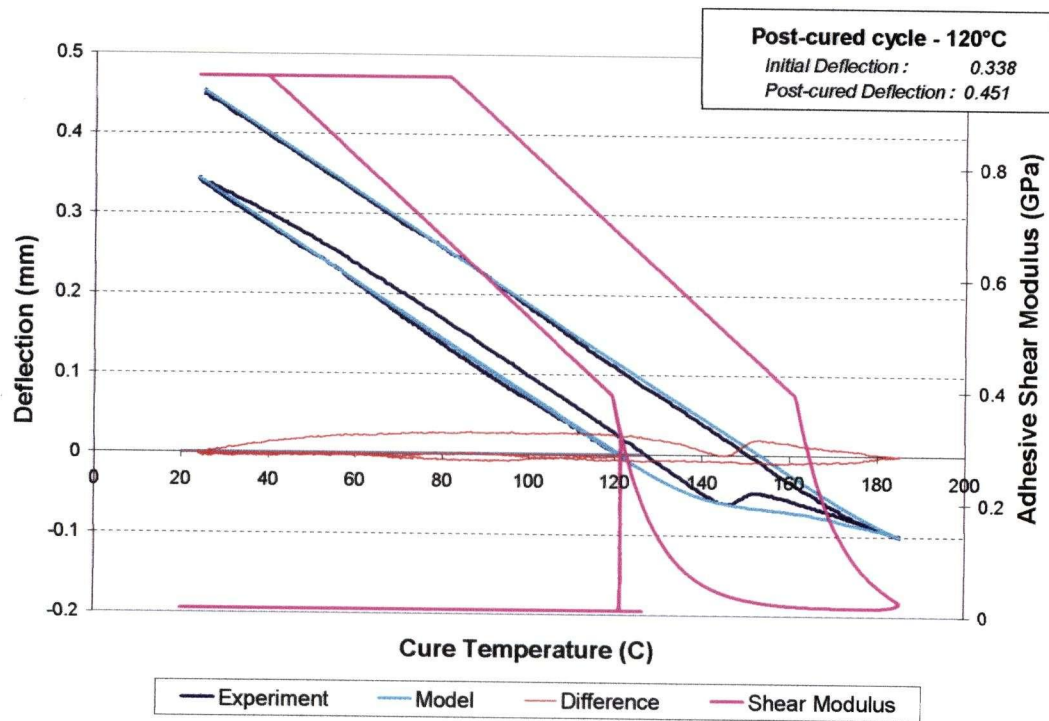**Figure 5.23 - Representative time domain results for post-cure cycles**

Figure 5.24 - Representative temperature domain results for post-cure cycles

80

The results for the post-cure cycles examined are listed in *Table 5.7*. In *Figure 5.25* the post-cure results are shown, along with the matching one-step cure cycles for comparison. These help illustrate a number of observations. Firstly, the final degree of cure is increased to near 100% by the post-cure, ensuring fully developed mechanical properties. Second, the results dispute the effectiveness of this approach. Although cure is advanced sufficiently, this is accompanied by a large increase in warpage during the cool-down from the post-cure temperature. These findings agree with those of Djokic [17]. Although the 120°C post-cured cycle seems to exhibit a larger final deflection than the 150°C post-cured cycle this is due to variability in specimen geometry, as only one specimen at each temperature was tested. Scaled results, similar to those produced for the one-step 177°C cycle, are presented in *Section 5.3.6*. Examining *Figure 5.24* for some additional insight into the results, we note that during the ramp to the post-cure temperature the adhesive's modulus drops to its minimum value and softening occurs. The softening causes a reduction in the "negative" warpage that is used to counteract the warpage generated during cool-down from the post-cure. The 177°C post-cured cycles show that post-curing does not affect the results if the adhesive is fully cured prior to the post-cure. The thermal softening model is thus shown to accurately predict the development of warpage through a cure cycle that shows considerable thermal softening.

Table 5.7 - Experimental Results - Post-cure cycles

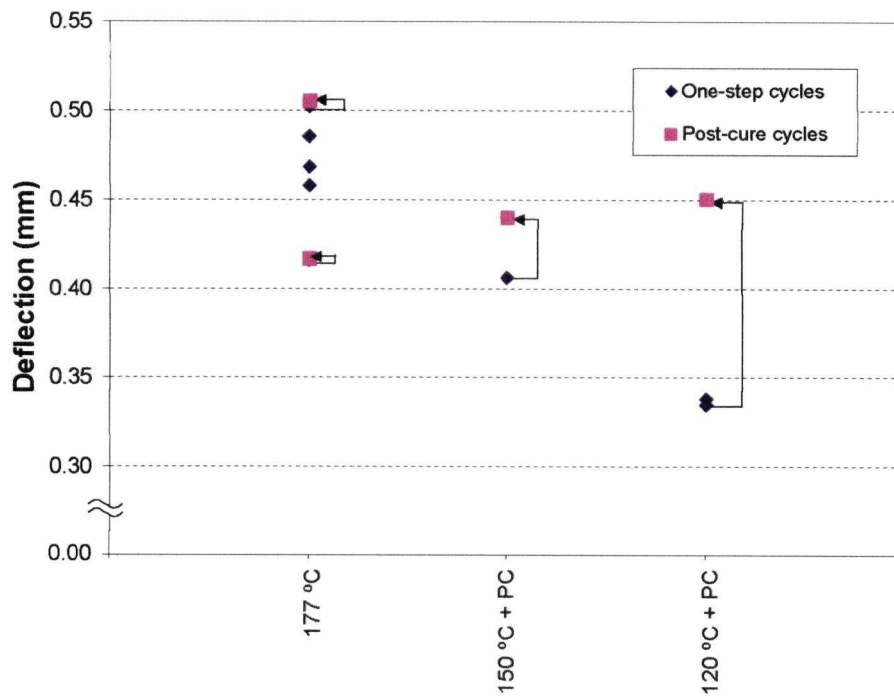| Cycle	Deflection			Model
	Experimental (mm)	Model (mm)	Difference (%)	DOC
[4] 177°C + post-cure *(a)*	0.506	0.508	-0.45	0.998
(b)	0.417	0.412	1.20	0.998
Average	0.461	0.460	0.29	0.998
Standard Deviation	0.044 (9.61%)	0.048 (10.43%)	0.83	
[5] 155°C + post-cure *(a)*	0.440	0.436	0.86	0.989
[6] 120°C + post-cure *(a)*	0.451	0.453	-0.44	0.984

Figure 5.25 - Experimental Results - post-cure cycles
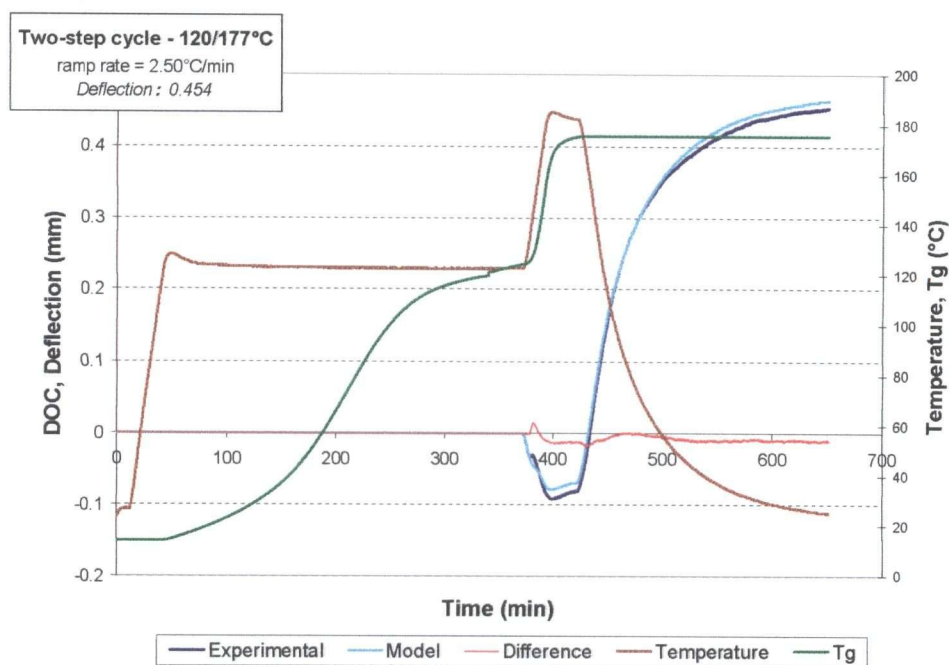
5.3.5   Two-step cycles

Another optimization method involves curing the adhesive in two steps - first at a lower cure temperature and then ramping to a higher cure temperature to complete the process. This method presupposes that if cure can be advanced sufficiently during the first hold such that an increase in modulus occurs, subsequent increases in temperature will create a "negative" thermal residual stress that will then counteract a portion of the cool-down residual stresses, effectively reducing the final warpage value. Two two-step cycles were examined, along with three ramp rates between the first and second dwell, resulting in six cycle permutations. These cycles are summarized in *Table 5.8*.

Table 5.8 - Two-step cure cycles

Description	Cycle			
	Temp (°C)	Dwell Time (min)	Heating Rate (°C/min)	Cooling Rate (°C/min)
[7] 2 step - 155°C /177°C (2.50 °C/min)	155	60	2.50	
	177	30	2.50	2.50
[8] 2 step - 120°C /177°C (2.50 °C/min)	120	330	2.50	
	177	30	2.50	2.50
[9] 2 step - 155°C /177°C (1.00 °C/min)	155	60	2.50	
	177	30	1.00	2.50
[10] 2 step - 120°C /177°C (1.00 °C/min)	120	330	2.50	
	177	30	1.00	2.50
[11] 2 step - 155°C /177°C (0.10 °C/min)	155	60	2.50	
	177	30	0.10	2.50
[12] 2 step - 120°C /177°C (0.10 °C/min)	120	330	2.50	
	177	30	0.10	2.50

The results of a representative 120/177°C cycle with a 2.5°C/min ramp rate are shown in *Figure 5.26* (in the time domain) and *Figure 5.27* (in the temperature domain). The results of a representative 120/177°C cycle with a 0.1°C/min ramp rate are shown in *Figure 5.28* (in the time domain) and *Figure 5.29* (in the temperature domain).

The model agrees well with the experimental results for two-step cycles. A small offset between the experimental and model deflection is seen at the second hold temperature, which is then carried through the final cool-down. This observation is once again more easily noticed in the temperature domain than in the time domain. The offset is likely due to inherent limitations of the modulus development model. As temperature ramps to the second hold, considerable time is spent in the region of the modulus development curve where errors in the warpage model, in terms of degree of cure, glass transition temperature, and modulus development modeling, are most likely to affect results.
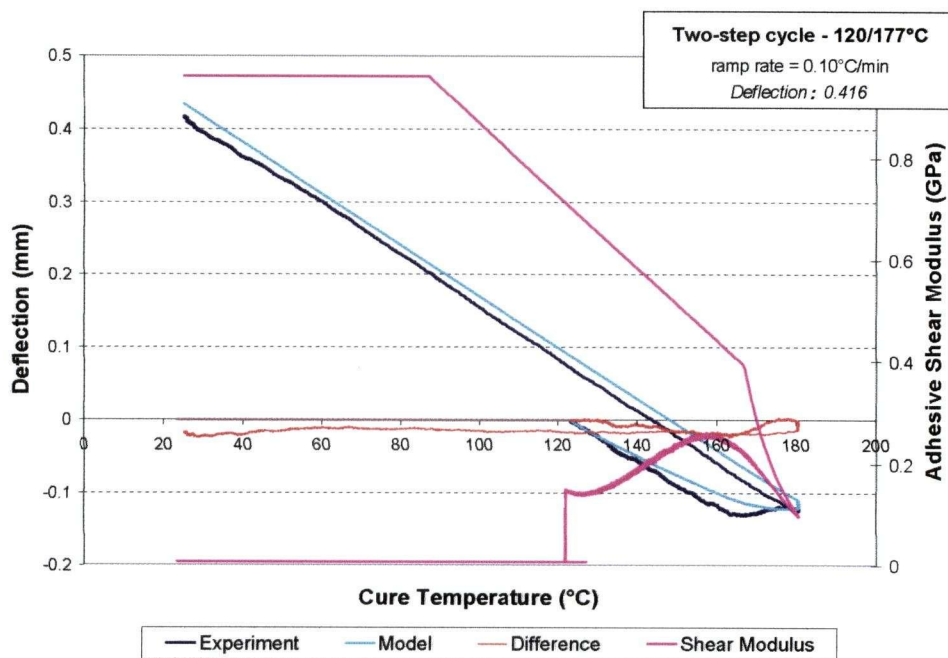
Figure 5.26 - Representative time domain results for two-step cycles

with a 2.50°C/min ramp rate
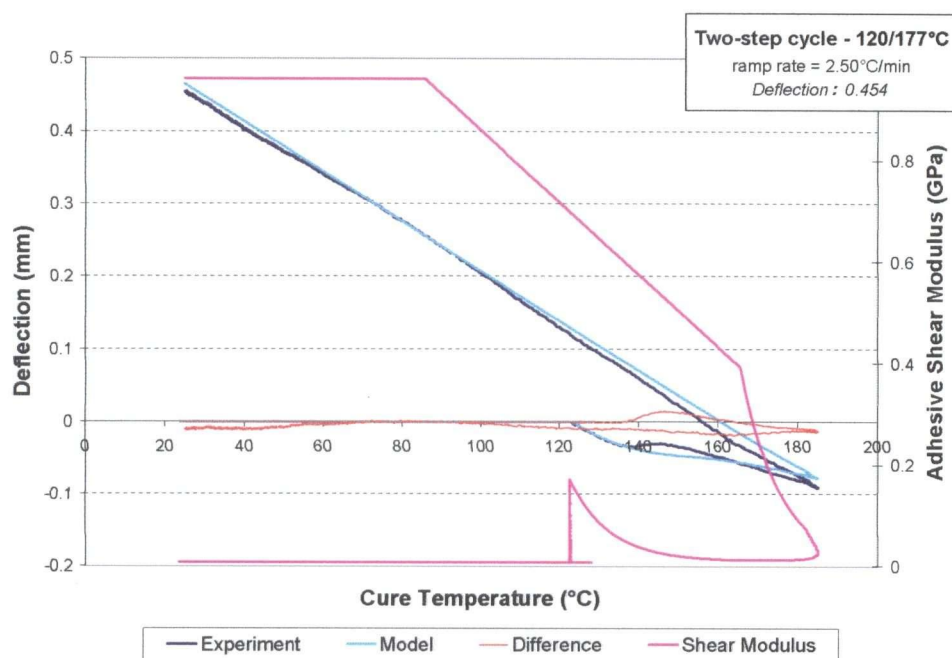
Figure 5.27 - Representative temperature domain results for two-step cycles

with a 2.50°C/min ramp rate

84
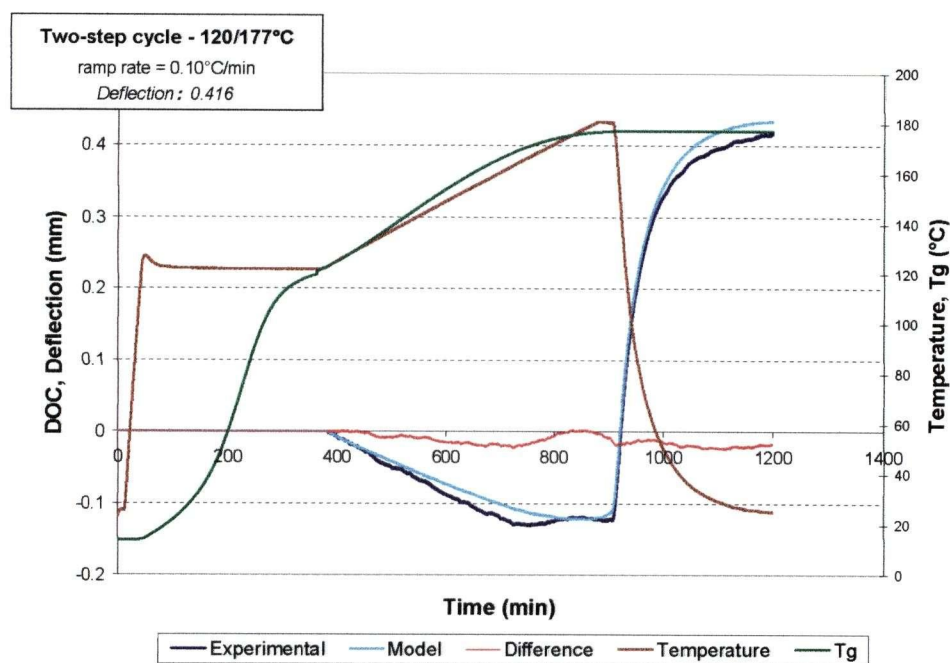
Figure 5.28 - Representative time domain results for two-step cycles

with a 0.10°C/min ramp rate

Figure 5.29 - Representative temperature domain results for two-step cycles

with a 0.10°C/min ramp rate

85

The results for the two-step cycles are listed in *Table 5.9*. In *Figure 5.30* the two-step cycle results are shown, along with the one-step 177°C cycles for comparison. Looking at the results we note a large degree of scatter. Once again, this is due to sensitivity of the results to geometry. Scaled results, similar to those produced for the one-step 177°C cycle, are presented later in *Section 5.3.6*. A slight trend to lower deflection values is evident for slow ramp rate cycles. At the fast ramp rate (2.5°C/min) the adhesive's shear modulus drops to its minimum value during the ramp to the second hold and thermal softening eliminates the advantages anticipated from the lower dwell cure. At slower ramp rates, however, the adhesive's modulus remains above the minimum and thus more of the deflection on heat up is maintained. Two-step 155/177°C cycles with 1.0 and 0.1°C/min ramp rates seem to show a higher warpage value than equivalent two-step 120/177°C cycles, however this is attributed to geometrical differences. The CHILE model modified to include thermal softening is once again shown to predict the softening response of a curing adhesive in a complicated cure cycle.
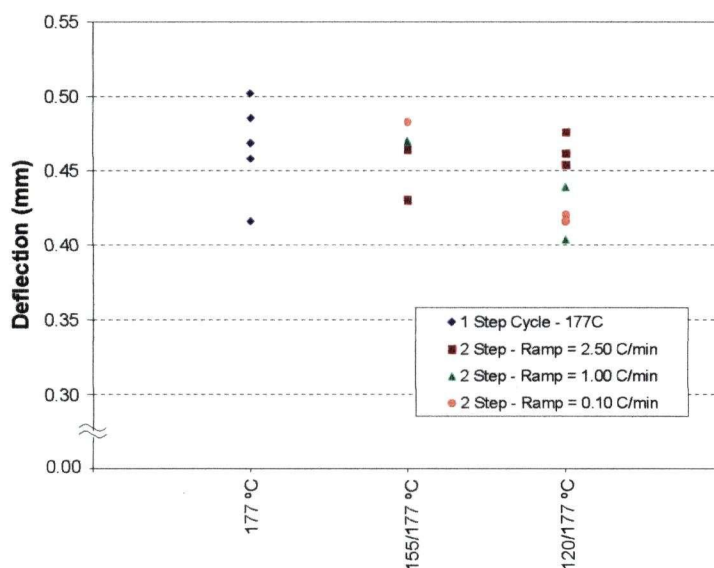

Figure 5.30 - Experimental Results - two-step cycles

An important observation is that there are no observable changes in deflection during the holds. This observation suggests that the system does not exhibit viscoelastic behaviour. In the Djokic study of FM300 [17], only the final deflection values for the two-step cycles are

quoted and thus no comparison of the development of warpage can be made. Conversely, in the Djokic study of FM73 [72], viscoelastic creep during the second hold is noted and a modulus defined by a power law and the Boltzmann superposition principal are used to model the development of defection. No attempt is made in this study to determine the underlying reasons for the fundamental difference in behaviour between FM73 and FM300.

Table 5.9 - Experimental Results - Two-step cycles

Cycle	Deflection			Model
	Experimental (mm)	**Model (mm)**	**Difference (%)**	**DOC**
[7] 2 step - 155°C /177°C *(a)*	0.430	0.440	-2.16	0.993
(b)	0.464	0.443	4.52	0.994
Average	0.447	0.442	1.31	0.994
Standard Deviation	0.017 (3.71%)	0.002 (0.49%)	3.34	
[8] 2 step - 120°C /177°C *(a)*	0.462	0.473	-2.40	0.994
(b)	0.454	0.465	-2.35	0.995
(c)	0.476	0.472	0.84	0.955
Average	0.464	0.470	-1.28	0.995
Standard Deviation	0.009 (1.96%)	0.004 (0.77%)	1.52	
[9] 2 step - 155°C /177°C *(a)*	0.470	0.452	3.79	0.995
[10] 2 step - 120°C /177°C *(a)*	0.439	0.418	4.78	0.994
(b)	0.404	0.415	-2.65	0.994
Average	0.422	0.416	1.22	0.994
Standard Deviation	0.018 (4.15%)	0.002 (0.40%)	3.72	
[11] 2 step - 155°C /177°C *(a)*	0.483	0.470	2.67	0.998
[12] 2 step - 120°C /177°C *(a)*	0.416	0.434	-4.33	0.998
(b)	0.421	0.425	-1.07	0.998
(c)	0.417	0.411	1.30	0.998
Average	0.418	0.423	-1.36	0.998
Standard Deviation	0.002 (0.48%)	0.009 (2.19%)	2.31	

5.3.6 Summary

As variations in specimen geometry were found to contribute to a large scatter in the experimental results, results were scaled to a standard adhesive layer thickness of 0.24 mm by running the model using the experimental temperature cycle. *Table 5.10* and *Figure 5.31* summarize the average deflection values, both experimentally and scaled to account for variations in the thickness of the adhesive layer, along with the degree of cure and the percent reduction in deflection based on the scaled results with the 1 step 177° cycle used as the baseline. Comparing the experimental results to those scaled to a standard adhesive layer thickness, we note that the thickness of the adhesive layer can have a large effect on the experimental results.

Table 5.10 - Experimental deflections

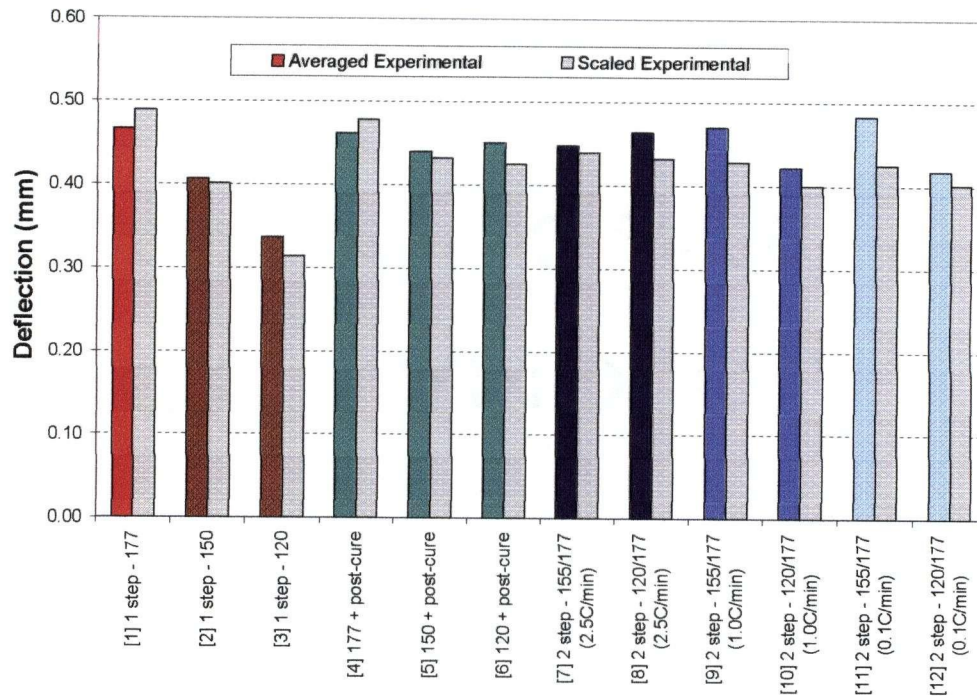| Cycle	Deflection (mm)		DOC	Reduction in deflection (%)
	Experimental	Scaled		
[1] 1 step - 177°C	0.466	0.489	0.997	-
[2] 1 step - 150°C	0.406	0.401	0.966	18
[3] 1 step - 120°C	0.336	0.311	0.865	36
[4] 177°C + post-cure	0.461	0.478	0.998	2
[5] 155°C + post-cure	0.440	0.432	0.989	12
[6] 120°C + post-cure	0.451	0.425	0.984	13
[7] 2 step - 155°C /177°C (2.5 °C/min)	0.447	0.439	0.994	10
[8] 2 step - 120°C /177°C (2.5 °C/min)	0.464	0.432	0.995	12
[9] 2 step - 155°C /177°C (1.0 °C/min)	0.470	0.428	0.995	12
[10] 2 step - 120°C /177°C (1.0 °C/min)	0.422	0.400	0.994	18
[11] 2 step - 155°C /177°C (0.1 °C/min)	0.483	0.425	0.998	13
[12] 2 step - 120°C /177°C (0.1 °C/min)	0.418	0.402	0.998	18

Figure 5.31 - Experimental deflections

Examining the scaled results we first note that for the one-step cycles, although a reduction in the cure temperature produces a reduction in deflection, a marked drop in the final degree of cure also occurs. As many mechanical properties are functions of the degree of cure, this drop is unacceptable for most applications. Post-curing the specimens, although increasing the final degree of cure, negates some of the benefit of a lower initial cure temperature. The two-step cycles show that reducing the first hold temperature can result in a reduction in the final deflections. This improvement is more pronounced for slower heating rates between the dwell temperatures, as fast heating rates result in a lag between the temperature increase and the development glass transition temperature.

5.3.7   Sources of Error

The test methodology incorporates a number of systemic errors. The first source of error is that the temperature of the specimens is not measured directly. Although thermocouples are placed approximately 2 mm from the specimens, it is still possible that a small difference in temperature exists between the specimen and the environment. A small temperature lag in the

specimens during ramps, which equilibrates during holds, may explain the difference between experimental and model results during ramps.

Second, due to the small specimen size, a significant amount of adhesive squeeze out was observed (*Figure 5.18*). This resulted in an initial change in total specimen thickness during the test, which was evident in the displacement of the load head (*Figure 5.16* and *Figure 5.17*). As this occurs early in the cure cycle when the adhesive viscosity drops, the deflection measurements are zeroed to the deflection values at the end of the first temperature dwell. To further prove the assumption that this initial deflection is an experimental artefact, a cycle was run where the temperature was ramped to 110°C, cooled to room temperature, ramped once more to 110°C, and cooled to room temperature before a standard 177°C cure cycle was applied. The time domain results of this test, shown in *Figure 5.32*, illustrate the effect of adhesive layer thinning. Initially an approximate 0.2 mm deflection is observed which corresponds to a physical change in the geometry of the specimen and not a thermal effect. This deflection is carried through the remainder of the experiment, before the expected thermally induced behaviour of the 177°C cure cycle is observed.
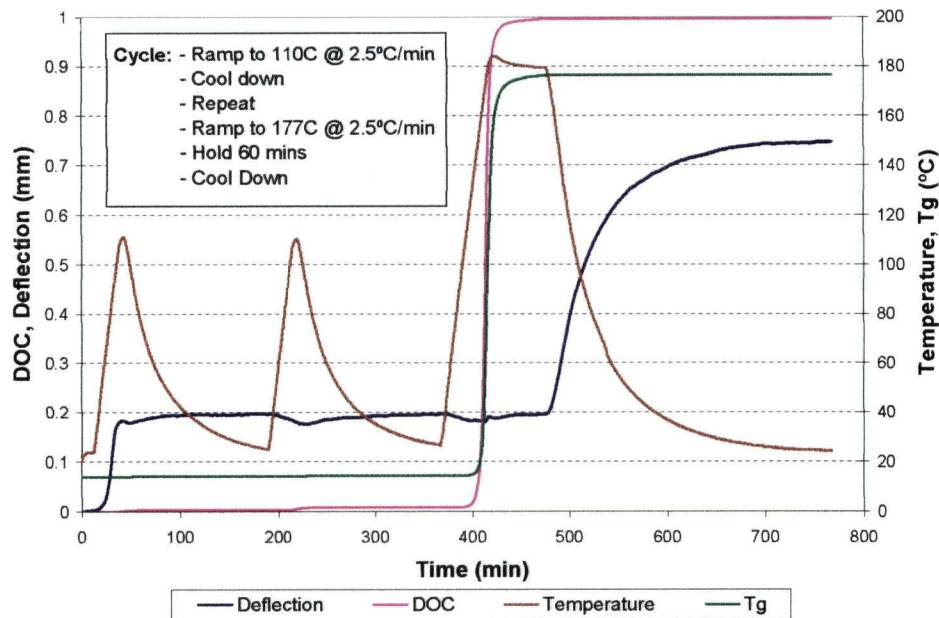

Figure 5.32 - Time domain results for a thickness test

5.4   Idealized cycles – Warpage

The experimental results did not exhibit some of the trends reported by other researchers. Temperature control, which was found to be a major source of consternation, affects the cycles in three major ways. First, although the temperatures were externally logged with three thermocouples, there is still the distinct possibility that the specimen temperatures differed slightly from the recorded temperatures, most notably during temperature ramps. These differences in temperature affect the specimen's cure history, and thus its shear modulus during the most important portion of the cycle. Second, loose temperature control creates overshoots when transitioning from ramps to holds. During these overshoots, the adhesive's shear modulus may drop below the intended minimum, causing a softening response which results in a larger than expected final deflection. Third, even though a smooth temperature ramp is programmed, the environmental temperature fluctuates about the target temperature. These oscillations can cause a small drop in modulus, resulting in additional thermal softening and an increase in final warpage.

The effect of poor temperature control was investigated by running the analytical model for idealized temperature cycles, following the same cycles outlined for the experimental program in *Table 4.3*. Temperature histories for idealized cure cycles were created such that the ramp rates and hold temperature exactly matched those stipulated in the cure cycle summary. The experimental cure cycles were simulated on a virtual specimen, with dimensions and properties shown *Table 5.11*.

Table 5.11 - Virtual specimen geometry and properties

Geometry			Material Properties		
Substrate Thickness	0.16	(mm)	Substrate Modulus	200	(GPa)
Patch Thickness	0.50	(mm)	Patch Modulus	140	(GPa)
Total Thickness	0.90	(mm)			
Adhesive Thickness	0.24	(mm)	Substrate CTE	15	($\mu\varepsilon$/°C)
Width	6.40	(mm)	Patch CTE	0	($\mu\varepsilon$/°C)
Length	40.00	(mm)			

5.4.1   One-Step Cycles

The ideal deflections for the three one-step cycles are shown in *Figure 5.33 (a)*, along with the corresponding shear moduli in *Figure 5.33 (b)*. Results are summarized in *section 5.4.4*. A near linear slope is observed, which is similar for all of the cycles, and the final deflection value is a function of the cure temperature.
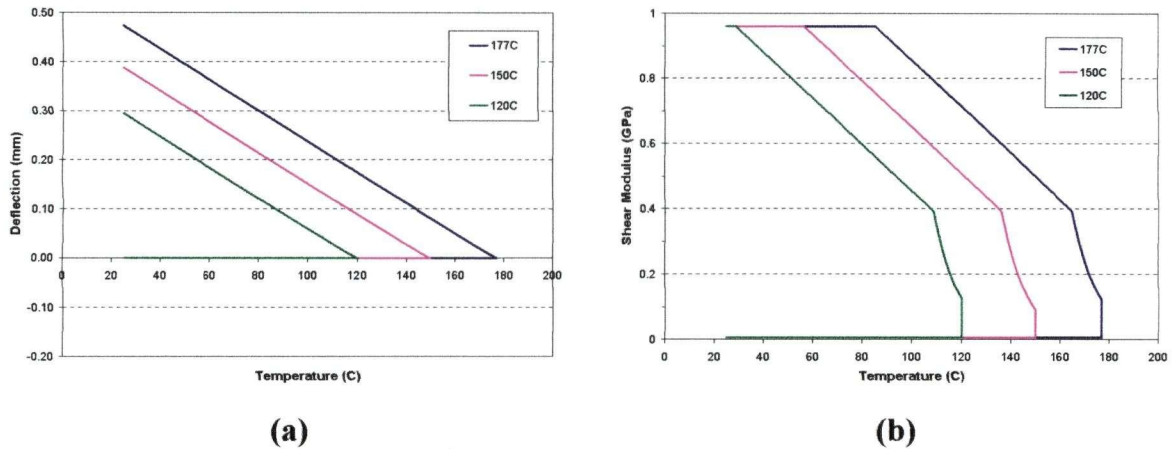

(a)   **(b)**

Figure 5.33 - Idealized one-step cure cycles: deflection (a) and shear modulus (b) versus temperature

5.4.2   Post Cure Cycles

The ideal deflections for the three post-cure cycles investigated are shown in *Figure 5.34 (a)*, along with the corresponding shear moduli in *Figure 5.34 (b)*.
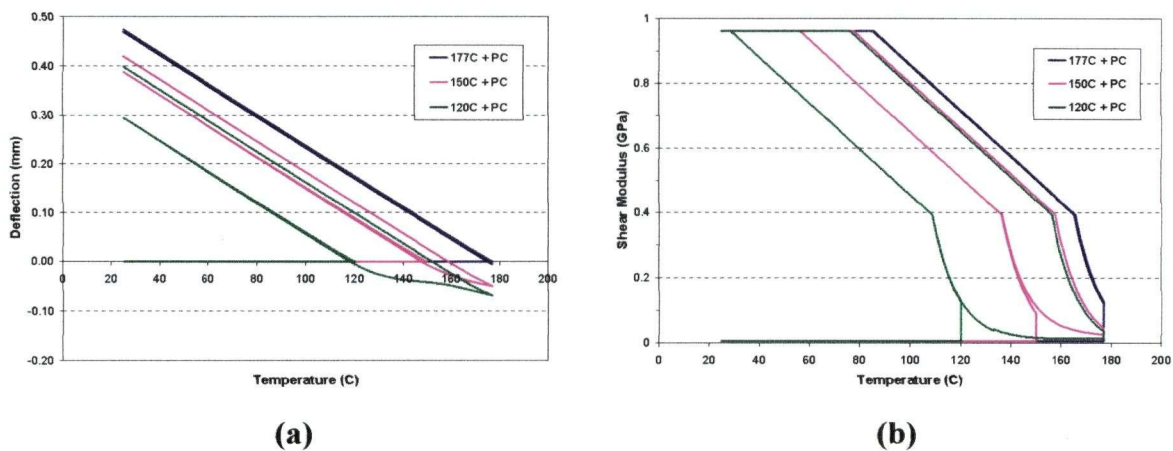

(a)   **(b)**

Figure 5.34 - Idealized post-cure cycles: deflection (a) and shear modulus (b) versus temperature

Results are summarized in *section 5.4.4*. The results for the initial heat-up and cool-down mirror those of the one-step cycles. During heat-up to the post-cure temperature, a slight softening response is observed, which begins slightly before the initial cure temperature is reached. This effect is most pronounced for the 120°C post-cure cycle, both in terms of absolute change in deflection and relative change in deflection. The absolute changes in deflection are due to the increase in temperature between the first dwell and the post-cure dwell. The relative change in deflection in the 120°C post-cure cycle is larger than for the other cycles due to the larger drop in shear modulus for this cycle, as evidenced in *Figure 5.34 (b)*.

5.4.3 Two-Step Cycles

The ideal deflections for the 155°C/177°C two-step cycles with different heating rates are shown in *Figure 5.35 (a)*, along with the corresponding shear moduli in *Figure 5.35 (b)*, while those for the 120°C/177°C two-step cycles with different heating rates are shown in *Figure 5.36 (a)*, along with the corresponding shear moduli in *Figure 5.36 (b)*. Results are summarized in *section 5.4.4*. From these results a number of important observations can be made. First we see that as the heat-up rate decreases, the behaviour of the adhesive's shear modulus development changes dramatically. For fast heat up rates, the adhesive's shear modulus drops to the fully relaxed value and thus the benefits of a two-step cure cycle are dramatically reduced. At slower heat-up rates, however, the minimum adhesive modulus reached is above the fully relaxed value, and thus the benefits of a two-step cycle are more pronounced. We also note that even though the heating rate is constant, the development of adhesive modulus may not be monotonic. This suggests that a non-constant heating rate may produce a more optimized cycle, both in terms of thermal residual stresses and in terms of cycle time.
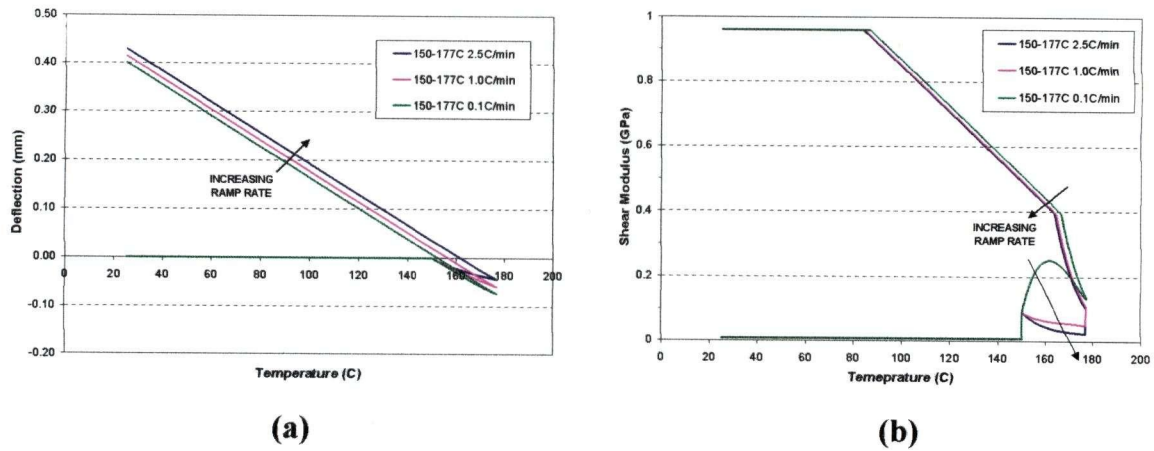
(a)

(b)

Figure 5.35 - Idealized two-step 155/177°C cycles: deflection (a) and shear modulus (b) versus temperature
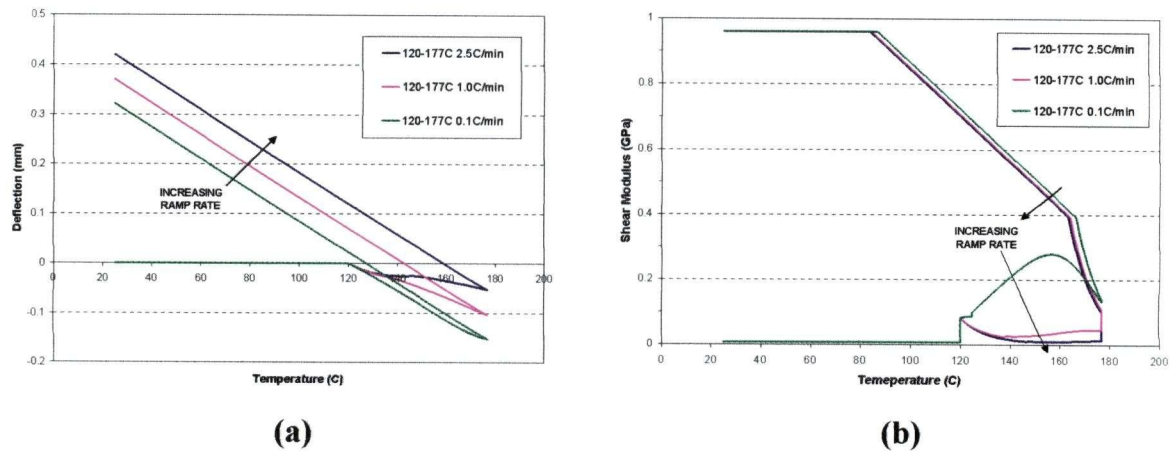

(a)

(b)

Figure 5.36 - Idealized two-step 120/177°C cycles: deflection (a) and shear modulus (b) versus temperature

5.4.4   Summary of idealized results

Idealized results, summarized in *Table 5.12* and *Figure 5.37*, show that a large reduction in warpage is possible by modifying the cure cycle. Results for idealized one-step cycles mirror those found experimentally; lowering the cure temperature results in a reduction in the induced warpage. As previously commented, this is generally accompanied by a reduction in the final degree of cure that may be unacceptable.

Idealized results for post-cured cycles also show similar trends to those determined experimentally. While post-curing does increase the final degree of cure, this is accompanied by a lessening in the reduction of warpage. For two-step cycles, however, trends shown by the idealized cycles are more pronounced than those found experimentally. The two-step idealized cycles show that reducing the temperature of the first dwell can result in an appreciable reduction in warpage that becomes more pronounced for slower ramp rates between the dwell temperatures. The maximum attainable percent reduction in deflection for the idealized cycles is shown to be 32% for a two-step 120°C/177°C cycle with a ramp rate of 0.1°C/min.

Table 5.12 - Idealized cycle deflections

| Cycle	Deflection (mm)	Percent Reduction	DOC
[1] 1 step - 177	0.474	0	0.994
[2] 1 step - 150	0.388	18	0.915
[3] 1 step - 120	0.294	38	0.839
[4] 177 + post-cure	0.470	1	0.995
[5] 150 + post-cure	0.420	11	0.974
[6] 120 + post-cure	0.399	16	0.970
[7] 2 step - 155/177 (2.5C/min)	0.437	8	0.990
[8] 2 step - 120/177 (2.5C/min)	0.420	11	0.989
[9] 2 step - 155/177 (1.0C/min)	0.429	9	0.992
[10] 2 step - 120/177 (1.0C/min)	0.370	22	0.991
[11] 2 step - 155/177 (0.1C/min)	0.416	12	0.997
[12] 2 step - 120/177 (0.1C/min)	0.322	32	0.997
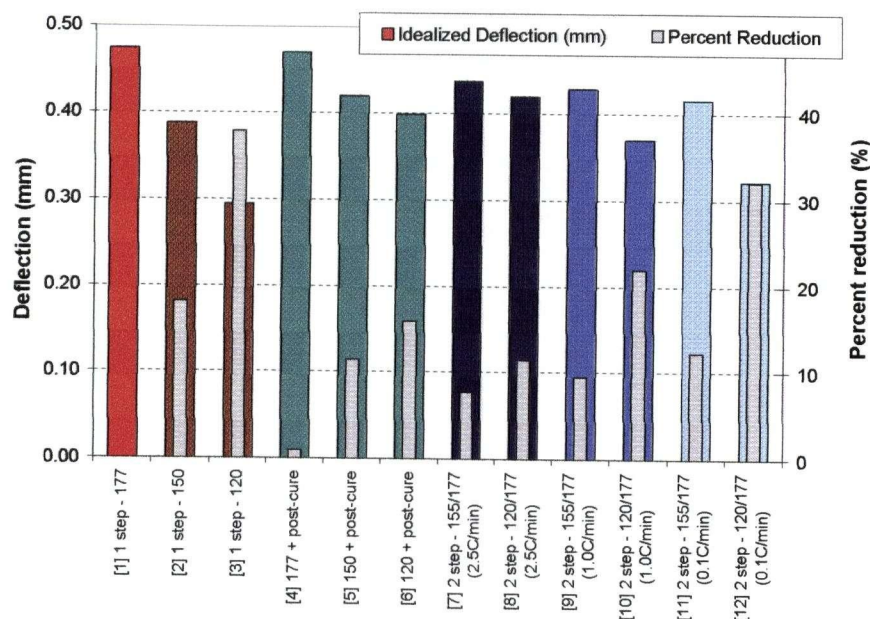
Figure 5.37 – Idealized cycle deflections

5.4.5   Comparison to experimental results

The results of the idealized cycles are listed (along with averaged and scaled experimental results) in *Table 5.13* and are compared to the scaled experimental results for each cycle studied. *Figure 5.38* also shows a graphical representation of the averaged experimental, scaled experimental, and idealized results.

Results show a large discrepancy between experimental and idealized results for a number of the cases investigated. Some of these are corrected by scaling the experimental results to account for variations in the adhesive layer thickness. However, taking variations in the adhesive layer thickness into account did not account all of the discrepancies. These discrepancies are believed to be caused by poor temperature control in the DMA during experimentation, both in terms of temperature control during ramps and overshoots when transitioning between ramps and holds. The results suggest that the cycles with the lowest hold temperature (120°C) are most sensitive to temperature variations. This may be due to the sensitivity of the cure kinetics to these lower temperatures, where cure rates are high and small variations impact the development of warpage. The relatively long ramps to the maximum cycle temperature (177°C) may also accentuate these discrepancies.
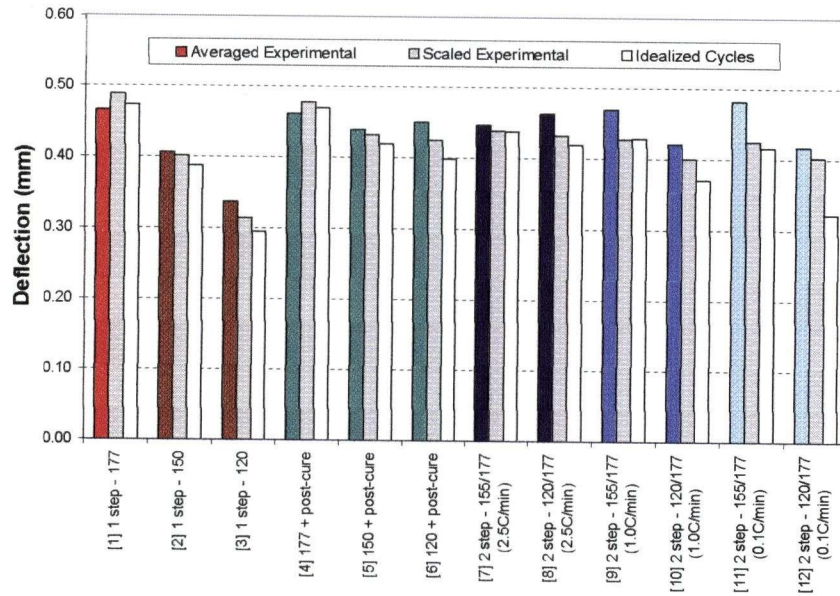
Figure 5.38 - Averaged experimental (left bars), scaled experimental (centre bars), and idealized (right bars) deflections

Table 5.13 - Comparing averaged experimental, scaled experimental, and idealized deflections

Cycles	Deflections			Percent Difference
	Averaged	**Scaled**	**Idealized**	**(Scaled vs. idealized)**
[1] 1 step - 177	0.466	0.489	0.474	3
[2] 1 step - 150	0.406	0.401	0.388	3
[3] 1 step - 120	0.336	0.311	0.294	6
[4] 177 + post-cure	0.461	0.478	0.470	2
[5] 150 + post-cure	0.440	0.432	0.420	3
[6] 120 + post-cure	0.451	0.425	0.399	7
[7] 2 step - 155/177 (2.5C/min)	0.447	0.439	0.437	0
[8] 2 step - 120/177 (2.5C/min)	0.464	0.432	0.420	3
[9] 2 step - 155/177 (1.0C/min)	0.470	0.428	0.429	0
[10]2 step - 120/177 (1.0C/min)	0.422	0.400	0.370	8
[11]2 step - 155/177 (0.1C/min)	0.483	0.425	0.416	2
[12]2 step - 120/177 (0.1C/min)	0.418	0.402	0.322	25

5.5   Idealized cycles - Thermal Residual Stresses

The purpose of modifying the cure cycle is to reduce the thermally induced residual stresses in the substrate layer of a bonded composite patch repair. In the DMA beam technique, warpage is used as a measure of the residual stresses. A reduction in warpage thus corresponds to a reduction in thermally induced residual stresses. *Table 5.14* lists the maximum thermally induced normal stresses in the patch and the substrate, as well as the maximum shear stresses in the adhesive layer for the idealized cycles. These results are shown graphically, along with the warpage for each cycle, in *Figure 5.39* and *Figure 5.40*. *Table* 5.15 lists the percent reductions in warpage and stresses for each cycle using the one-step 177°C cycle as the baseline. The results show that the percent reduction in warpage corresponds to a similar reduction in normal stresses. Shear stresses in the adhesive, while following the same trends as the normal stresses, do not show the same percent reductions.

Table 5.14 - Maximum Stresses

| Cycle	Idealized Deflection (mm)	Maximum Stress (MPa)		
		Patch,σ	Substrate,σ	Adhesive,τ
[1] 1 step - 177	0.4740	-221	462	16.1
[2] 1 step - 150	0.3878	-181	379	12.6
[3] 1 step - 120	0.2944	-138	288	9.2
[4] 177 + post-cure	0.4695	-220	461	15.3
[5] 150 + post-cure	0.4198	-195	407	14.5
[6] 120 + post-cure	0.3988	-183	383	14.4
[7] 2 step - 155/177 (2.5C/min)	0.4374	-202	422	15.6
[8] 2 step - 120/177 (2.5C/min)	0.4200	-192	402	15.4
[9] 2 step - 155/177 (1.0C/min)	0.4290	-197	413	15.5
[10] 2 step - 120/177 (1.0C/min)	0.3700	-166	347	14.8
[11] 2 step - 155/177 (0.1C/min)	0.4160	-191	400	15.3
[12] 2 step - 120/177 (0.1C/min)	0.3218	-144	300	13.9
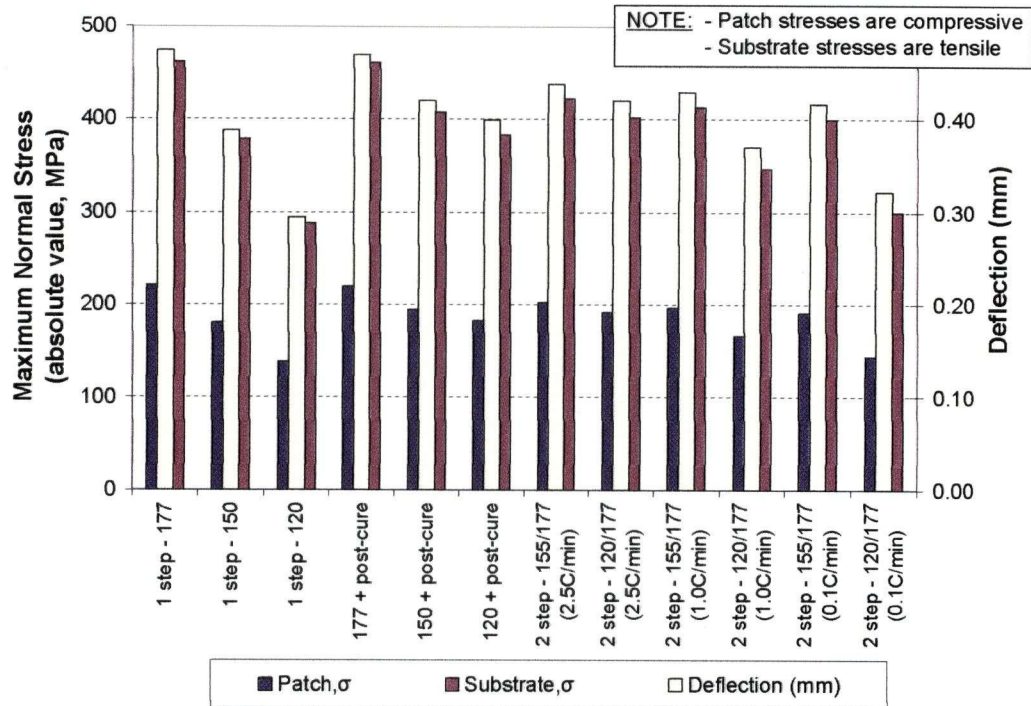
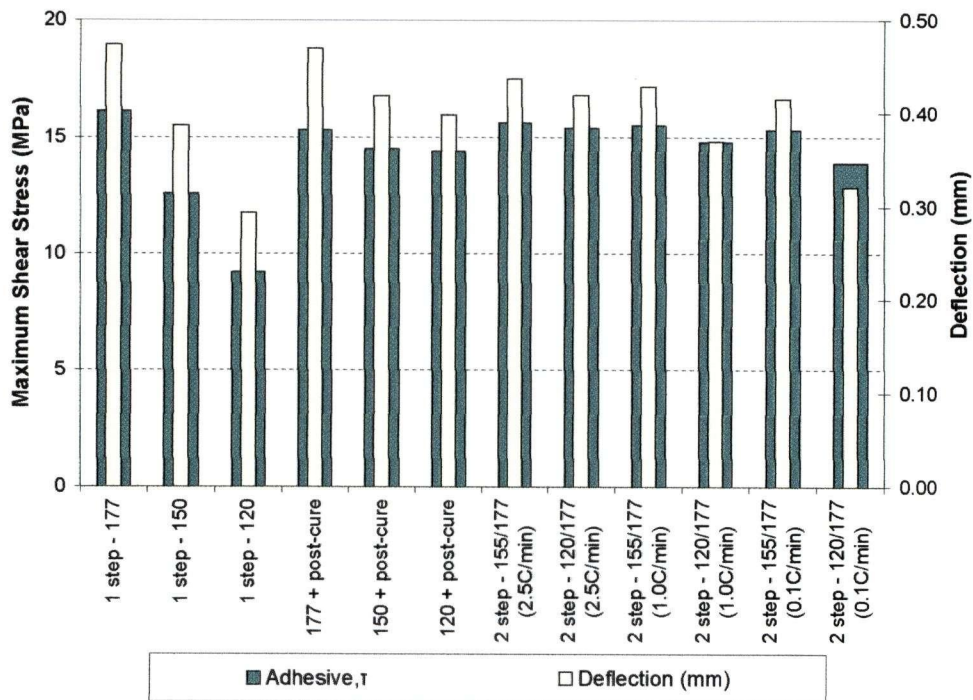**Figure 5.39 - Maximum normal stresses in the *x*-direction in the patch and the substrate**

Figure 5.40 - Maximum shear stresses in the adhesive layer

Table 5.15 – Percent reductions of maximum stresses

Cycle	Percent Reduction			
	Deflection (mm)	Patch,σ	Substrate,σ	Adhesive,τ
[1] 1 step – 177	-	-	-	-
[2] 1 step - 150	18	18	18	0.22
[3] 1 step - 120	38	38	38	0.43
[4] 177 + post-cure	1	0	0	0.05
[5] 150 + post-cure	11	12	12	0.10
[6] 120 + post-cure	16	17	17	0.11
[7] 2 step - 155/177 (2.5C/min)	08	9	9	0.03
[8] 2 step - 120/177 (2.5C/min)	11	13	13	0.04
[9] 2 step - 155/177 (1.0C/min)	9	11	11	0.04
[10] 2 step - 120/177 (1.0C/min)	22	25	25	0.08
[11] 2 step - 155/177 (0.1C/min)	12	14	13	0.05
[12] 2 step - 120/177 (0.1C/min)	32	35	35	0.14

5.6   Effects of thermal softening on the CHILE model

The effect of thermal softening on CHILE model predictions is investigated by running the CHILE model, both with and without the thermal softening component, on the scaled experimental cycles presented in *section 5.3.6. Table 5.16* and *Figure 5.41* show the resulting model deflections for both the CHILE model with thermal softening (CHILE w/TS) and the standard CHILE model (CHILE), as well as the percent difference between the two models.

From these results we note that the introduction of a thermal softening component can only result in an increase in predicted deflections. For the 1-step cycles, no difference between the two variations of the model is observed. This is expected since the thermal softening component of the CHILE model only affects the deflection during heat-ups and in the 1-step cycles the only heat up occurs prior to gelation of the adhesive.

100

Table 5.16 - Comparing CHILE with thermal hardening

Cycle	CHILE w/TS (mm)	CHILE (mm)	Difference (%)
[1] 1 step - 177	0.489	0.489	0.00
[2] 1 step - 150	0.401	0.401	0.00
[3] 1 step - 120	0.311	0.311	0.00
[4] 177 + post-cure	0.478	0.483	-1.05
[5] 155 + post-cure	0.433	0.412	4.85
[6] 120 + post-cure	0.425	0.383	9.88
[7] : step - 155°C /177°C (2.5 °C/min)	0.439	0.424	3.42
[8] : step - 120°C /177°C (2.5 °C/min)	0.432	0.394	8.80
[9] : step - 155°C /177°C (1.0 °C/min)	0.429	0.418	2.56
[10] : step - 120°C /177°C (1.0 °C/min)	0.400	0.363	9.25
[11] : step - 155°C /177°C (0.1 °C/min)	0.425	0.407	4.24
[12] : step - 155°C /177°C (2.5 °C/min)	0.402	0.318	20.90
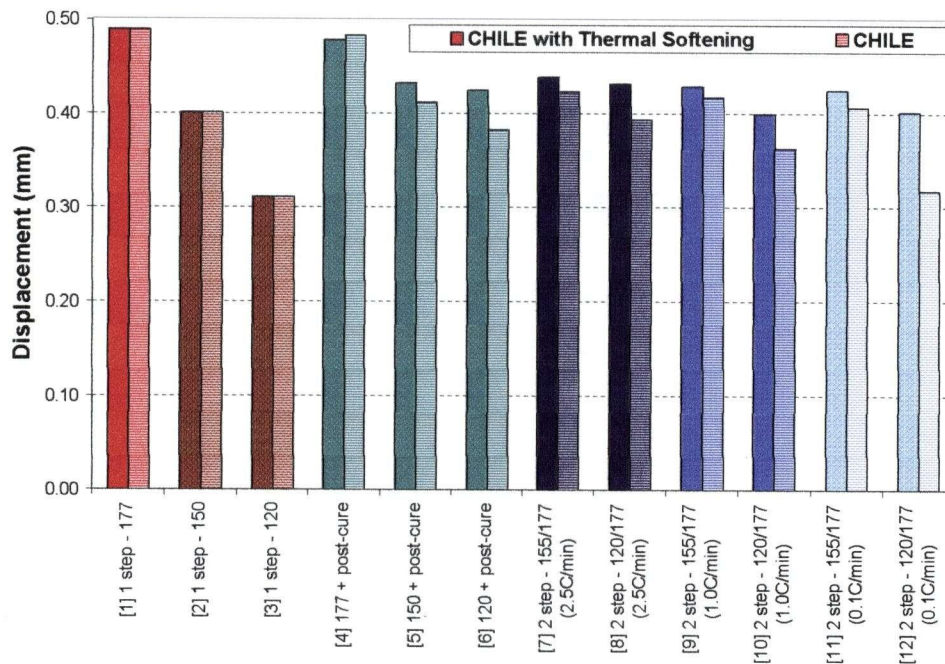
Figure 5.41 – Comparing the standard CHILE model with the modified, thermal softening CHILE model
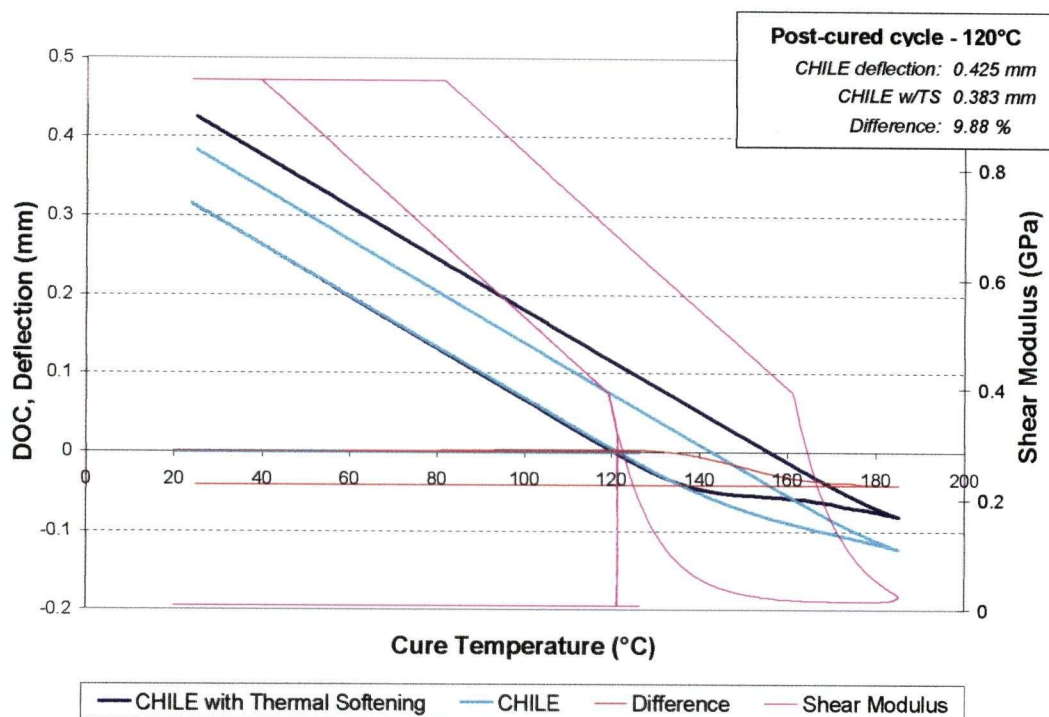
Figure 5.42 – Effect of thermal softening on a post cured 120°C idealized cure cycle
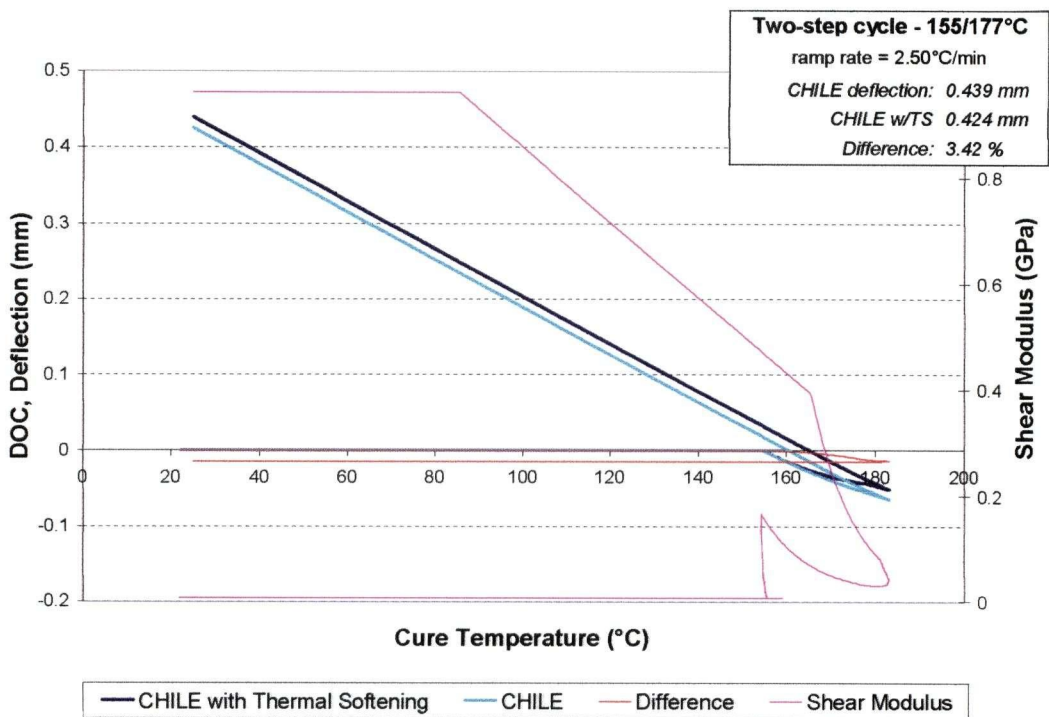
Figure 5.43 - Effect of thermal softening on a 2-step 155°C/177°C idealized cure cycle

with a 2.50°C/min ramp rate
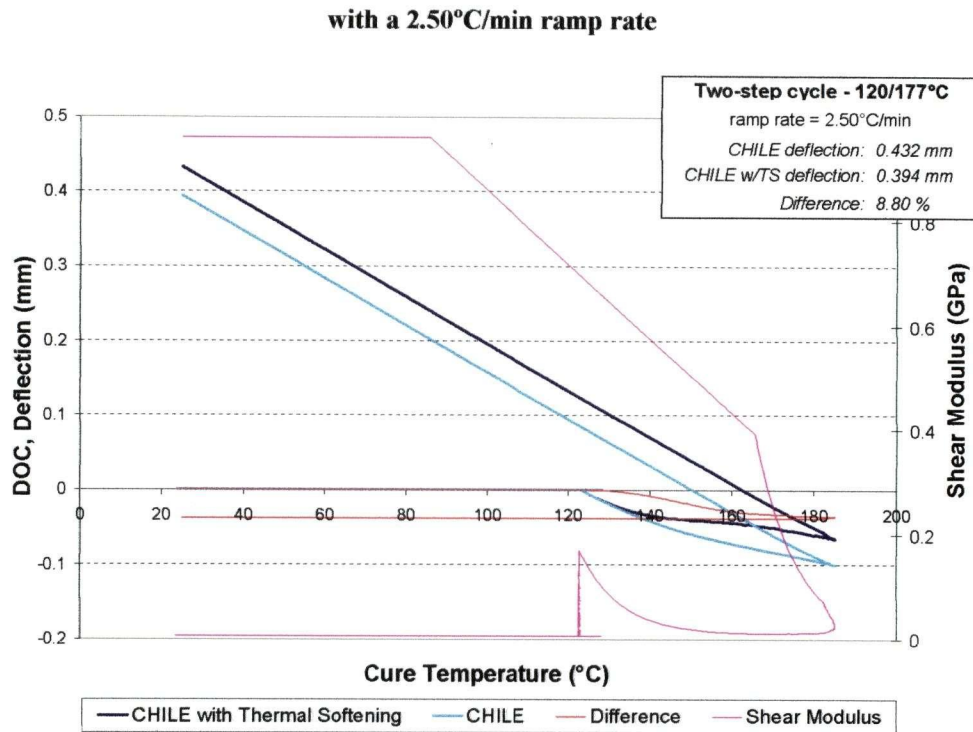
Figure 5.44 - Effect of thermal softening on a 2-step 120°C/177°C idealized cure cycle

with a 2.50°C/min ramp rate
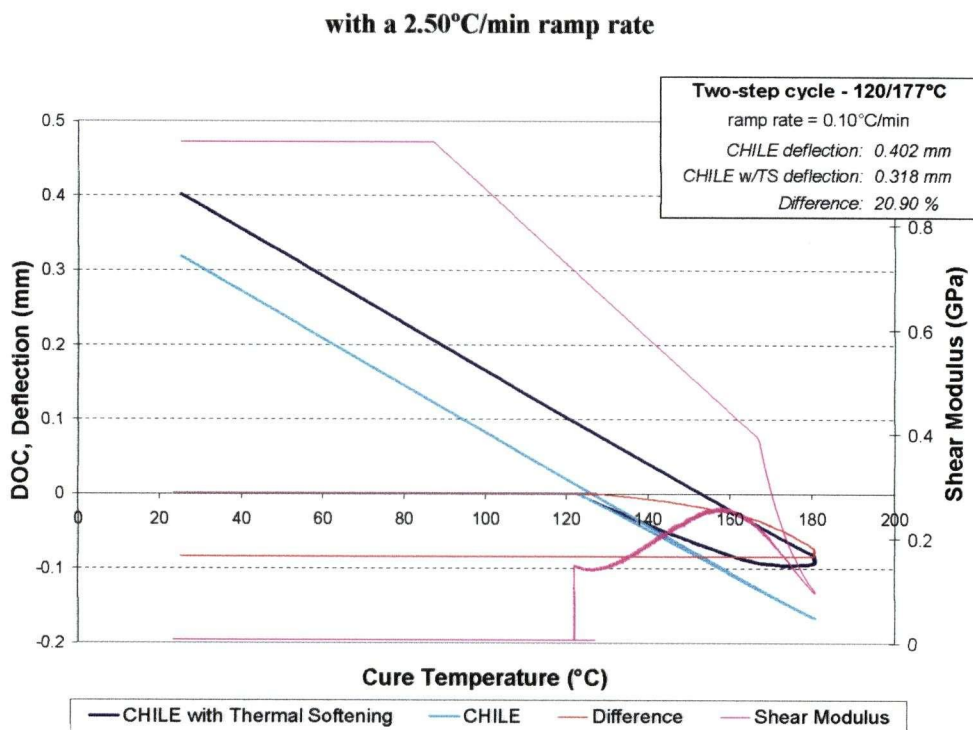
Figure 5.45 - Effect of thermal softening on a 2-step 120°C/177°C idealized cure cycle

with a 0.10°C/min ramp rate

For post-cure cycles, the effect of thermal softening increases as the initial cure temperature decreases. The results of an idealized 120°C post cured cycle are shown in *Figure 5.42*, for models run with and without thermal softening. Thermal softening occurs during the reheat portion of the cycle since the modulus drops as the rate of development of the glass transition temperature lags the temperature ramp. Thermal softening causes a reduction in "negative" warpage on the reheat portion of the cycle, resulting in a larger final deflection than that obtained with a simple CHILE model. The slope on cool-down is unaffected by thermal softening.

Similarly, the results for the two-step cycles show that the effect of thermal softening increases as the first dwell temperature decreases. The results for a two-step 155°C/177°C cure cycle with a ramp rate of 2.5°C/min are shown in *Figure 5.43*, while those for a two-step 120°C/177°C cure cycle with a ramp rate of 2.5°C/min are shown in *Figure 5.44*. These figures present the model results, both with and without thermal softening. The results for the two-step cycles also show that the effect of thermal softening becomes more pronounced as the heating rate between first and second dwells is increased. The results of a two-step 120°C/177°C cure cycle with a ramp rate of 0.1°C/min are shown in *Figure 5.45*, for model predictions with and without thermal softening. A slow ramp rate between the first and second dwell allows the development of glass transition temperature to keep pace with the increase in temperature. Increasing the ramp rate causes the development of glass transition temperature to lag behind the temperature, resulting in a drop in modulus and consequently an increased in the effect of thermal softening.

5.7   Cycle Times

While reducing thermal residual stresses is important to the long-term durability and fatigue life of bonded composite patch repairs, the cycle time is also a concern. As modified cycles may require more sophisticated heating and temperature control technologies and increased cycle times result in longer downtimes, a compromise between reduced thermal residual stresses and increased cycle times is often required. *Table 5.17* lists the cycle times for the idealized cycles investigated, as well as the percent increase in cycle time over the

idealized cycles investigated, as well as the percent increase in cycle time over the manufacturer recommended one-step 177°C cycle. Also shown are the idealized warpage values and the corresponding percent decreases in warpage. A comparison between percent increase in cycle time and percent reduction in warpage is shown in *Figure 5.46*. These values can help determine an acceptable trade off between increased cycle time and reduction in warpage.

Table 5.17 - Cycle Times

Cycles	Cycle Time (minutes)	Percent increase	Idealized warpage (mm)	Percent decrease
[1] 1 step - 177	191	-	0.474	-
[2] 1 step - 150	269	41	0.388	18.2
[3] 1 step - 120	565	196	0.294	37.9
[4] 177 + post-cure	317	66	0.470	0.9
[5] 150 + post-cure	396	108	0.420	11.4
[6] 120 + post-cure	692	263	0.399	15.9
[7] 2 step - 155/177 (2.5C/min)	221	16	0.437	7.7
[8] 2 step - 120/177 (2.5C/min)	491	157	0.420	11.4
[9] 2 step - 155/177 (1.0C/min)	234	23	0.429	9.5
[10] 2 step - 120/177 (1.0C/min)	525	175	0.370	21.9
[11] 2 step - 155/177 (0.1C/min)	432	127	0.416	12.2
[12] 2 step - 120/177 (0.1C/min)	1038	444	0.322	32.1
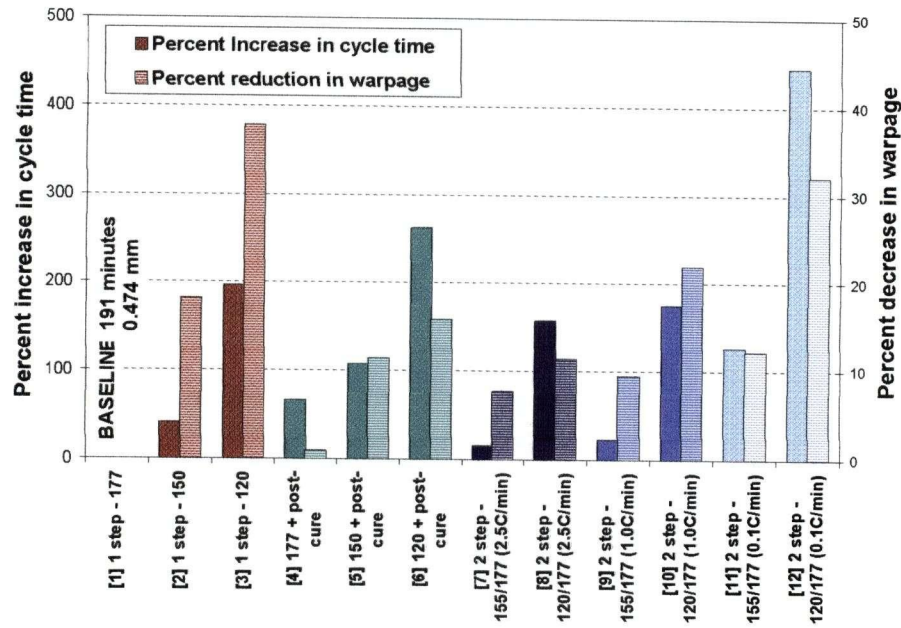
Figure 5.46 – Increase in cycle time and reduction in warpage comparison

177°C cycle used as a baseline

5.8   Model Sensitivities

The sensitivity of the cure hardening, instantaneously linear elastic model (modified to include thermal softening effects) to variations in geometry and cure conditions was investigated by running the model under idealized cycle conditions. The sensitivity of the model to specimen geometry was investigated by modifying the adhesive layer thickness. The sensitivity of the model to cure conditions was investigated by modifying an idealized two-step cure cycle's ramp rate between the first and second temperature dwells, as well as the maximum cure cycle temperature.

5.8.1   Sensitivity of idealized cycles to the adhesive layer thickness

To determine the sensitivity of the model to the adhesive layer thickness, a two-step cycle was simulated on the virtual specimen of *section 5.5* with different adhesive thicknesses. The two-step cycle consisted of a 120°C dwell for 330 minutes followed by a ramp to 177°C at 0.1°C/min and a hold for 30 minutes. The adhesive thicknesses ranged from 0.15 mm to 0.35

mm to span the variation in experimentally observed thicknesses. The virtual specimen with an adhesive layer thickness of 0.24 mm was used as the baseline for comparison.
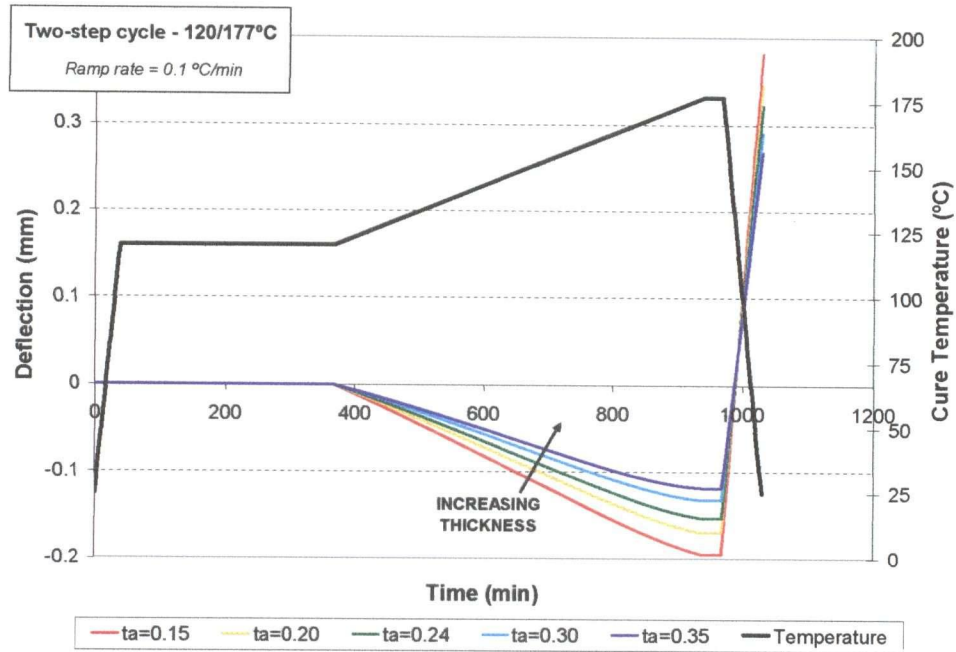
Figure 5.47 - Time domain results for thickness sensitivity of an idealized two-step cycle
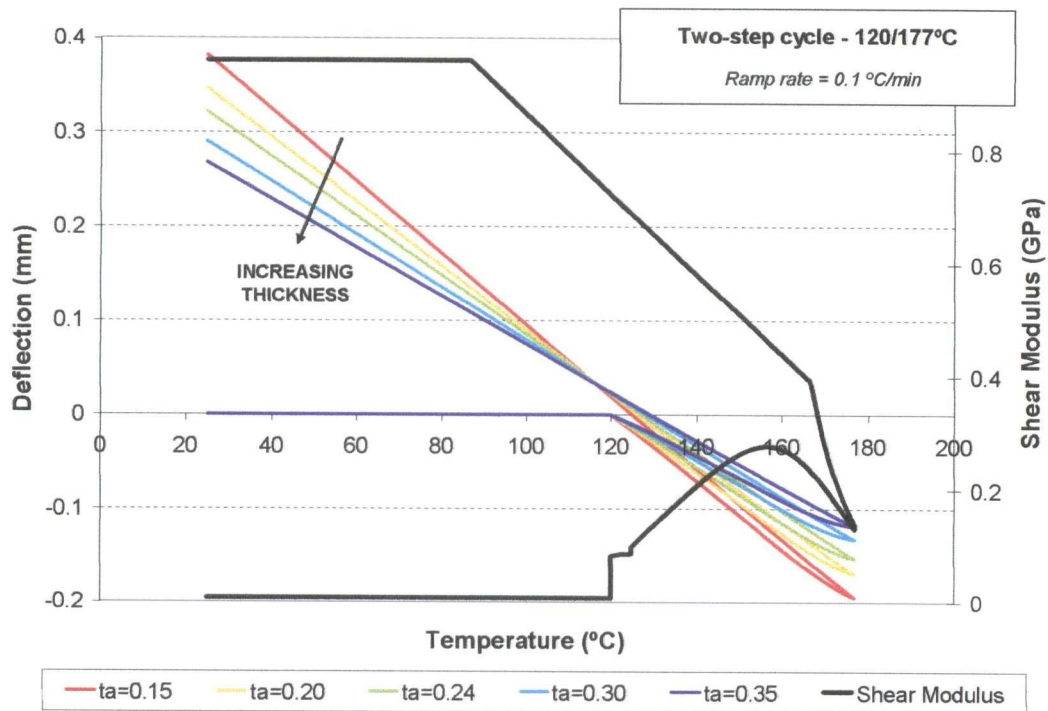
Figure 5.48 - Temperature domain results for thickness sensitivity of an idealized two-step cycle

Figure 5.47 shows the temperature cycle and the resulting deflections for the different adhesive layer thicknesses in the time domain. Similarly, *Figure 5.48* shows the modulus development, which is the same for all the cycles, and resulting deflections for the different adhesive layer thicknesses in the temperature domain.

Table 5.18 - Sensitivity to adhesive layer thickness

Thickness (mm)	Deflection (mm)	Difference (%)
0.15	0.3818	18.6503
0.20	0.3463	7.6240
0.24	0.3218	0.0000
0.30	0.2903	-9.7826
0.35	0.2681	-16.6891

The results of the thickness sensitivity study and the relative differences are tabulated in *Table 5.18* and presented graphically in *Figure 5.49*. These results illustrate the importance of accurately measuring thickness. From the results we note that increasing the adhesive layer thickness results in a more compliant system, which corresponds to less warpage at the end of the cycle.
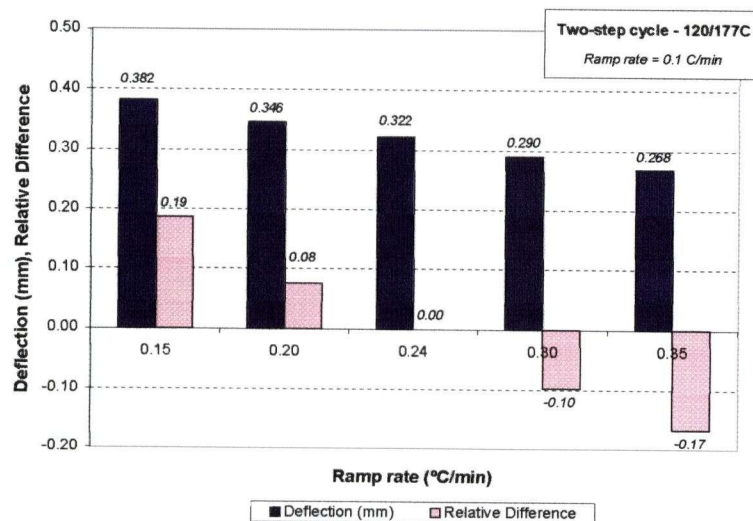
Figure 5.49 - Sensitivity of an idealized two-step cycle to the adhesive layer thickness

5.8.2   Sensitivity of idealized cycles to the maximum temperature

To determine the sensitivity of the model to temperature overshoots, two-step cycles with different second dwell temperatures were simulated on virtual specimens. The two-step cycles consisted of a 120°C dwell for 330 minutes followed by a ramp to the maximum cure temperature and a hold for 30 minutes. Ramp rates of 0.1°C/min and 2.5 °C/min were investigated. The second dwell temperature was varied between 170 and 185°C to determine the effect on the final deflection, with a maximum cycle temperature of 177°C chosen as the baseline for relative difference calculations.
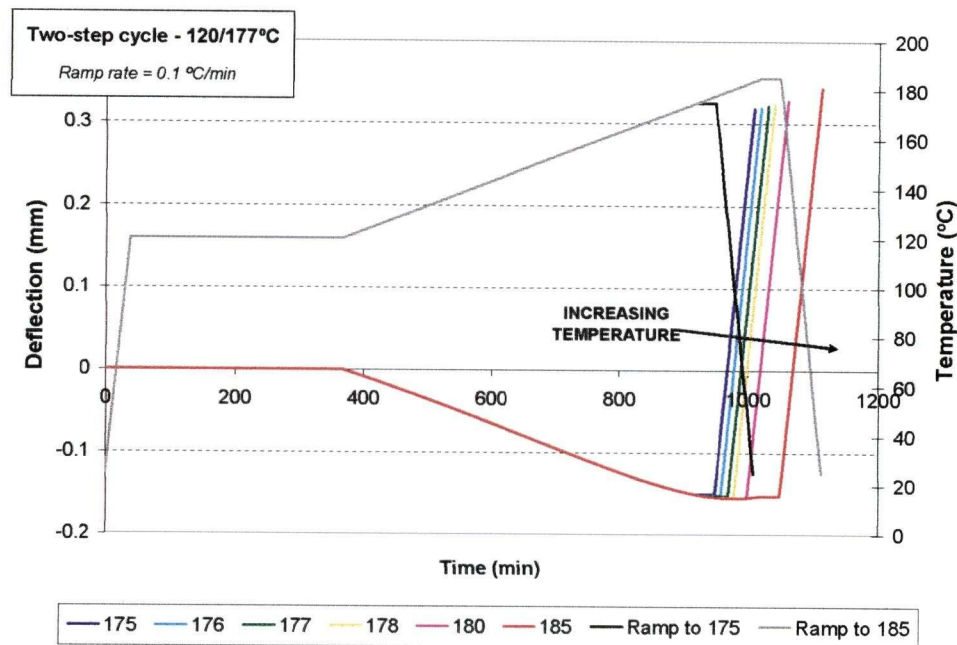
Figure 5.50 - Time domain results for temperature sensitivity of an idealized two-step cycle with a 0.10 °C/min ramp rate
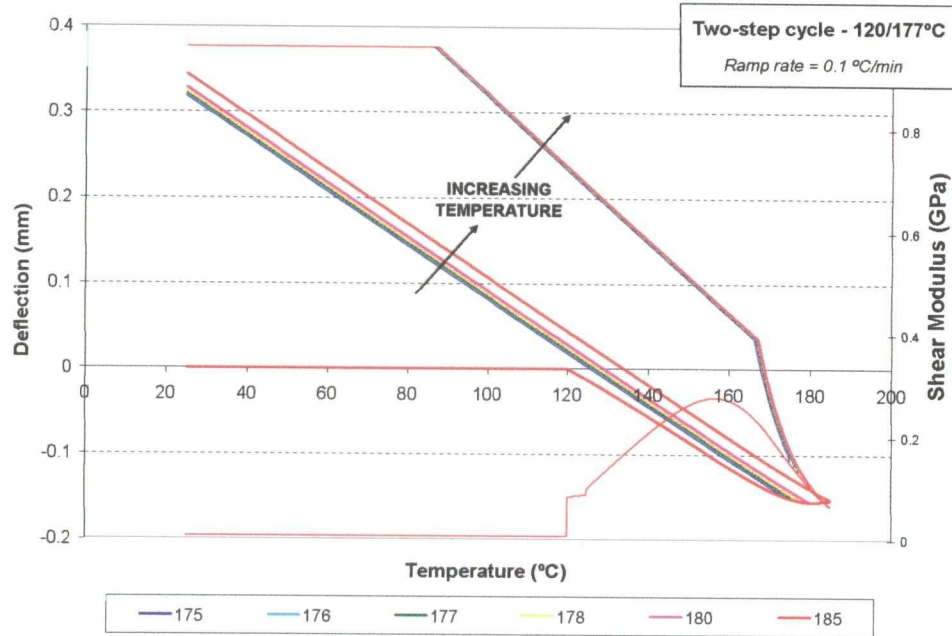
Figure 5.51 - Temperature domain results for temperature sensitivity of an idealized two-step cycle with a 0.10 °C/min ramp rate
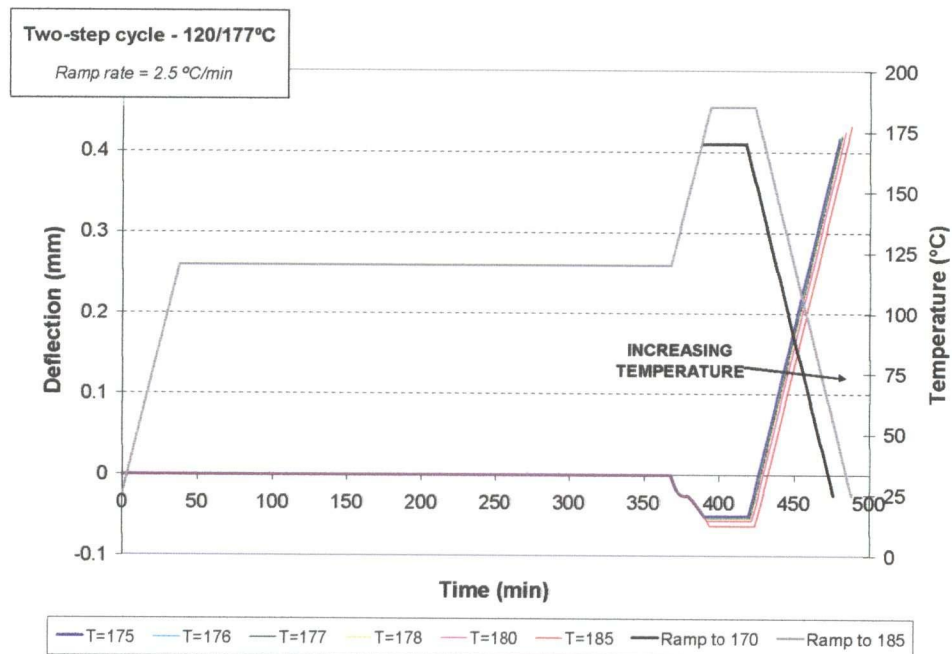
Figure 5.52 - Time domain results for temperature sensitivity of an idealized two-step cycle with a 2.50 °C/min ramp rate
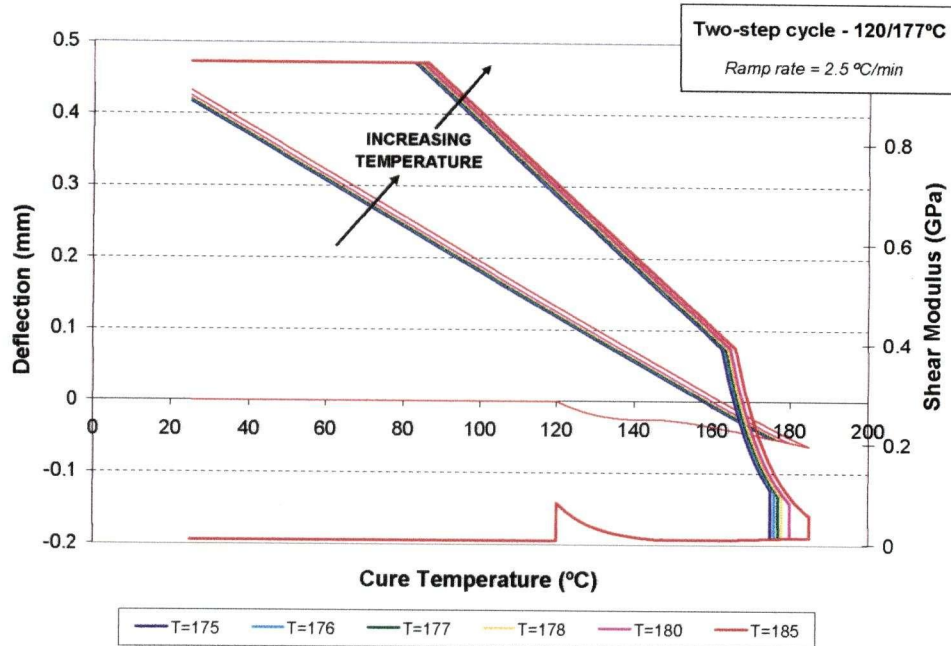
Figure 5.53 - Temperature domain results for temperature sensitivity of an idealized two-step cycle

with a 2.50 °C/min ramp rate

Figure 5.50 and *Figure 5.52* show the results in the time domain for cycles with a 0.1°C/min and a 2.5°C/min ramp rate respectively. These figures show the temperature cycles for the 175°C and 185°C maximum temperatures and the deflection values for varying maximum cycle temperatures. *Figure 5.51* and *Figure 5.53* show the results in the temperature domain for cycles with a 0.1°C/min and a 2.5°C/min ramp rate respectively. These figures show the deflection values for varying maximum cycle temperatures and the adhesive's shear modulus throughout the various cycles.

The results of the maximum cure cycle temperature study and the relative differences are tabulated in *Table 5.19* and presented graphically in *Figure 5.54*. These results show that for slow heating rates, variations in the maximum temperature achieved during the cure cycle had a more profound effect on the final deflection value than for fast heating rates. Since fast heating rates cause the modulus to drop to the fully relaxed modulus, temperature overshoots result in a slightly larger warpage due to the magnitude of the overshoot. For slow heating rates, the overshoot not only increases the warpage due to a slightly higher temperature, but

also causes a reduction in the modulus, resulting in an increase in warpage due to thermal softening.

Table 5.19 - Sensitivity to maximum temperature

Temperature (°C)	0.10 °C/min		2.50 °C/min	
	Deflection (mm)	Difference (%)	Deflection (mm)	Difference (%)
185	0.3436	6.77	0.4320	2.86
180	0.3281	1.97	0.4249	1.17
178	0.3237	0.59	0.4217	0.40
177	0.3218	0.00	0.4200	0.00
176	0.3201	-0.53	0.4183	-0.41
175	0.3185	-1.01	0.4165	-0.83
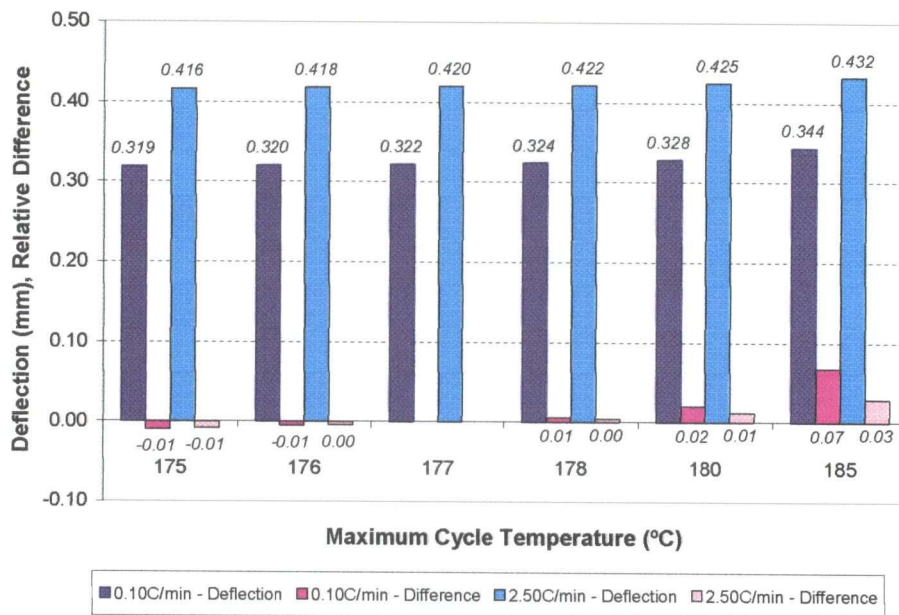
Figure 5.54 - Sensitivity of an idealized two-step cycle to the maximum cycle temperature

5.8.3   Sensitivity of idealized cycles to the ramp rate

To determine the sensitivity of the idealized cycle to the ramp rate, a two-step cycle was simulated on virtual specimens with different ramp rates between the first and second dwell temperatures. The two-step cycle consisting of a 120°C dwell for 330 minutes followed by a ramp to 177°C at 2.5°C/min and a hold for 30 minutes was chosen as the baseline for relative difference calculations. The ramp rate was then varied between 0.1°C/min and 10.0°C/min to determine the effect on the final deflection.

Figure 5.55 shows the temperature profiles for two-step cycles with ramp rates of 0.1 °C/min and 10.0 °C/min and the resulting deflections for the different ramp rates in the time domain. Similarly *Figure 5.56* shows the development of the adhesive layer's shear modulus and the resulting deflections for the different ramp rates in the temperature domain.
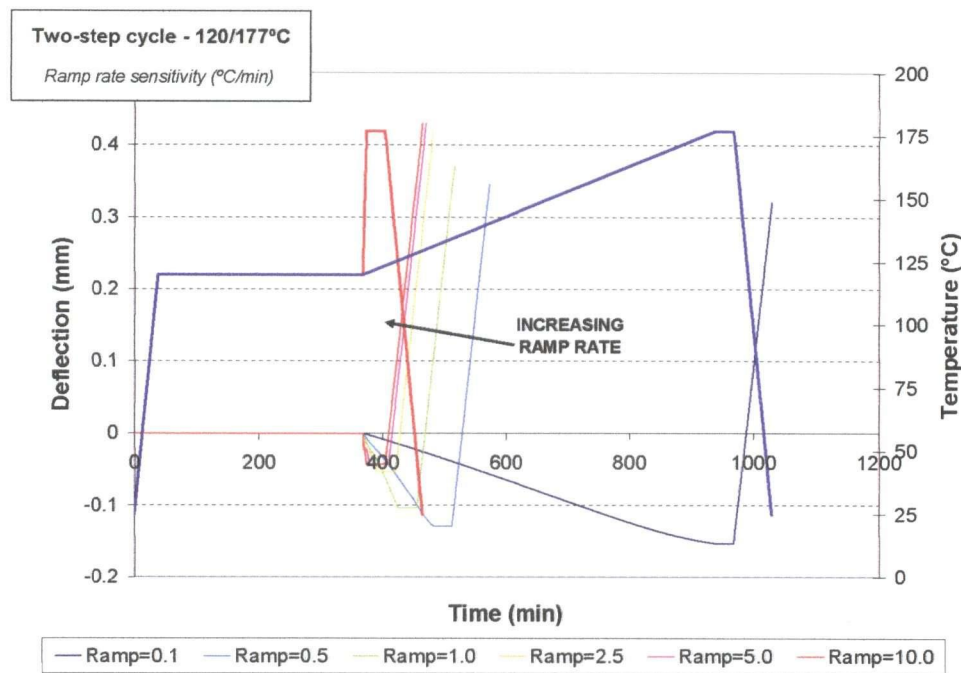
Figure 5.55 - Time domain results for ramp rate sensitivity of an idealized two-step cycle
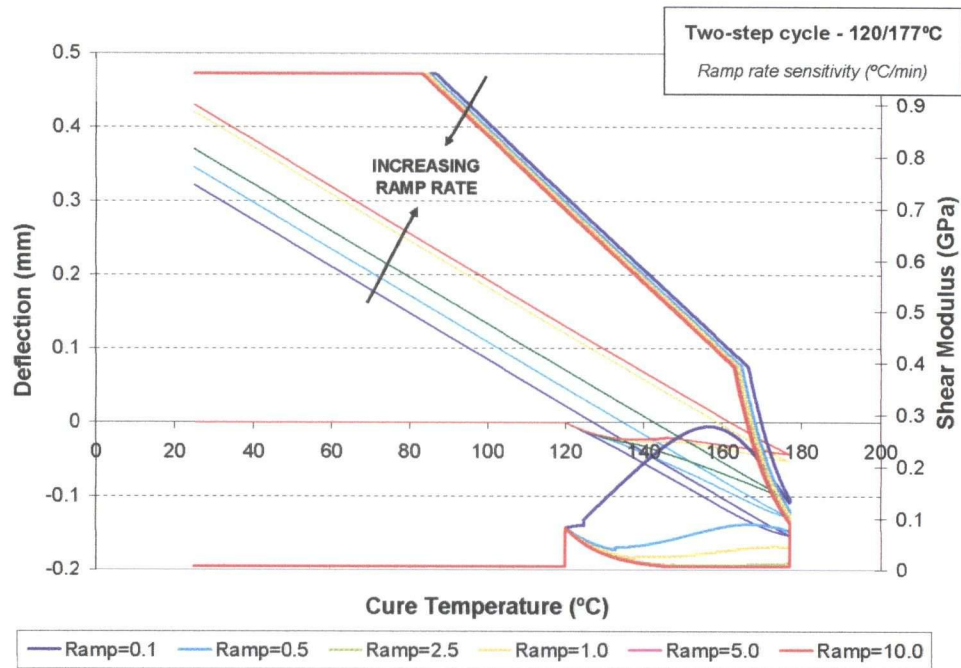
Figure 5.56 - Temperature domain results for ramp rate sensitivity of an idealized two-step cycle

Table 5.20 - Sensititvity to ramp rate

Ramp rate (°C/min)	Deflection (mm)	Difference (%)
0.1	0.3220	-23.33
0.5	0.3450	-17.86
1.0	0.3700	-11.90
2.5	0.4200	0.00
5.0	0.4300	2.38
10.0	0.4300	2.38

114
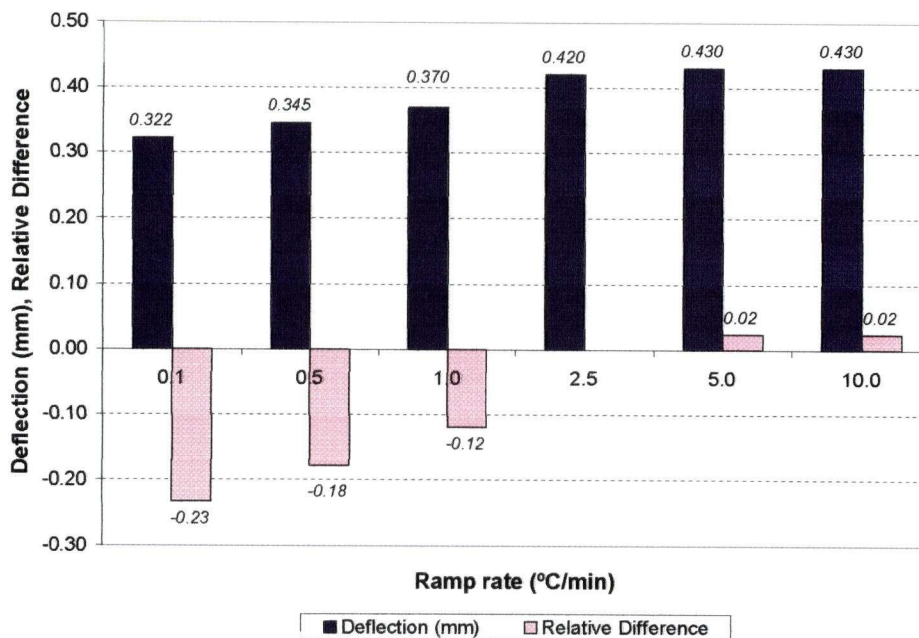
Figure 5.57 - Sensitivity of an idealized two-step cycle to the ramp rate

The results of the ramp rate sensitivity study and the relative differences are tabulated in *Table 5.20* and presented graphically *Figure 5.57*. These results show how important accurate temperature control is during the ramp. In *Figure 5.56* we see that when slower ramp rates are used the shear modulus during the ramp can remain considerably higher than the fully relaxed shear modulus. For faster heating rate, however, the effect of two-step curing is largely negated due to thermal softening during heat-up as the adhesive's shear modulus drops towards the fully relaxed value. For the two fastest heating rates investigated, the final deflection values are equal, as the adhesive's shear modulus dropped to the fully relaxed modulus in both cycles.

6. __Conclusions__

The objective of this thesis was to develop and validate a simple and efficient technique for cure cycle optimization of bonded composite patch repair using a Dynamic Mechanical Analyzer (DMA). Thus the DMA beam technique was shown to be an effective, versatile method of characterizing materials, as well as monitoring the out of plane deflection of bonded composite patch repair specimens throughout a cure cycle. Insight gained from these measurements can be used to optimize cure cycles so as to reduce the thermally induced residual stresses in real applications of bonded composite patch repairs.

Bimaterial beam technique

A bimaterial beam technique was used to extract unknown viscoelastic material properties of a polymeric material from the system's material properties. Relaxation tests were performed in a DMA on both monolithic Lexan specimens and bimaterial steel/Lexan specimens. The viscoelastic response of Lexan was then extracted from the bimaterial system response and compared to the monolithic response. Tests were conducted well below the glass transition temperature of Lexan and results showed good agreement between the relaxation modulus of Lexan as extracted from the bimaterial system response and the monolithic Lexan response, with an error of less than 8% for the highest temperatures tested and better agreement at lower temperatures.

Material Characterization

The modulus of an aerospace grade adhesive, FM300, was characterized using a DMA bimaterial beam technique. Bimaterial beams consisting of an elastic shim and an uncured layer of FM300 were cured in the DMA at a variety of isothermal temperatures, while a cyclic deflection was applied. Using a cure kinetics model and a glass transition temperature model, the modulus was shown to be an instantaneous function of the difference between the temperature and the glass transition temperature.

Bonded Composite Patch Repair Specimens

The development of deflection in bonded composite patch repair specimens consisting of an elastic substrate (steel), a curing adhesive (FM300), and a composite patch (AS4/3501-6), throughout a cure cycle were measured in-situ using a DMA. The effect of modifying the cure cycle on the development of thermally induced warpage was investigated. For one-step cycles, although a reduction in the cure cycle temperature results in a reduction in the final deflection values, a marked drop in the final degree of cure also occurs that may be unacceptable for some applications. Post-curing the specimens increases the final degree of cure but negates some of the benefits of a lower initial cure temperature. For the two-step cycles, reducing the first dwell temperature results in a reduction in warpage. The ramp rate between the first and second dwell was found to be an important factor in the generation of warpage. Slow ramp rates allow the glass transition temperature to develop and keep pace with the increase in temperature. For faster rates, the temperature increase outpaces the development of glass transition temperature resulting in thermal softening, which adversely affects warpage. Thus slow rates result in a reduction in warpage when compared to faster rates.

A wide scatter in experimental results was noted. Due to the small specimen size the experimental method is sensitive to variations in geometry, most notably in the adhesive layer thickness. Scaling the results to a standard adhesive layer thickness reduced the degree of scatter considerably.

Bonded Composite Patch Repair Model

A modified CHILE model, which incorporates both cure hardening and thermal softening behaviour for the adhesive layer, was shown to accurately predict the development of warpage in bonded composite patch repair specimens. Model results agree well with experimental values for a wide range of cure cycles. The addition of a thermal softening term has the potential to expand the applicability of pseudo-viscoelastic models.

The modified CHILE model was then used to study the response of a virtual specimen subjected to idealized cycles. Results showed a number of differences between the idealized

117

cycles and the actual DMA cycles. These differences are attributed to temperature control problems in the DMA, both due to poor control during temperature ramps, which result a temperature profile that oscillates about the desired ramp rate, and overshoots when transitioning from a ramp to a hold. The results indicate that improved temperature control could improve the effectiveness of cure cycle optimization by as much as 25%.

In an attempt to quantify the effects of variation in specimen geometry and poor temperature control, the sensitivity of the model to changes in adhesive layer thickness, ramp rate, and maximum cycle temperature were examined. Results show that considerable variations in deflection occur as a result of changes to the adhesive layer thickness or ramp rate, while the maximum cure cycle temperature was not found to affect deflections significantly.

7. **Future Work**

As the main impetus for the design of an optimized cure cycle is an increase in the fatigue life of the repair, it is important to correlate reductions in thermally induced residual stresses (or conversely warpage) with increases in fatigue life. While other researchers have studied the long-term effects of cure cycle optimization, no such attempt has been made herein. Long-term fatigue tests of the cure cycles investigated in this work should be performed to determine how reductions in warpage affect the patch repair's fatigue life. Such a study would help designers determine what trade-offs, in terms of costs associated with processing time and sophistication of heating and temperature control systems versus increased fatigue life, are acceptable for specific repair applications.

Although the developed CHILE with thermal softening model agrees well with experimental results for FM300, results from other researchers into the behaviour of similar adhesives show very different constitutive responses. Work by Djokic [73] on FM73 shows significant stress relaxation throughout the cure cycle. Stress relaxation, much like thermal softening, results in a lessening of the benefits of cure cycle optimization. No attempt was made in this work to determine the causes of the difference in behaviour between these adhesive systems. It may therefore prove fruitful to test bonded composite patch repair specimens with FM73 adhesive. Results could help determine whether the thermal softening phenomena is an artefact of the experimental method and/or specimen size. Should FM73 exhibit behaviour similar to that reported for FM300, experiments could be undertaken to determine if FM300 exhibits viscoelastic behaviour in larger sized bonded composite patch repair specimens. These results could help quantify the effect of size on the analysis method proposed herein.

Cocuring of the adhesive layer has been proposed as a method of decreasing the downtime associated with structural repair. Patches could easily be designed to mate with complex aerodynamic surfaces and cured in-situ without the need for a tool or an autoclave. To the best of the author's knowledge, no studies have focused on the effects of cocuring the patch. Cocuring may also negate the need for an adhesive layer, as it may be possible to design the curing patch's material such that adhesion with the substrate is assured.

119

Newer DMA models such as the TA Instruments Q800 DMA may allow the operator to measure the out of plane deflection caused by thermally induced stresses, while simultaneously applying a small dynamic disturbance. This would allow measurement of both thermally induced deflection and instantaneous modulus in-situ throughout the entire cure cycle. This test methodology would eliminate a number of the intermediate steps necessary for model predictions and the associated error. It would also effectively combine characterization of the adhesive layer's instantaneous modulus and development of deflection in bonded composite patch repairs. Characterizing the adhesive layer's modulus in this type of test would also improve dimensional stability, a major source of error for the modulus characterization test; Having the patch layer on top of the adhesive minimizes adhesive flow and creates a more consistent adhesive layer thickness.

Slowing the ramp rate between the first and second dwell temperatures has been shown to be an effective method of optimization. This method has however been shown to have a practical limitation, as the model predicts a maximum achievable modulus at the end of the ramp, $G_a(T^* = T_{max} - T_{g,\infty})$. In some cases, constant ramp rates allow the modulus to increase above this value during the ramp, indicating a ramp rate that is slower than necessary. Conversely, if the modulus drops below this value thermal softening will occur, adversely affecting warpage and indicating that the ramp rate that is too fast. Building on this technique further, a feedback control scheme could be developed whereby the rate of temperature increase could be controlled using a measurement of the material's instantaneous modulus; should the modulus drop below a preset threshold, the thermal ramp rate would be slowed, while if it rises above the theoretical maximum achievable modulus, the ramp rate could be increased.

8. <u>References</u>

[1]   Chester,R.J., Walker,K.F., and Chalkley,P.D., "Adhesively Bonded Repairs to Primary Aircraft Structure", International Journal of Adhesion and Adhesives, Vol. 19, No. 1, pp. 1-8, 1999.

[2]   Ong,C.L. and Shen,S.B., "The Reinforcing Effect of Composite Patch Repairs on Metallic Aircraft Structures", International Journal of Adhesion and Adhesives, Vol. 12, No. 1, pp. 19-26, 1992.

[3]   Hyer,M.W., "Stress Analysis of Fiber-Reinforced Composite Materials", 1998.

[4]   Canadian Institute of Steel Construction, "Handbook of Steel Construction", Vol. 4th, 1985.

[5]   Cho,J. and Sun,C.T., "Lowering Thermal Residual Stresses in Composite Patch Repairs in Metallic Aircraft Structure", AIAA Journal, Vol. 39, No. 10, pp. 2013-2018, 2001.

[6]   Umamaheswar,T.V.R.S. and Singh,R., "Modelling of a Patch Repair to a Thin Cracked Sheet", Engineering Fracture Mechanics, Vol. 62, No. 2-3, pp. 267-289, 1999.

[7]   Davis,M. and Bond,D., "Principles and Practices of Adhesive Bonded Structural Joints and Repairs", International Journal of Adhesion and Adhesives, Vol. 19, No. 2-3, pp. 91-105, 1999.

[8]   Baker,A.A. and Chester,R.J., "Recent Advances in Bonded Composite Repair Technology for Metallic Aircraft Components", pp. 45-49, 1993.

[9]   Kerr,A. and Ruddy,J., "Development of a Bonded Repair for the F-16FS479 Bulkhead Vertical Tail Attach Bosses", Applied Composite Materials, Vol. 6, No. 4, pp. 239-249, 1999.

[10] Bartholomeusz,R.A., Baker,A.A., Chester,R.J., and Searl,A., "Bonded Joints With Through-Thickness Adhesive Stresses - Reinforcing the F/A-18 Y470.5 Bulkhead", International Journal of Adhesion and Adhesives, Vol. 19, No. 2-3, pp. 173-180, 1999.

[11] Baker,A.A., Rose,L.R.F., Walker,K.F., and Wilson,E.S., "Repair Substantiation for a Bonded Composite Repair to F111 Lower Wing Skin", Applied Composite Materials, Vol. 6, No. 4, pp. 251-267, 1999.

[12] Jones,R., Molent,L., and Pitt,S., "Study of Multi-Site Damage of Fuselage Lap Joints", Theoretical and Applied Fracture Mechanics, Vol. 32, No. 2, pp. 81-100, 1999.

[13] Lange,J., Toll,S., Manson,J.A.E., and Hult,A., "Residual Stress Build-Up in Thermoset Films Cured Below Their Ultimate Glass Transition Temperature", Polymer, Vol. 38, No. 4, pp. 809-815, 1997.

[14] Sourour,S. and Kamal,M.R., "Differential Scanning Calorimetry of Epoxy Cure - Isothermal Cure Kinetics", Thermochimica Acta, Vol. 14, No. 1-2, pp. 41-59, 1976.

[15] Shutilin,Y.F., "On Application of Williams-Landel-Ferry and Arrhenius Equations to Description of Relaxational Properties of Polymers and Polymer Homologs", Vysokomolekulyarnye Soedineniya Seriya A, Vol. 33, No. 1, pp. 120-127, 1991.

[16] Hutchinson,J.M. and Montserrat,S., "A Theoretical Model of Temperature-Modulated Differential Scanning Calorimetry in the Glass Transition Region", Thermochimica Acta, Vol. 305, pp. 257-265, 1997.

[17] Djokic,D., Johnston,A., Rogers,A., Lee-Sullivan,P., and Mrad,N., "Residual Stress Development During the Composite Patch Bonding Process: Measurement and Modeling", Composites Part A-Applied Science and Manufacturing, Vol. 33, No. 2, pp. 277-288, 2002.

[18] Sideridou,I., Achilias,D.S., and Kyrikou,E., "Thermal Expansion Characteristics of Light-Cured Dental Resins and Resin Composites", Biomaterials, Vol. 25, No. 15, pp. 3087-3097, 2004.

[19] Ramis,X., Cadenato,A., Morancho,J.M., and Salla,J.M., "Curing of a Thermosetting Powder Coating by Means of DMTA, TMA and DSC", Polymer, Vol. 44, No. 7, pp. 2067-2079, 2003.

[20] Rieger,J., "The Glass Transition Temperature T-g of Polymers - Comparison of the Values From Differential Thermal Analysis (DTA, DSC) and Dynamic Mechanical Measurements (Torsion Pendulum)", Polymer Testing, Vol. 20, No. 2, pp. 199-204, 2001.

[21] Chern,C.S. and Poehlein,G.W., "A Kinetic-Model for Curing Reactions of Epoxides With Amines", Polymer Engineering and Science, Vol. 27, No. 11, pp. 788-795, 1987.

[22] Hojjati,M. and Johnson,A.F., "Stress Relaxation Behaviour of Cytec FM73 Adhesive During Cure", 2002.

[23] Kim,Y.K. and White,S.R., "Stress Relaxation Behavior of 3501-6 Epoxy Resin During Cure", Polymer Engineering and Science, Vol. 36, No. 23, pp. 2852-2862, 1996.

[24] Kim,J., Moon,T.J., and Howell,J.R., "Cure Kinetic Model, Heat of Reaction, and Glass Transition Temperature of AS4/3501-6 Graphite-Epoxy Prepregs", Journal of Composite Materials, Vol. 36, No. 21, pp. 2479-2498, 2002.

[25]   McCrum,N.G., Buckley,C.P., and Bucknall,C.B., "Principles of Polymer Engineering", Vol. 2nd, 1997.

[26]   Roylance,D., "Engineering Viscoelasticity", 2001.

[27]   Flügge,W., "Viscoelasticity", Vol. 7th, 1967.

[28]   Ferry,J.D., "Viscoelastic Properties of Polymers", Vol. 3rd, 1980.

[29]   Brostow,W., "Temperature Shift Factor - Polymer Mechanical-Properties Above and Below Glass-Transition", Materials Chemistry and Physics, Vol. 13, No. 1, pp. 47-57, 1985.

[30]   Brostow,W., "Time-Stress Correspondence in Viscoelastic Materials: an Equation for the Stress and Temperature Shift Factor", Materials Research Innovations, Vol. 3, No. 6, pp. 347-351, 2000.

[31]   Akinay,A.E., Brostow,W., Castano,V.M., Maksimov,R., and Olszynski,P., "Time-Temperature Correspondence Prediction of Stress Relaxation of Polymeric Materials From a Minimum of Data", Polymer, Vol. 43, No. 13, pp. 3593-3600, 2002.

[32]   Akinay,A.E. and Brostow,W., "Long-Term Service Performance of Polymeric Materials From Short-Term Tests: Prediction of the Stress Shift Factor From a Minimum of Data", Polymer, Vol. 42, No. 10, pp. 4527-4532, 2001.

[33]   Simon,S.L., McKenna,G.B., and Sindt,O., "Modeling of the Evolution of the Dynamic Mechanical Properties of a Commercial Epoxy During Cure After Gelation", Journal of Applied Polymer Science, Vol. 76, pp. 495-508, 2000.

[34]   Eom,Y., Boogh,L., Michaud,V., Sunderland,P., and Manson,J.A., "Time-Cure-Temperature Superposition for the Prediction of Instantaneous Viscoelastic Properties During Cure", Polymer Engineering and Science, Vol. 40, No. 6, pp. 1281-1292, 2000.

[35]   O'Brien,D.J., Mather,P.T., and White,S.R., "Viscoelastic Properties of an Epoxy Resin During Cure", Journal of Composite Materials, Vol. 35, No. 10, pp. 883-904, 2001.

[36]   Zobeiry,N., Vaziri R., and Poursartip A., "Computationally Efficient Pseudo-Viscoelastic Models for Evaluation of Residual Stresses in Thermoset Polymer Composites During Cure", to be published in Composites: Part A, 2005.

[37]   Cook,W.D., Scott,T.F., Quay-Thevenon,S., and Forsythe,J.S., "Dynamic Mechanical Thermal Analysis of Thermally Stable and Thermally Reactive Network Polymers", Journal of Applied Polymer Science, Vol. 93, No. 3, pp. 1348-1359, 2004.

[38]   Johnston,A., Vaziri,R., and Poursartip,A., "A Plane Strain Model for Process-Induced Deformation of Composite Structures", Journal of Composite Materials, 2001.

[39] Svanberg,J.M. and Holmberg,J.A., "Prediction of Shape Distortions Part I. FE-Implementation of a Path Dependent Constitutive Model", Composites Part A-Applied Science and Manufacturing, Vol. 35, No. 6, pp. 711-721, 2004.

[40] Svanberg,J.M. and Holmberg,J.A., "Prediction of Shape Distortions. Part II. Experimental Validation and Analysis of Boundary Conditions", Composites Part A-Applied Science and Manufacturing, Vol. 35, No. 6, pp. 723-734, 2004.

[41] Sun,C.T., Klug,J., and Arendt,C., "Analysis of Cracked Aluminum Plates Repaired With Bonded Composite Patches", AIAA Journal, Vol. 34, No. 2, pp. 369-374, 1996.

[42] Klug,J., Maley,S., and Sun,C.T., "Characterization of Fatigue Behavior of Bonded Composite Repairs", Journal of Aircraft, Vol. 36, No. 6, pp. 1016-1022, 1999.

[43] Lena,M.R., Klug,J.C., and Sun,C.T., "Composite Patches As Reinforcements and Crack Arrestors in Aircraft Structures", Journal of Aircraft, Vol. 35, No. 2, pp. 318-323, 1998.

[44] Naboulsi,S. and Mall,S., "Modeling of a Cracked Metallic Structure With Bonded Composite Patch Using the Three Layer Technique", Composite Structures, Vol. 35, No. 3, pp. 295-308, 1996.

[45] Naboulsi,S. and Mall,S., "Nonlinear Analysis of Bonded Composite Patch Repair of Cracked Aluminum Panels", Composite Structures, Vol. 41, No. 3-4, pp. 303-313, 1998.

[46] Schubbe,J.J. and Mall,S., "Investigation of a Cracked Thick Aluminum Panel Repaired With a Bonded Composite Patch", Engineering Fracture Mechanics, Vol. 63, No. 3, pp. 305-323, 1999.

[47] Rose,L.R.F., "An Application of the Inclusion Analogy for Bonded Reinforcements", International Journal of Solids and Structures, Vol. 17, No. 8, pp. 827-838, 1981.

[48] Wang,C.H., Rose,L.R.F., Callinan,R., and Baker,A.A., "Thermal Stresses in a Plate With a Circular Reinforcement", International Journal of Solids and Structures, Vol. 37, No. 33, pp. 4577-4599, 2000.

[49] Daverschot,D.R., Vlot,A., and Woerden,H.J.M., "Thermal Residual Stresses in Bonded Repairs", Applied Composite Materials, Vol. 9, No. 3, pp. 179-197, 2002.

[50] Hojjati,M., Xiao,X., and Johnson,A.F., "Modelling of Residual Stress Development During Composite Patch Repair of Metallic Structures: a Litterature Review", 2000.

[51] Hojjati,M. and Johnson,A.F., "Closed-Form Solution for Residual Stress Development in a Simple Single-Sided Bonded Patch Repair", 2002.

[52]   White,S.R. and Hahn,H.T., "Process Modeling of Composite Materials: Residual Stress Development During Cure. Part II. Experimental Validation", Journal of Composite Materials, Vol. 26, No. 16, pp. 2423-2453, 1992.

[53]   Crasto,A., Kim,R.Y., and Russell,J.D., "In Situ Monitoring of Residual Strain Development During Composite Cure", 44th International SAMPE Symposium, pp. 1706-1717, 1999.

[54]   Crasto,A.S. and Kim,R.Y., "On the Determination of Residual-Stresses in Fiber-Reinforced Thermoset Composites", Journal of Reinforced Plastics and Composites, Vol. 12, No. 5, pp. 545-558, 1993.

[55]   Cho,J. and Sun,C.T., "Lowering Thermal Residual Stresses in Bonded Composite Patch Repairs", Technical Conference, Vol. 14, 1999.

[56]   Kim,K.S. and Hahn,H.T., "Residual Stress Development During Processing of Graphite/Epoxy Composites", Composite Science and Technology, Vol. 36, pp. 121-132, 1989.

[57]   White,S.R. and Hahn,H.T., "Cure Cycle Optimization for the Reduction of Processing-Induced Residual-Stresses in Composite-Materials", Journal of Composite Materials, Vol. 27, No. 14, pp. 1352-1378, 1993.

[58]   Ramani,K. and Zhao,W.P., "The Evolution of Residual Stresses in Thermoplastic Bonding to Metals", International Journal of Adhesion and Adhesives, Vol. 17, No. 4, pp. 353-357, 1997.

[59]   Findik,F., Mrad,N., and Johnston,A., "Strain Monitoring in Composite Patched Structures", Composite Structures, Vol. 49, No. 3, pp. 331-338, 2000.

[60]   Ochi,M., Yamashita,K., and Shimbo,M., "The Mechanism for Occurrence of Internal-Stress During Curing Epoxide-Resins", Journal of Applied Polymer Science, Vol. 43, No. 11, pp. 2013-2019, 1991.

[61]   Schoch,K.F., Panackal,P.A., and Frank,P.P., "Real-Time Measurement of Resin Shrinkage During Cure", Thermochimica Acta, Vol. 417, No. 1, pp. 115-118, 2004.

[62]   Lange,J., Manson,J.A.E., and Hult,A., "Build-Up of Structure and Viscoelastic Properties in Epoxy and Acrylate Resins Cured Below Their Ultimate Glass Transition Temperature", Polymer, Vol. 37, No. 26, pp. 5859-5868, 1996.

[63]   Lange,J., Toll,S., Manson,J.A.E., and Hult,A., "Residual-Stress Buildup in Thermoset Films Cured Above Their Ultimate Glass-Transition Temperature", Polymer, Vol. 36, No. 16, pp. 3135-3141, 1995.

[64]   Motahhari,S. and Cameron,J., "The Contribution to Residual Stress by Differential Resin Shrinkage", Journal of Reinforced Plastics and Composites, Vol. 18, No. 11, pp. 1011-1020, 1999.

[65]   Kim,Y.K. and White,S.R., "Stress Relaxation Behavior of 3501-6 Epoxy Resin During Cure", Polymer Engineering and Science, Vol. 36, No. 23, pp. 2852-2862, 1996.

[66]   White,S.R. and Kim,Y.K., "Process-Induced Residual Stress Analysis of AS4/3501-6 Composite Material", Mechanics of Composite Materials and Structures, Vol. 5, No. 2, pp. 153-186, 1998.

[67]   White,S.R. and Hahn,H.T., "Process Modeling of Composite Materials: Residual Stress Development During Cure. Part I. Model Formation", Journal of Composite Materials, Vol. 26, No. 16, pp. 2402-2422, 1992.

[68]   Gopal,A.K., Adali,S., and Verijenko,V.E., "Optimal Temperature Profiles for Minimum Residual Stress in the Cure Process of Polymer Composites", Composite Structures, Vol. 48, No. 1-3, pp. 99-106, 2000.

[69]   Bogetti,T.A. and Gillespie,J.W., Jr., "Process-Induced Stress and Deformation in Thick-Section Thermoset Composite Laminates", Journal of Composite Materials, Vol. 26, No. 5, pp. 626-659, 1992.

[70]   Bogetti,T.A., Gillespie,J.W., and McCullough,R.L., "Influence of Processing on the Development of Residual Stresses in Thick Section Thermoset Composites", International Journal of Materials & Product Technology, Vol. 9, No. 1-3, pp. 170-182, 1994.

[71]   Cho,J. and Sun,C.T., "Modeling Thermal Residual Stresses in Composite Patch Repairs During Multitemperature Bonding Cycles", Journal of Aircraft, Vol. 40, No. 6, pp. 1200-1205, 2003.

[72]   Djokic,D., Hojjati,M., Johnston,A., and Lee-Sullivan,P., "Process Optimization for Reduction of Composite Patch Repair Residual Stresses", International SAMPE Technical Conference, Vol. 33, pp. 356-368, 2001.

[73]   Djokic, D., (2002). "Reduction of residual thermal stresses during bonded composite patch repair", M.S.Eng., University of New Brunswick,

[74]   Hojjati,M., Johnson,A.F., and Cole,K.C., "Cure Kinetics of Cytec FM73 Epoxy Adhesive", 2001.

[75]   Findik,F. and Unal,H., "Development of Thermal Residual Strains in a Single Sided Composite Patch", Composites Part B-Engineering, Vol. 32, No. 4, pp. 379-383, 2001.

[76]   Hibbeler,R.C., "Mechanics of Materials", Vol. 4th, 1999.

[77]   Rogers,A.D. and Lee-Sullivan,P., "An Alternative Model for Predicting the Cure Kinetics of a High Temperature Cure Epoxy Adhesive", Polymer Engineering and Science, Vol. 43, No. 1, pp. 14-25, 2003.

[78]   Twigg,G.A. and Poursartip A., 2005.

[79]   Hojjati,M., Johnston,A., Hoa,S.V., and Denault,J., "Viscoelastic Behavior of Cytec FM73 Adhesive During Cure", Journal of Applied Polymer Science, Vol. 91, No. 4, pp. 2548-2557, 2004.

[80]   Kim,K.S. and Hahn,H.T., "Residual-Stress Development During Processing of Graphite Epoxy Composites", Composites Science and Technology, Vol. 36, No. 2, pp. 121-132, 1989.

[81]   Loctite Corporation, "Hysol 9392 Epoxy Paste Adhesive", Vol. Rev 1, 2001.

[82]   Rheometric Scientific Incorporated, "Dynamic Mechanical Analyzer DMTA V, Document Manual 925-50010", No. Rev A, 1999.

[83]   Cytec Engineered Materials, "FM300 High Shear Strength Modified Epoxy Film Adhesive", 2005.

[84]   LaPlante,G. and Lee-Sullivan,P., "Moisture Effects on FM300 Structural Film Adhesive: Stress Relaxation, Fracture Toughness, and Dynamic Mechanical Analysis", Journal of Applied Polymer Science, Vol. 95, No. 5, pp. 1285-1294, 2005.

[85]   Roy,A.K. and Kim,R.Y., "Measurements for Determining the Thermal-Expansion Coefficient (CTE) of Laminated Orthotropic Rings", Journal of Reinforced Plastics and Composites, Vol. 12, No. 4, pp. 378-385, 1993.

Appendix A

Additional Bonded Composite Patch Repair Experimental Results
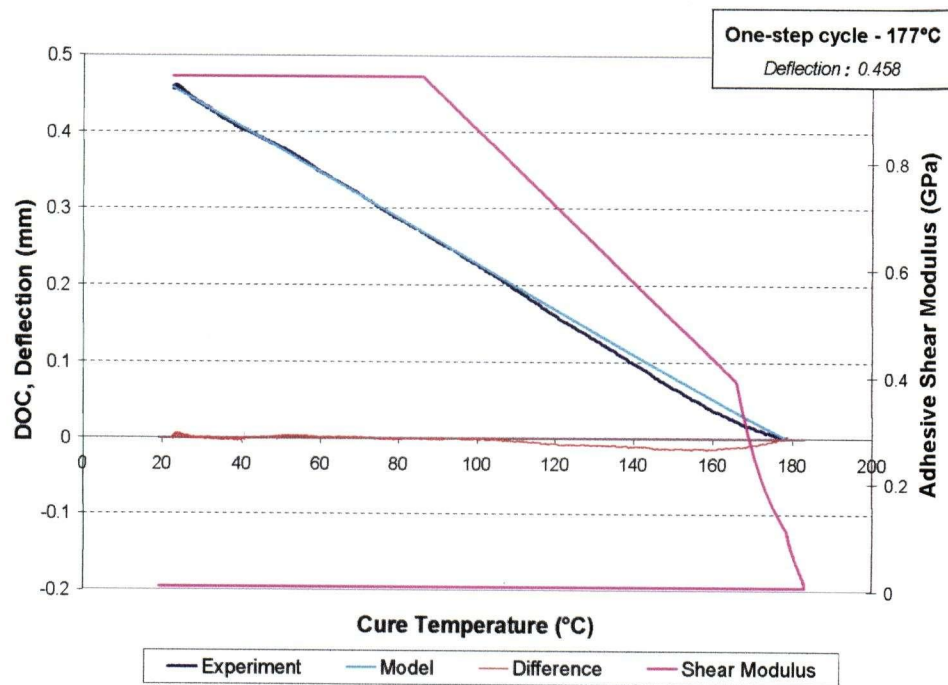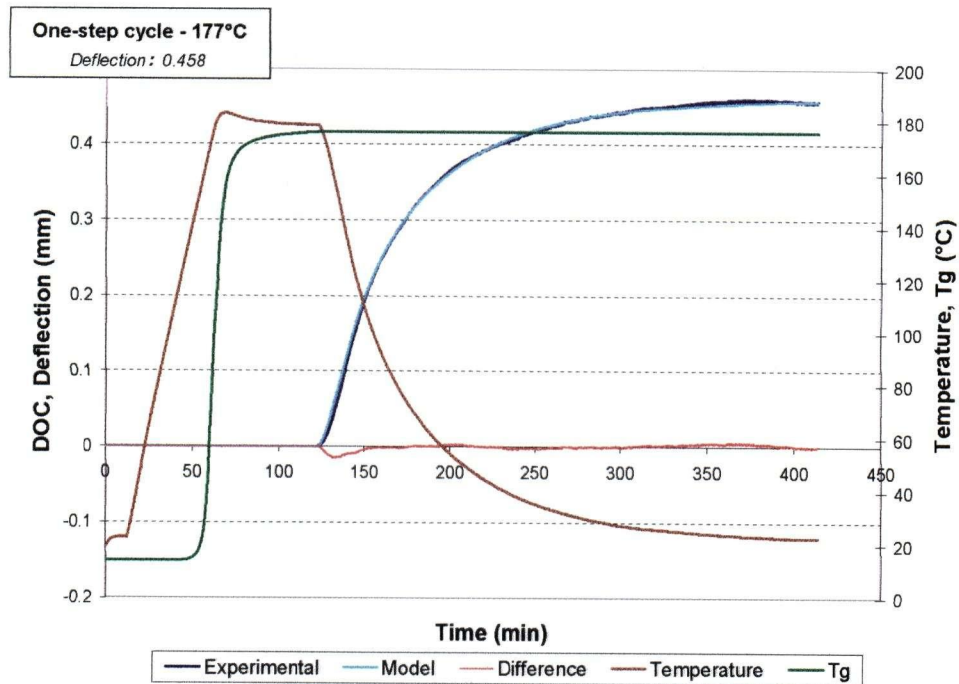
Figure A.1 - One-step cycle – 177°C - Specimen 1(a)

Experimental and model results in the time and temperature domains
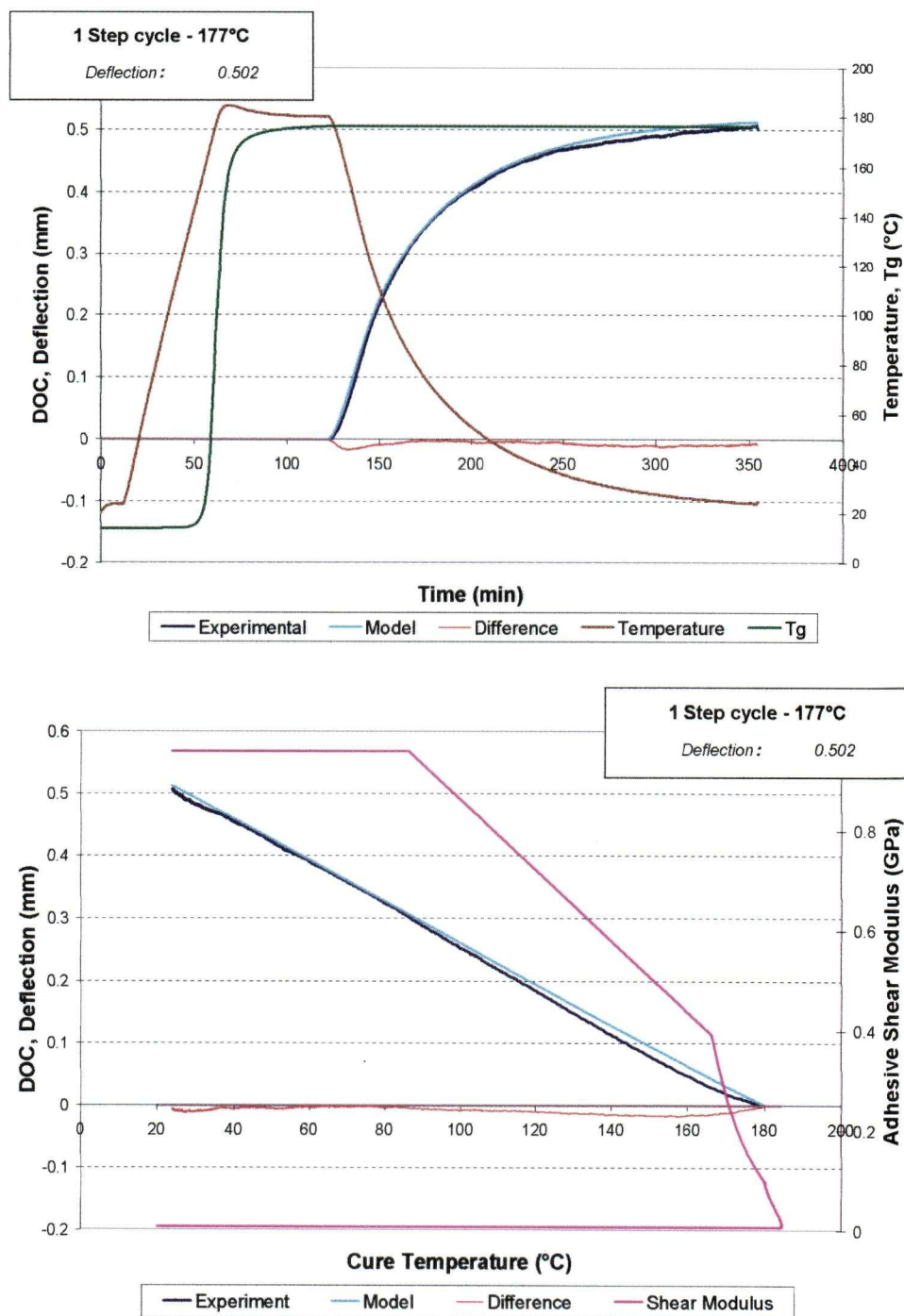
Figure A.2 - One-step cycle – 177°C - Specimen 1(b)

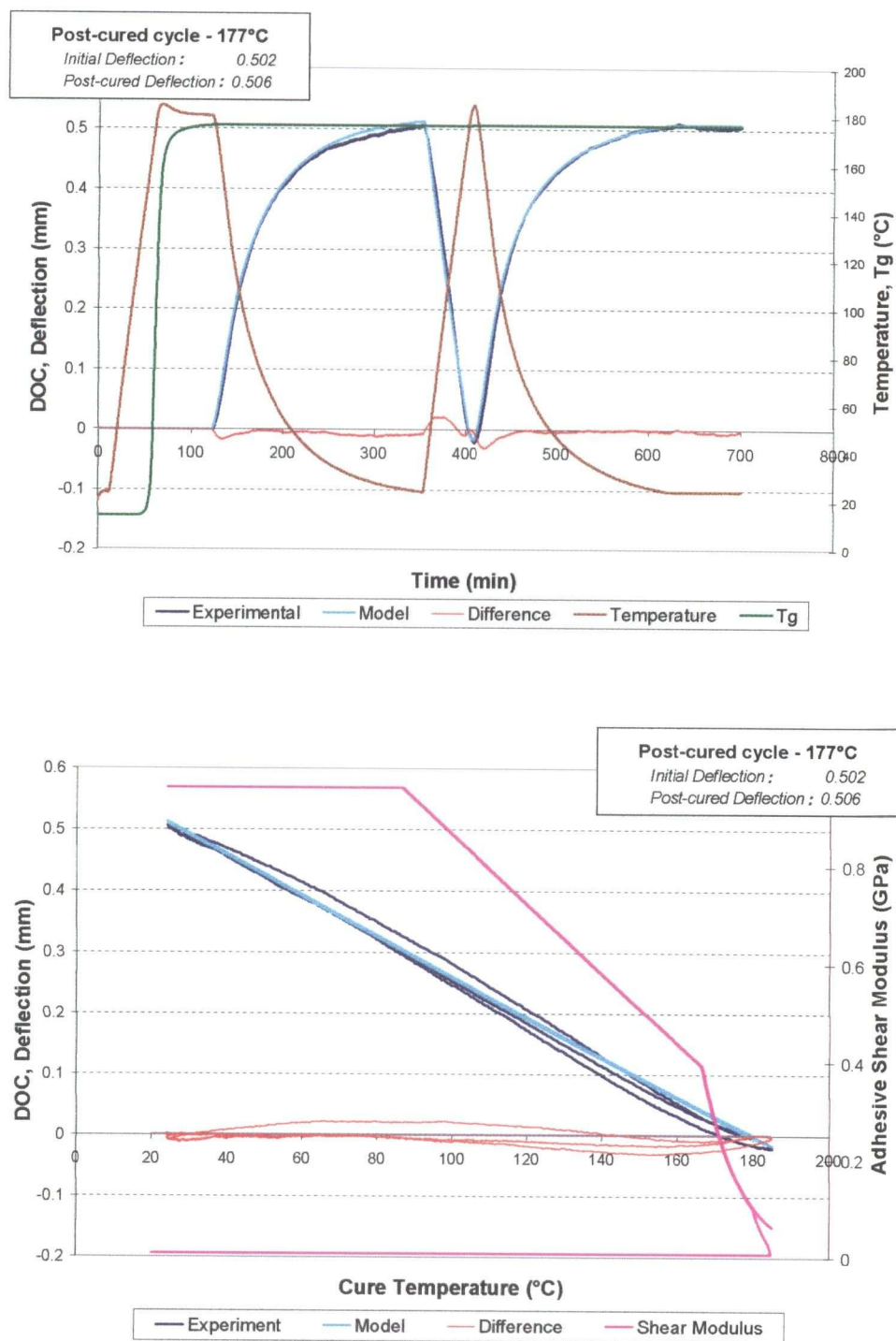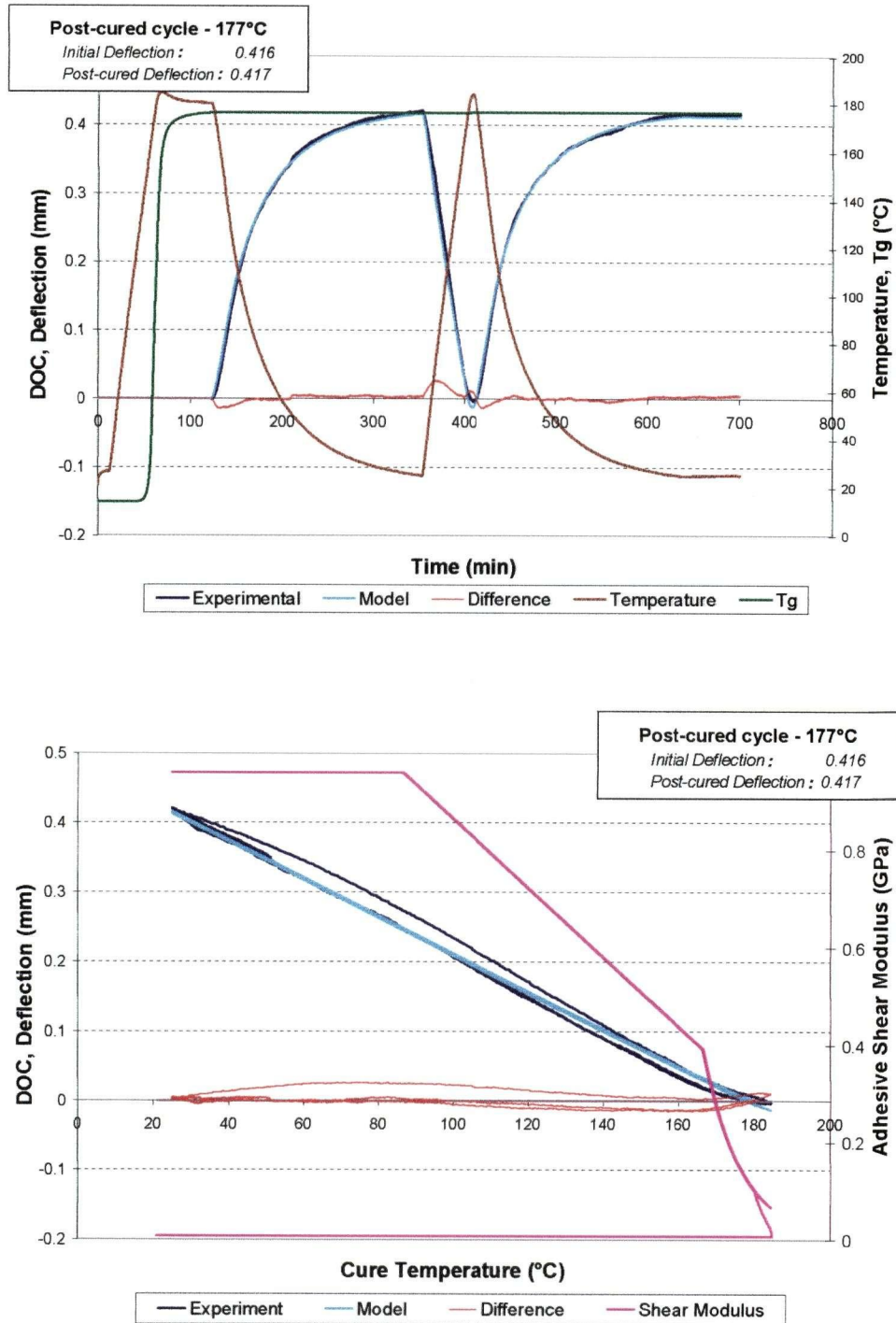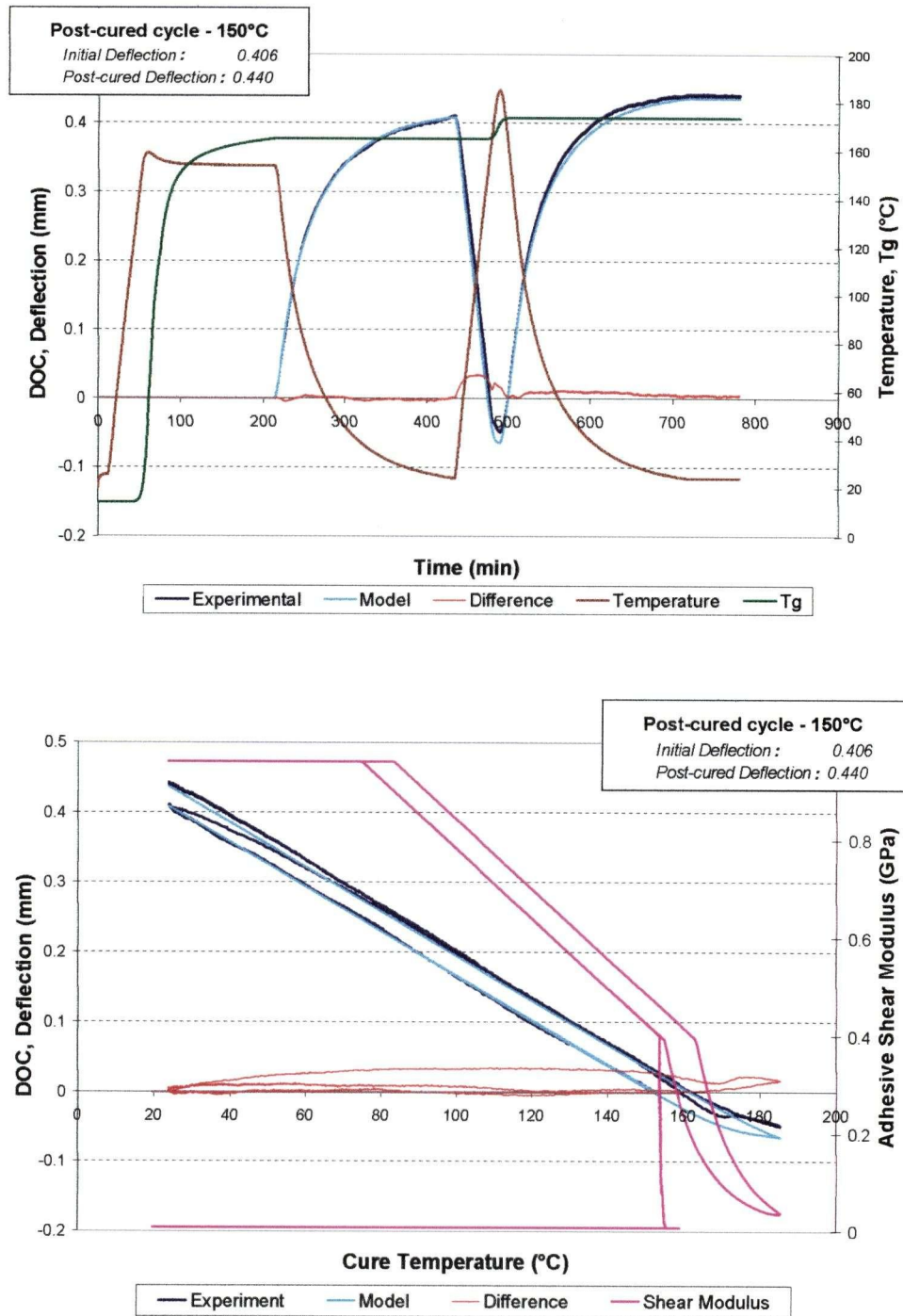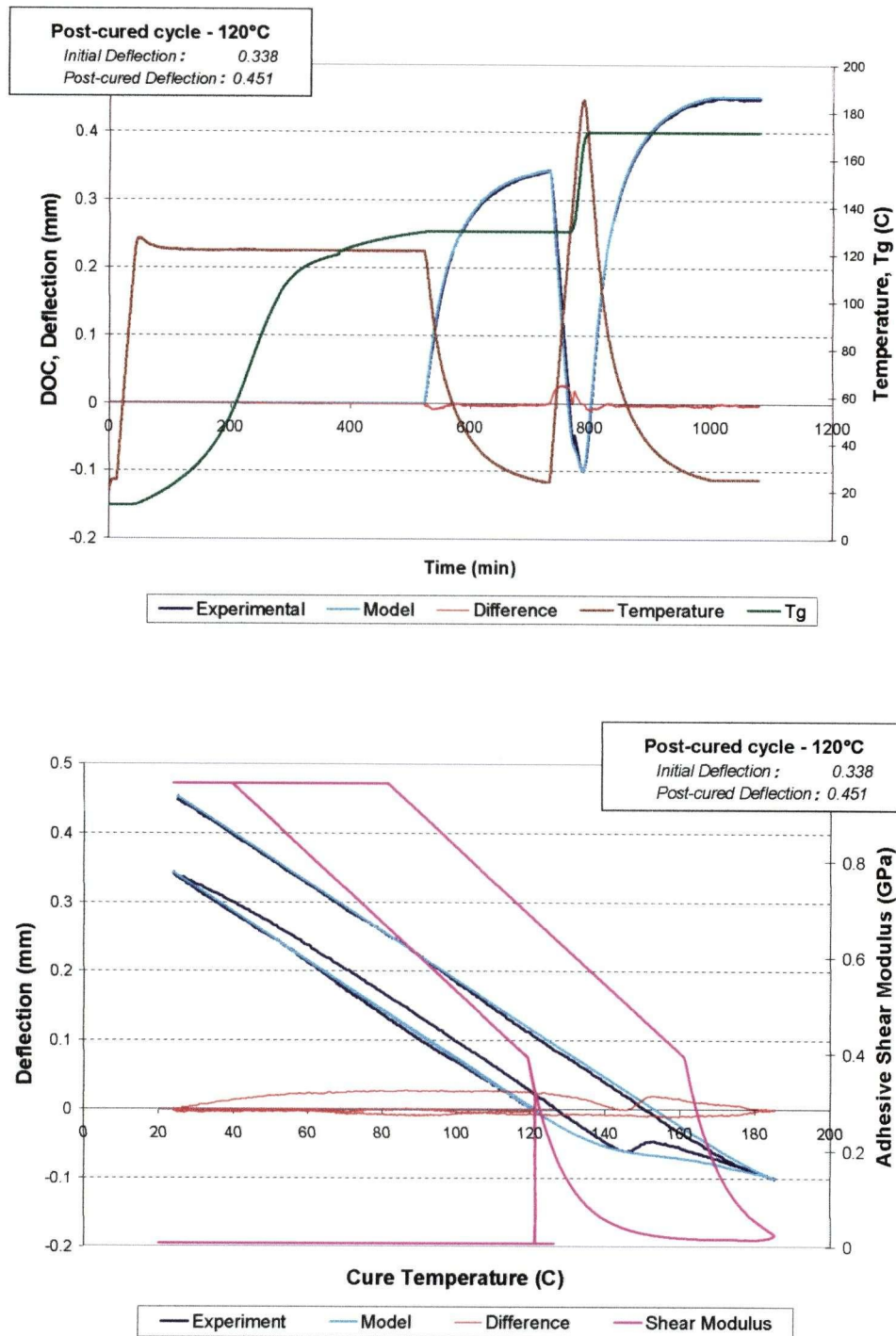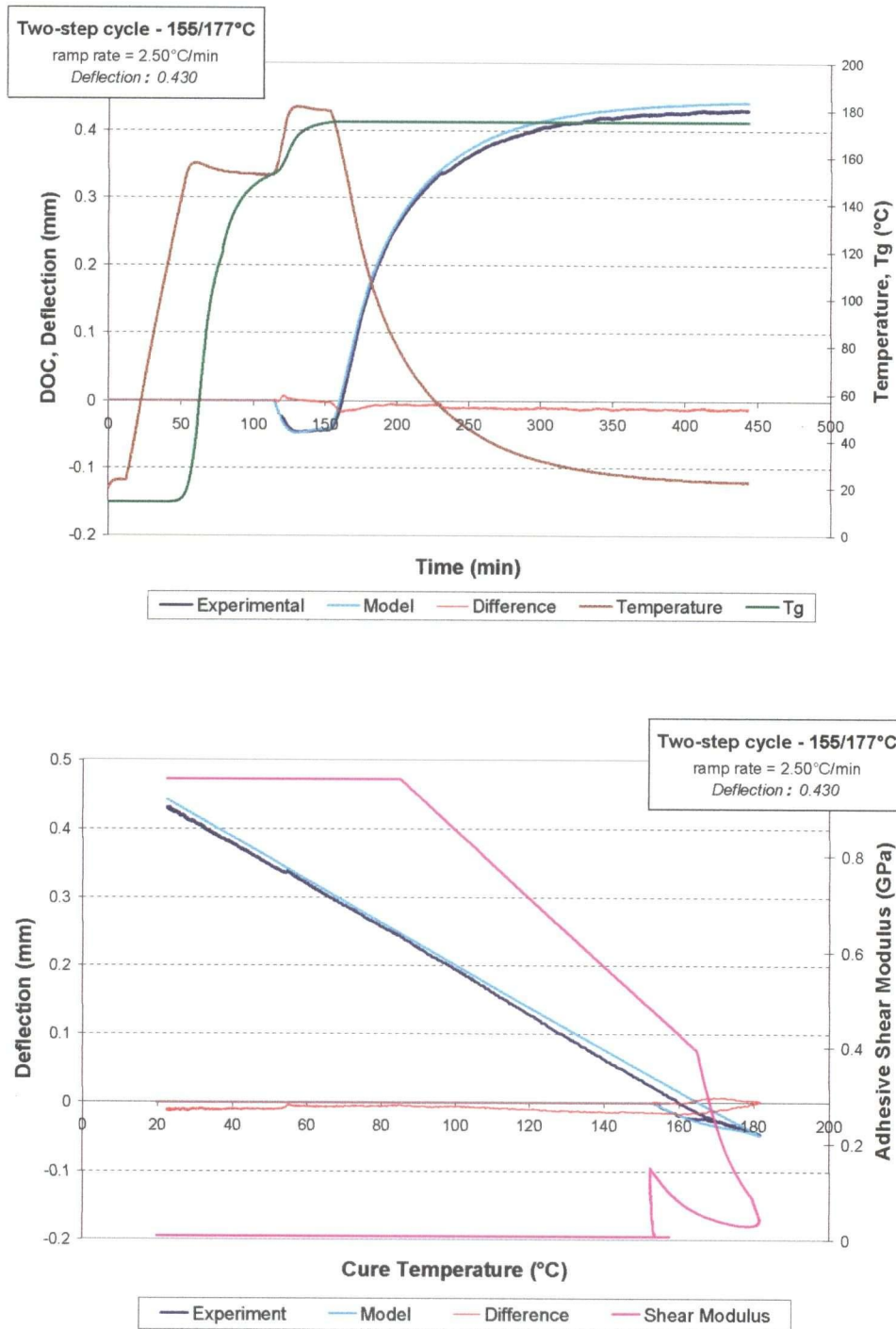**Experimental and model results in the time and temperature domains**
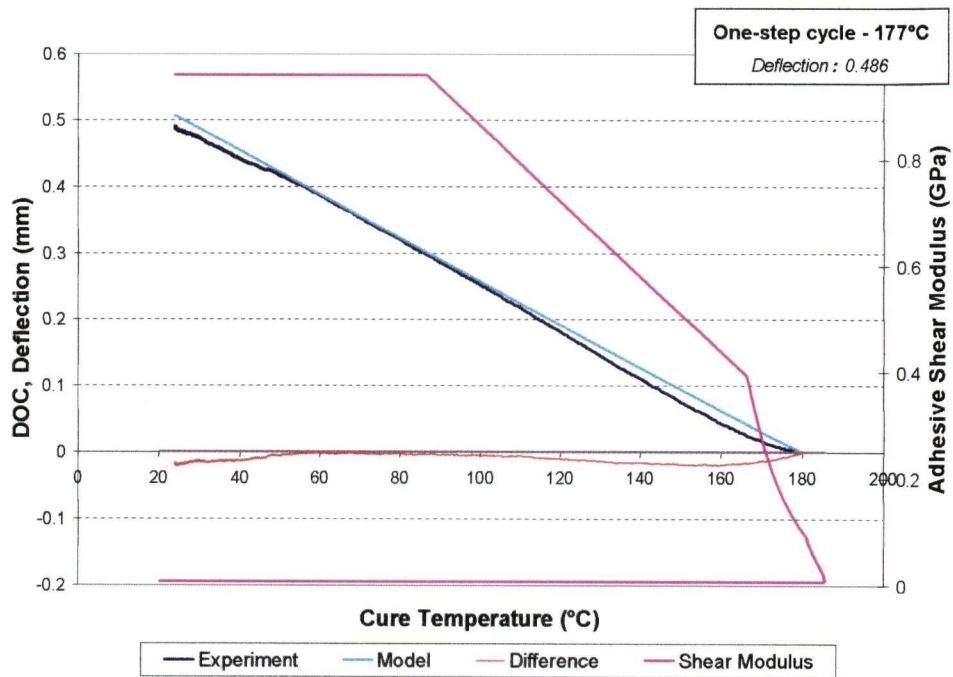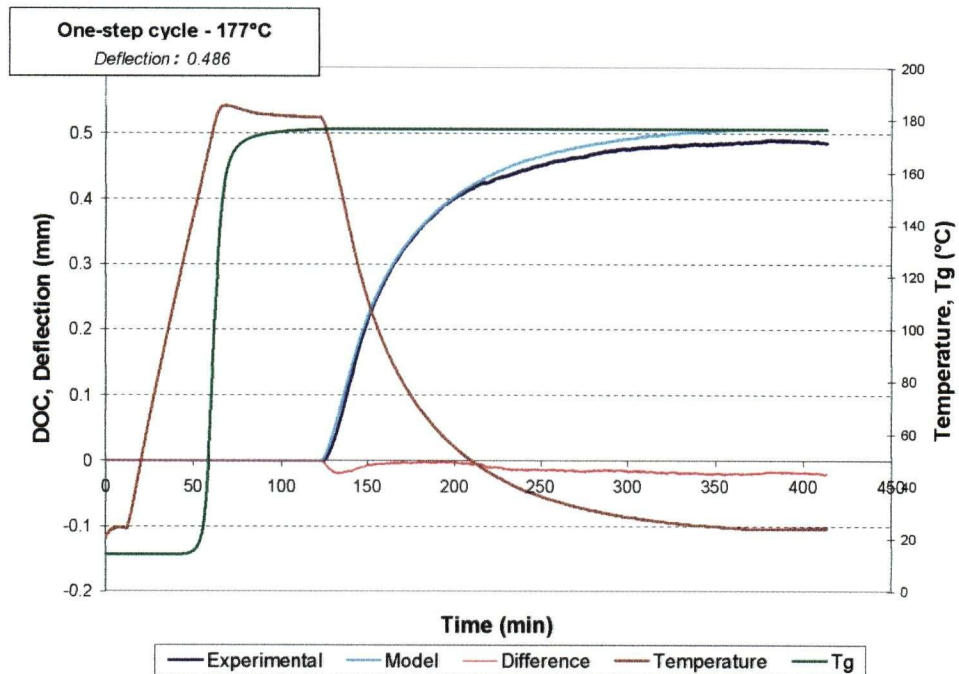
Figure A.3 - One-step cycle – 177°C - Specimen 1(c)

Experimental and model results in the time and temperature domains
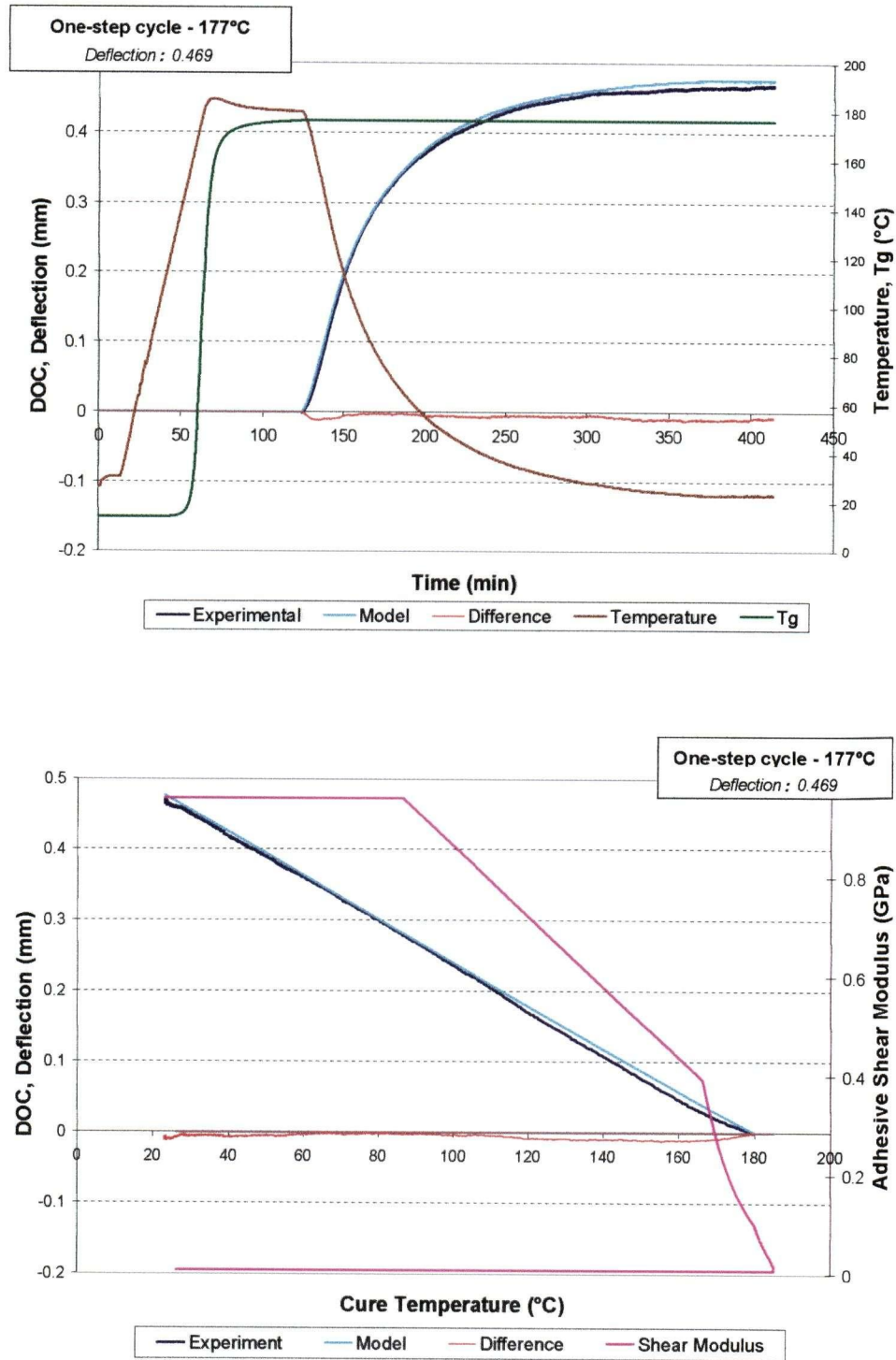
Figure A.4 - One-step cycle – 177°C - Specimen 1(d)

Experimental and model results in the time and temperature domains
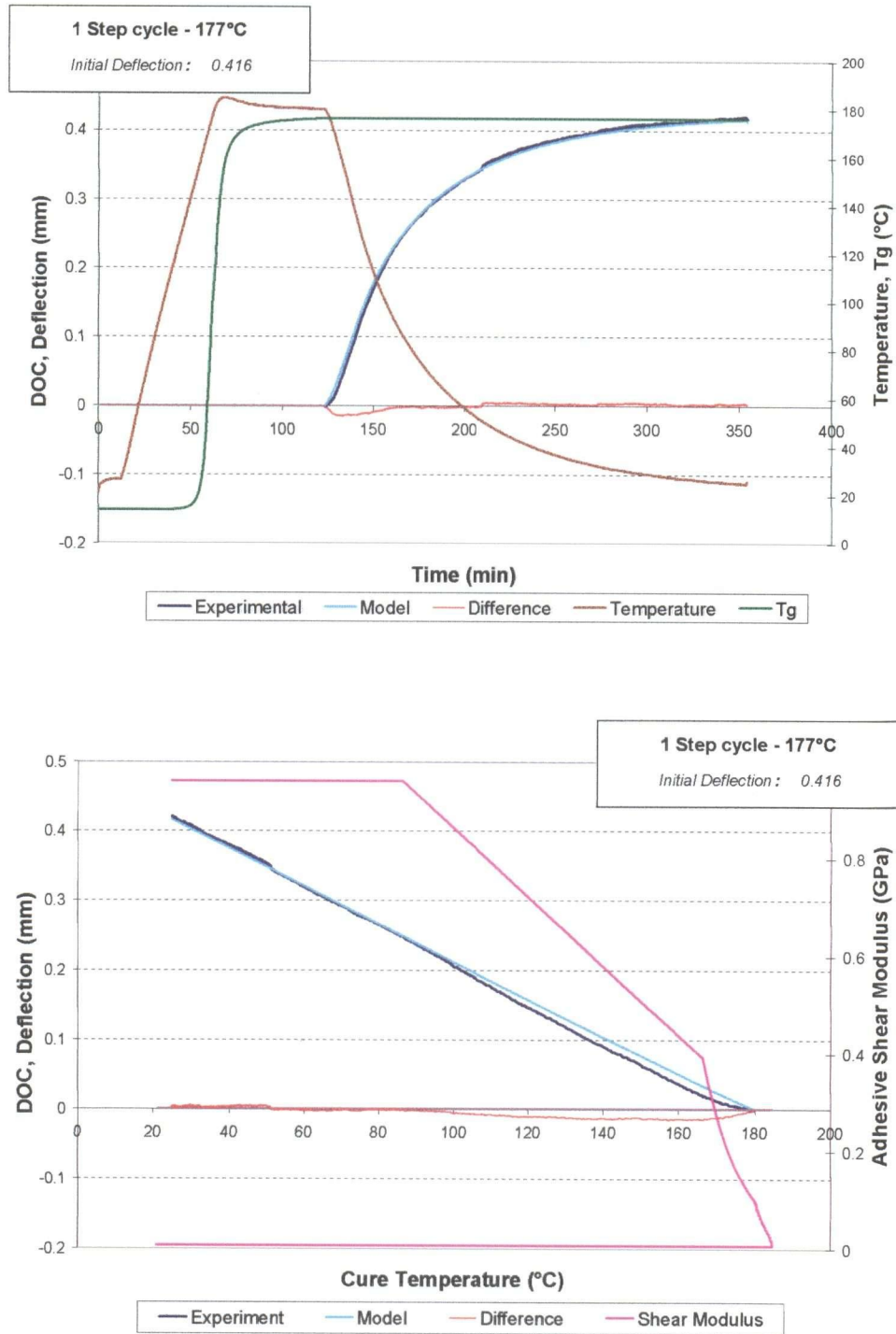
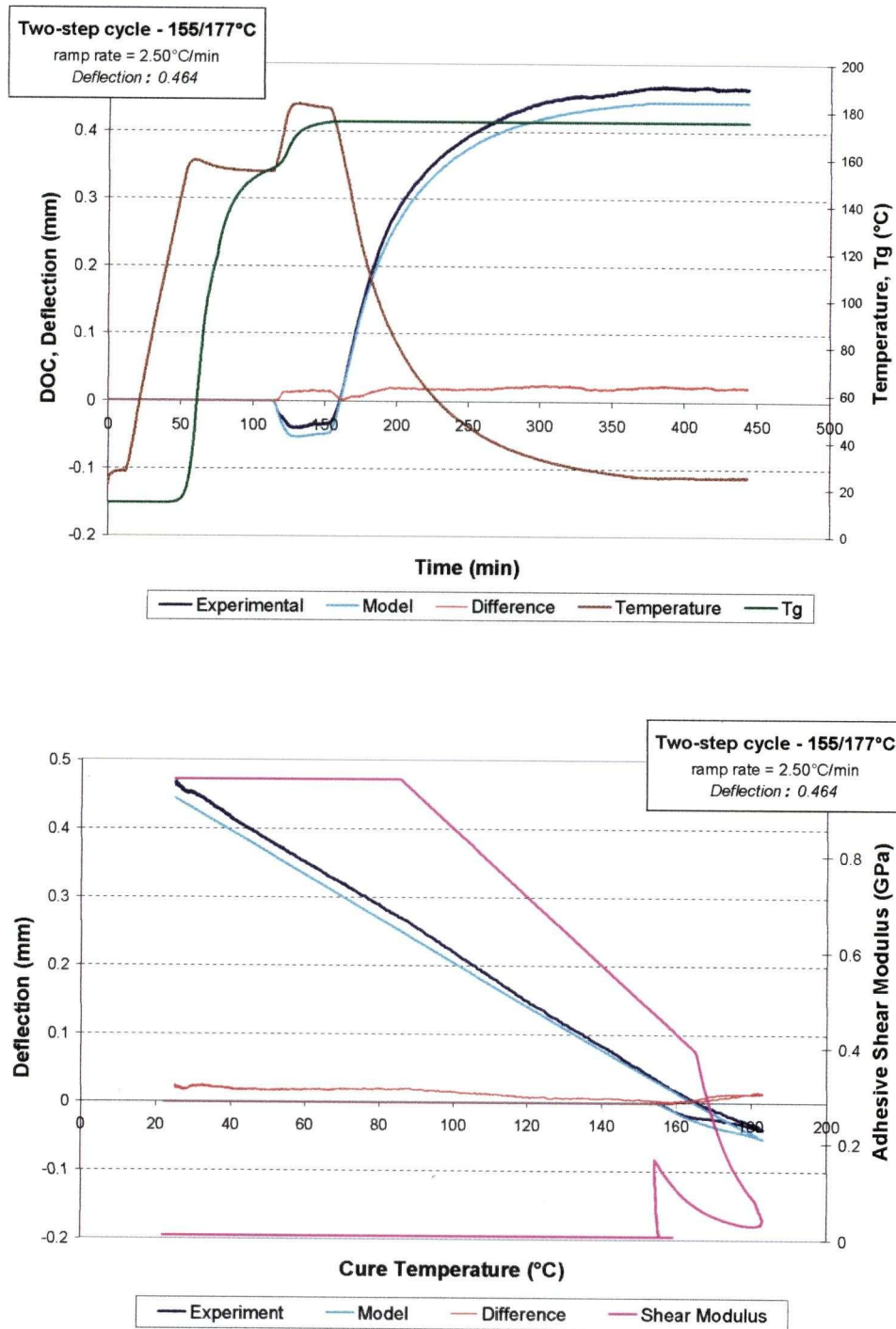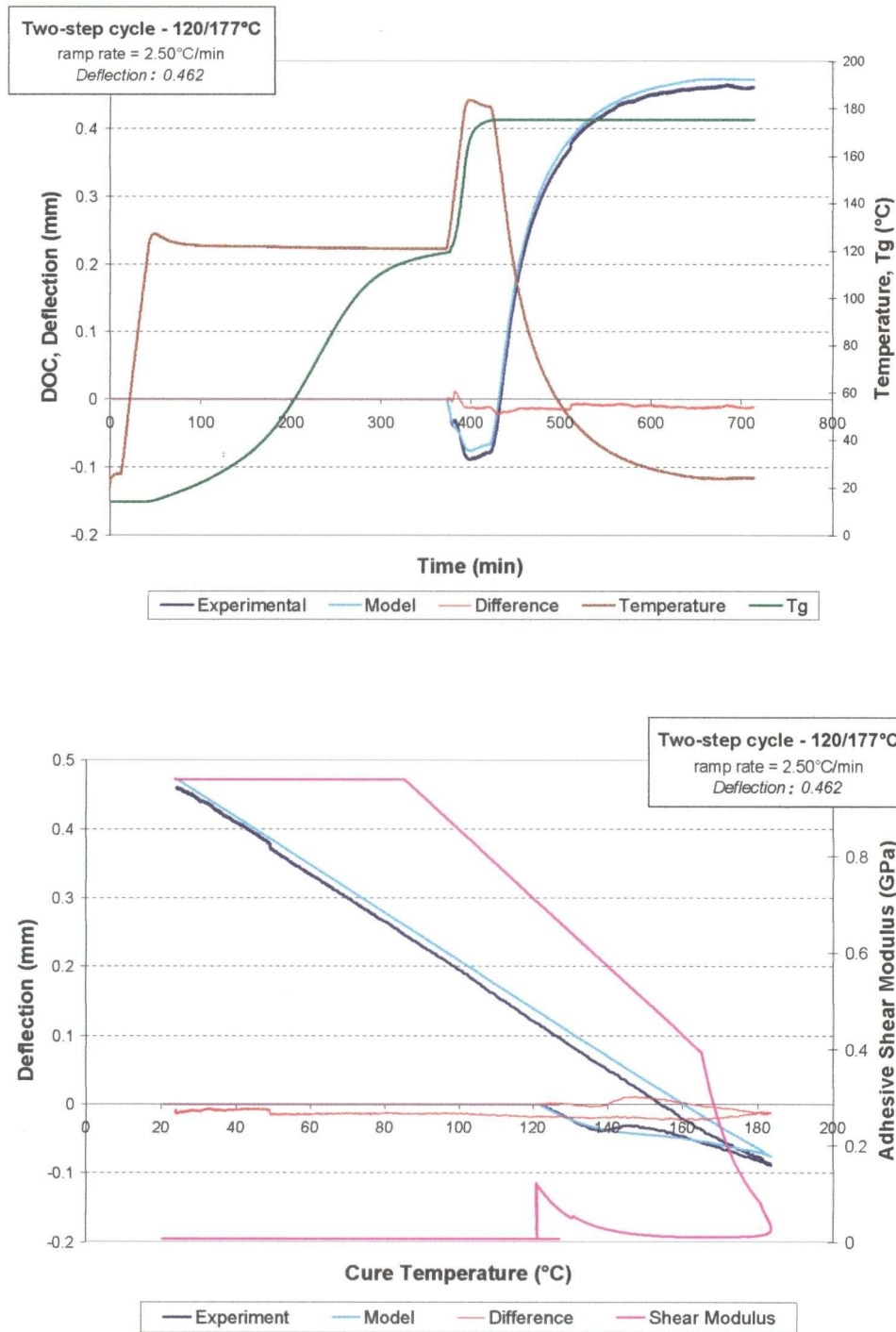**Figure A.5 - One-step cycle – 177°C - Specimen 1(e)**

Experimental and model results in the time and temperature domains
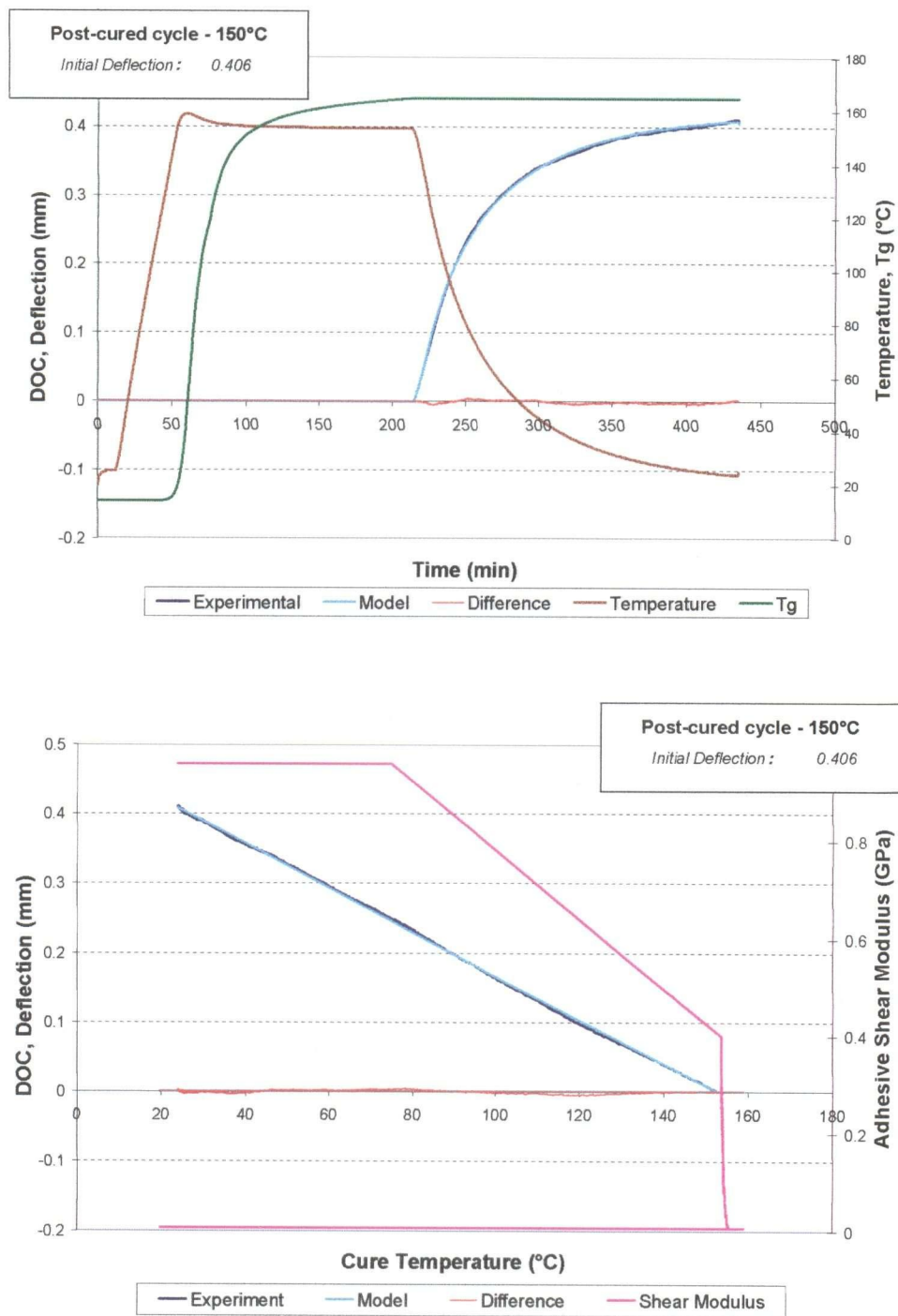
Figure A.6 - One-step cycle – 150°C - Specimen 2(a)

Experimental and model results in the time and temperature domains
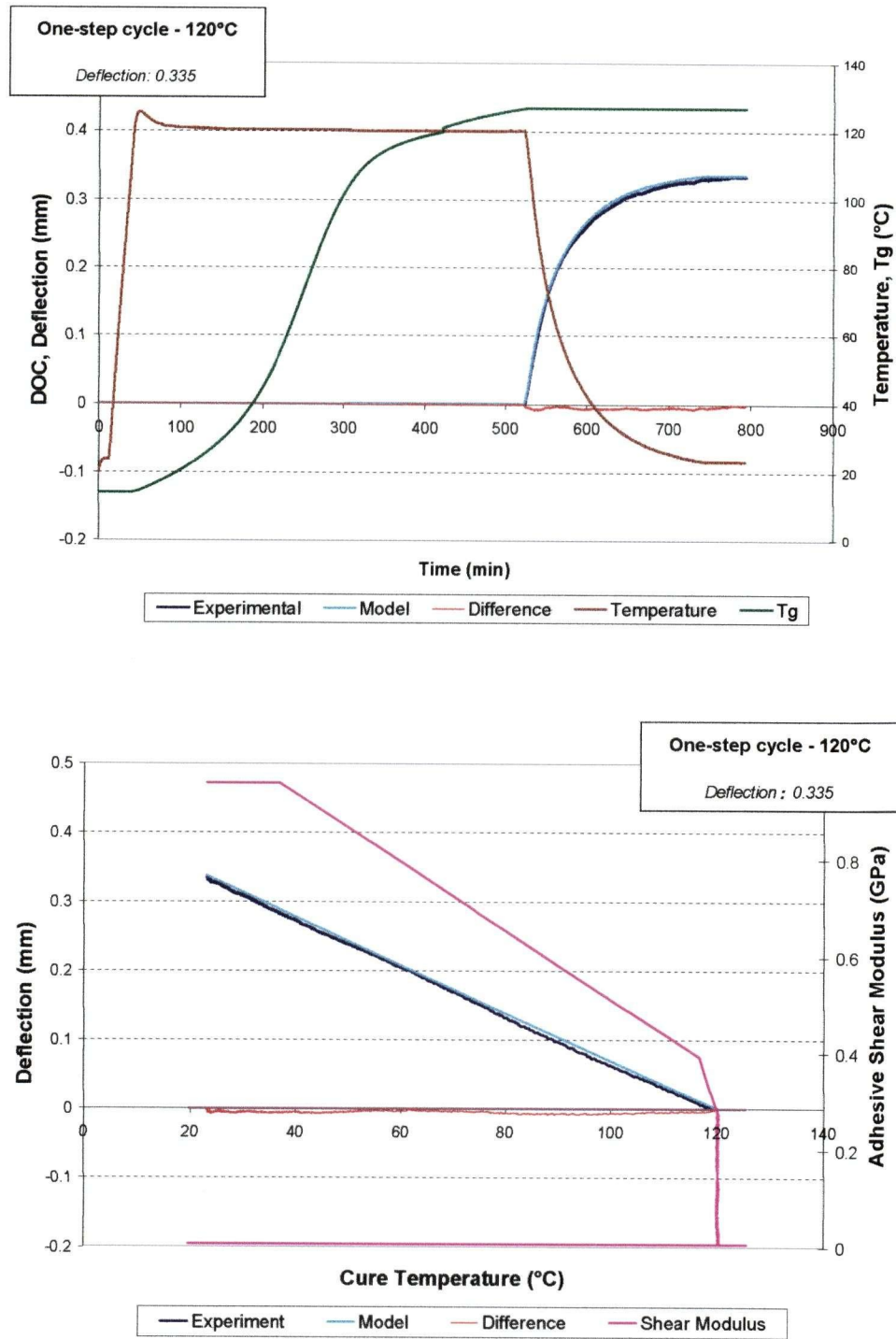
Figure A.7 - One-step cycle – 120°C - Specimen 3(a)

Experimental and model results in the time and temperature domains
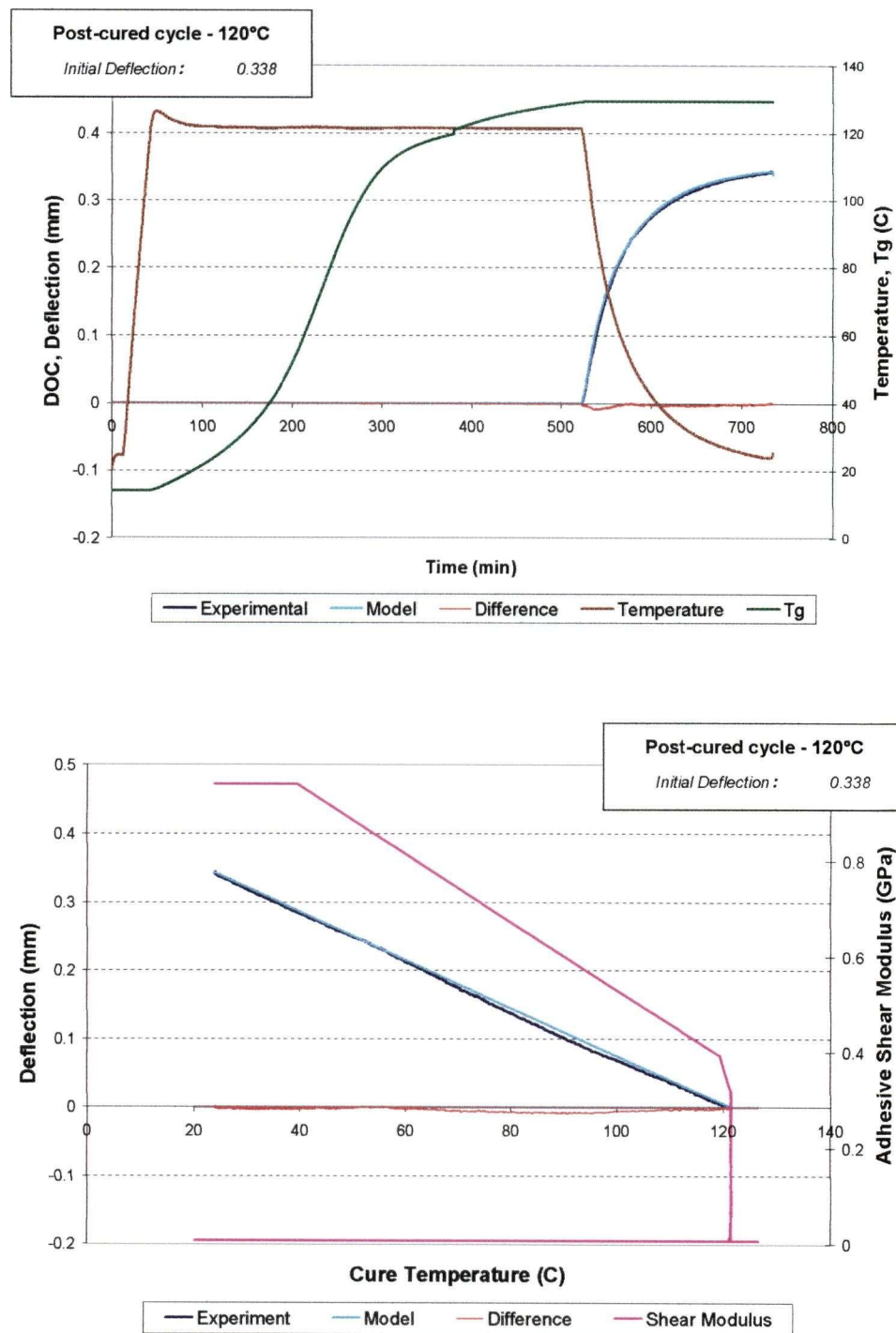
Figure A.8 - One-step cycle – 120°C - Specimen 3(b)

Experimental and model results in the time and temperature domains

**Figure A.9 – Post cure cycle – 177/177°C - Specimen 4(a)**

Experimental and model results in the time and temperature domains

Figure A.10 – Post cure cycle – 177/177°C - Specimen 4(b)

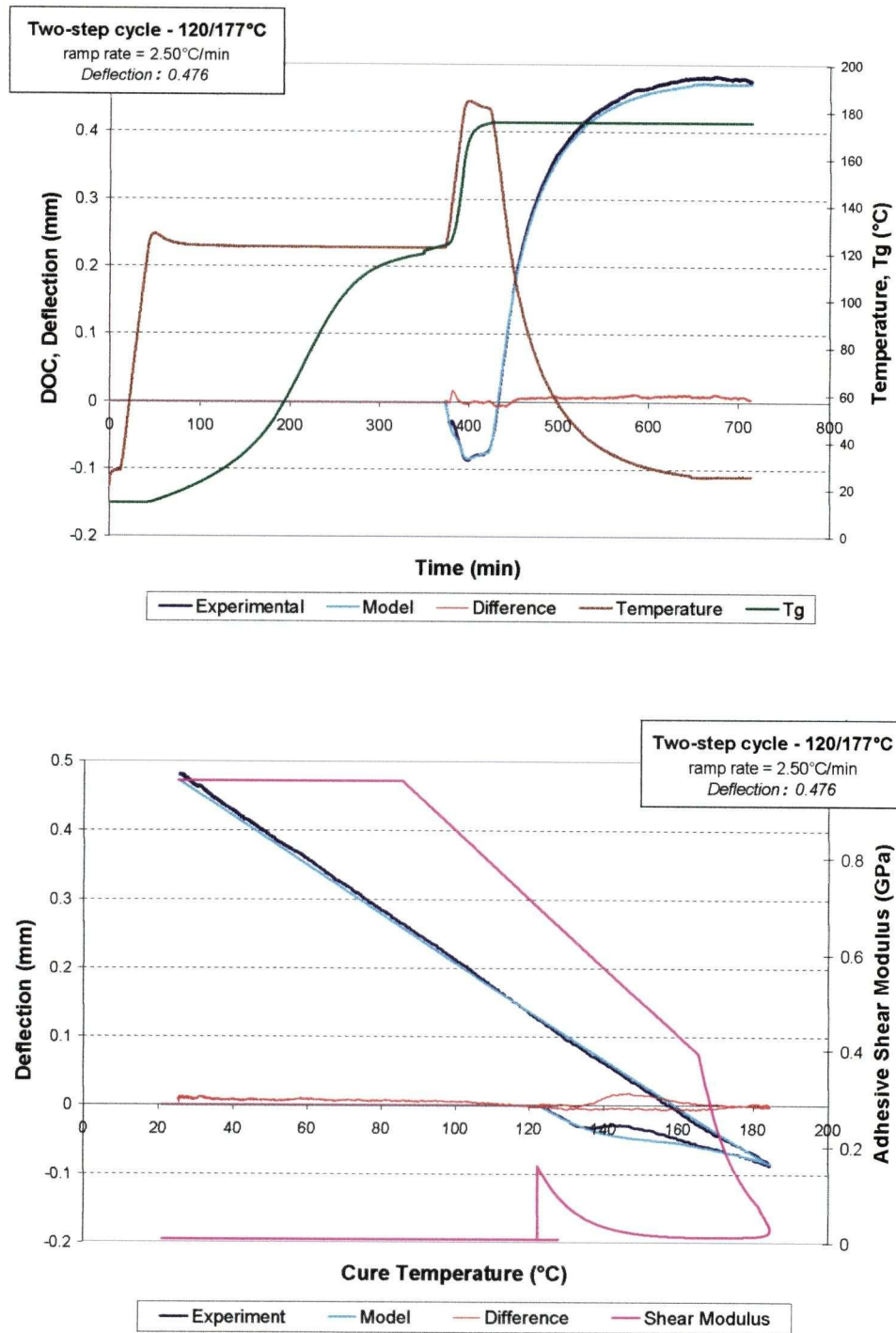**Experimental and model results in the time and temperature domains**

Figure A.11 – Post cure cycle – 150/177°C - Specimen 5(a)

Experimental and model results in the time and temperature domains

Figure A.12 – Post cure cycle – 120/177°C - Specimen 6(a)

Experimental and model results in the time and temperature domains

Figure A.13 - Two-step cycle – 155/177ºC, 2.5ºC/min - Specimen 7(a)

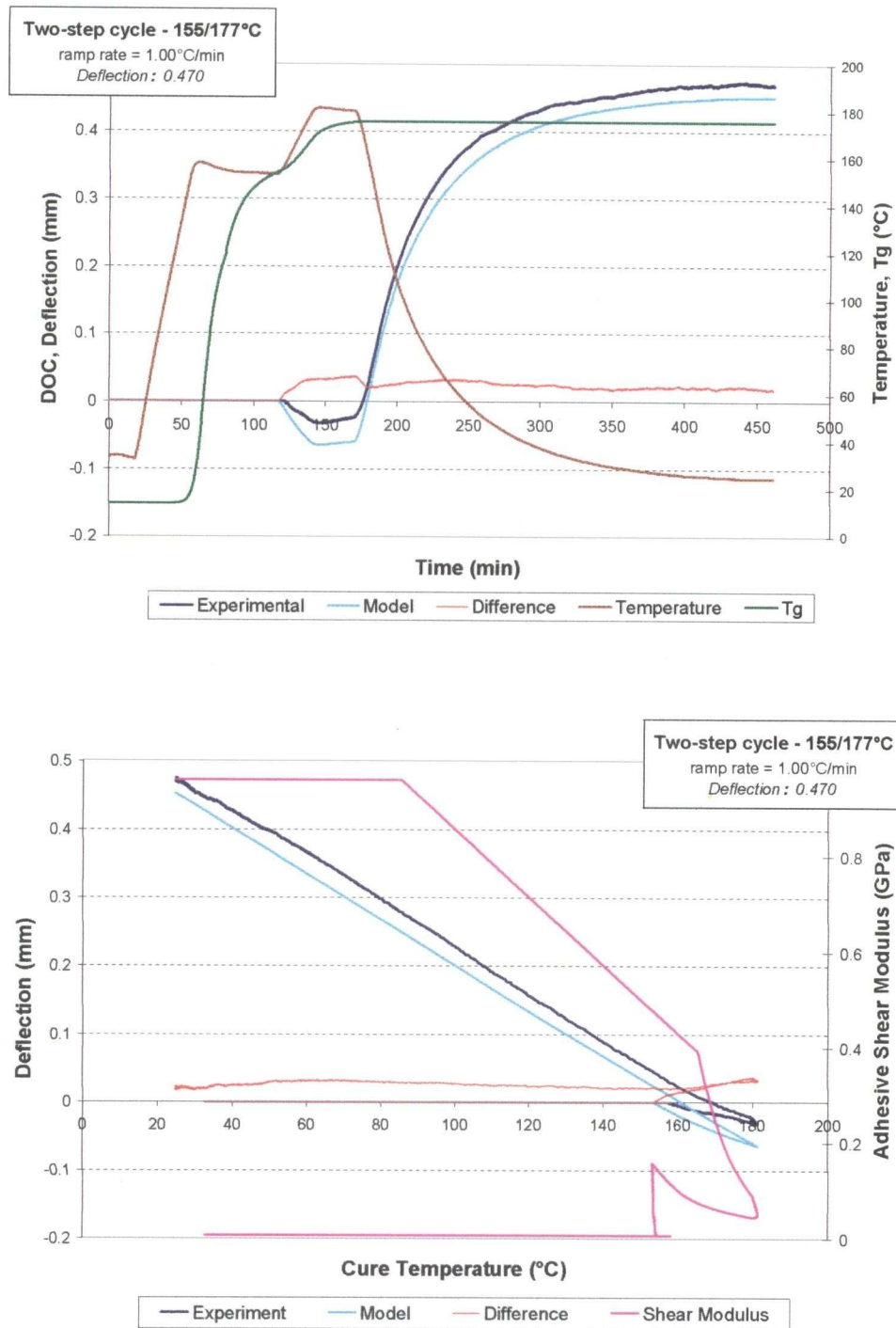**Experimental and model results in the time and temperature domains**

Figure A.14 - Two-step cycle – 155/177ºC, 2.5ºC/min - Specimen 7(b)

Experimental and model results in the time and temperature domains

Figure A.15 - Two-step cycle – 120/177°C, 2.5°C/min - Specimen 8(a)

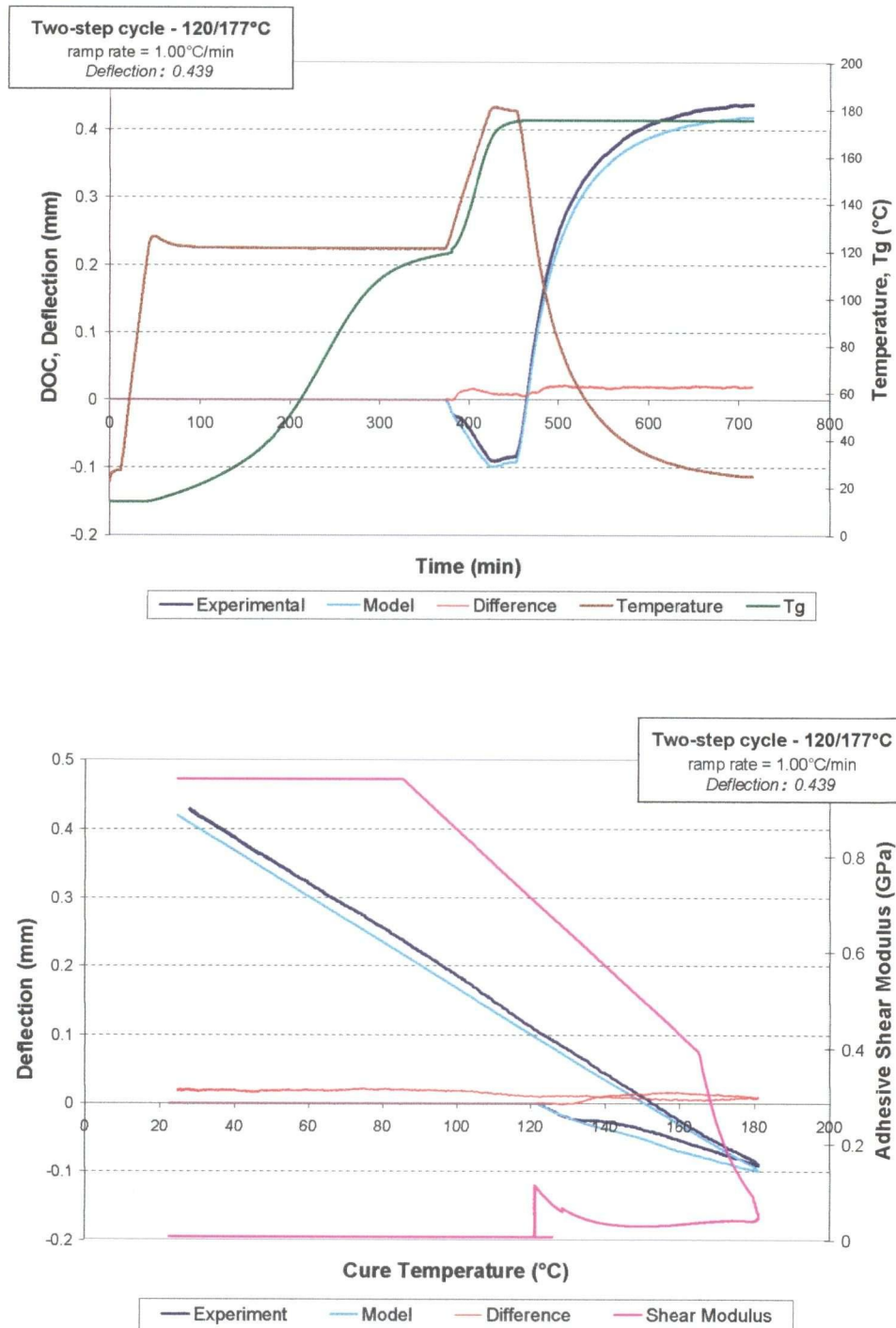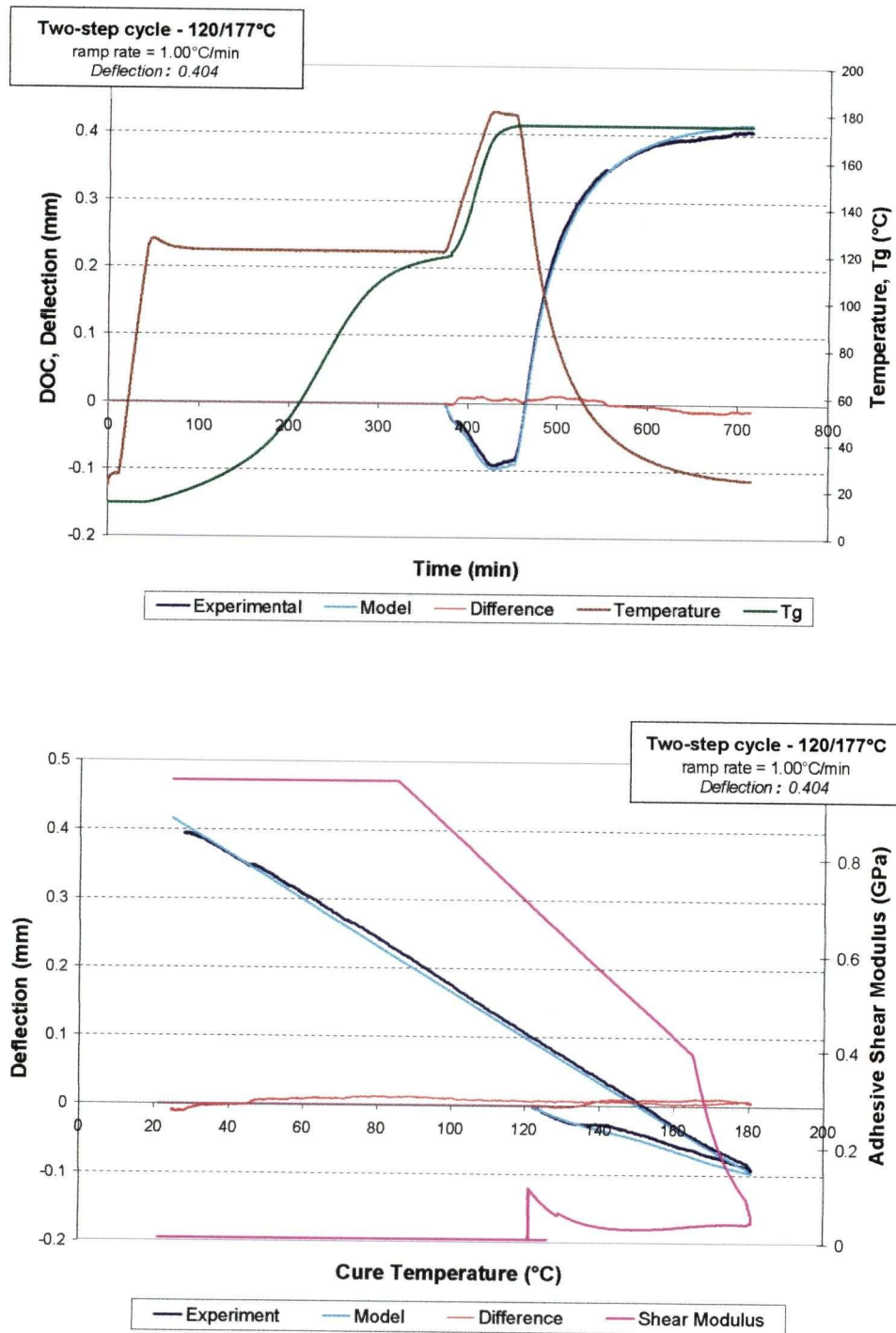**Experimental and model results in the time and temperature domains**
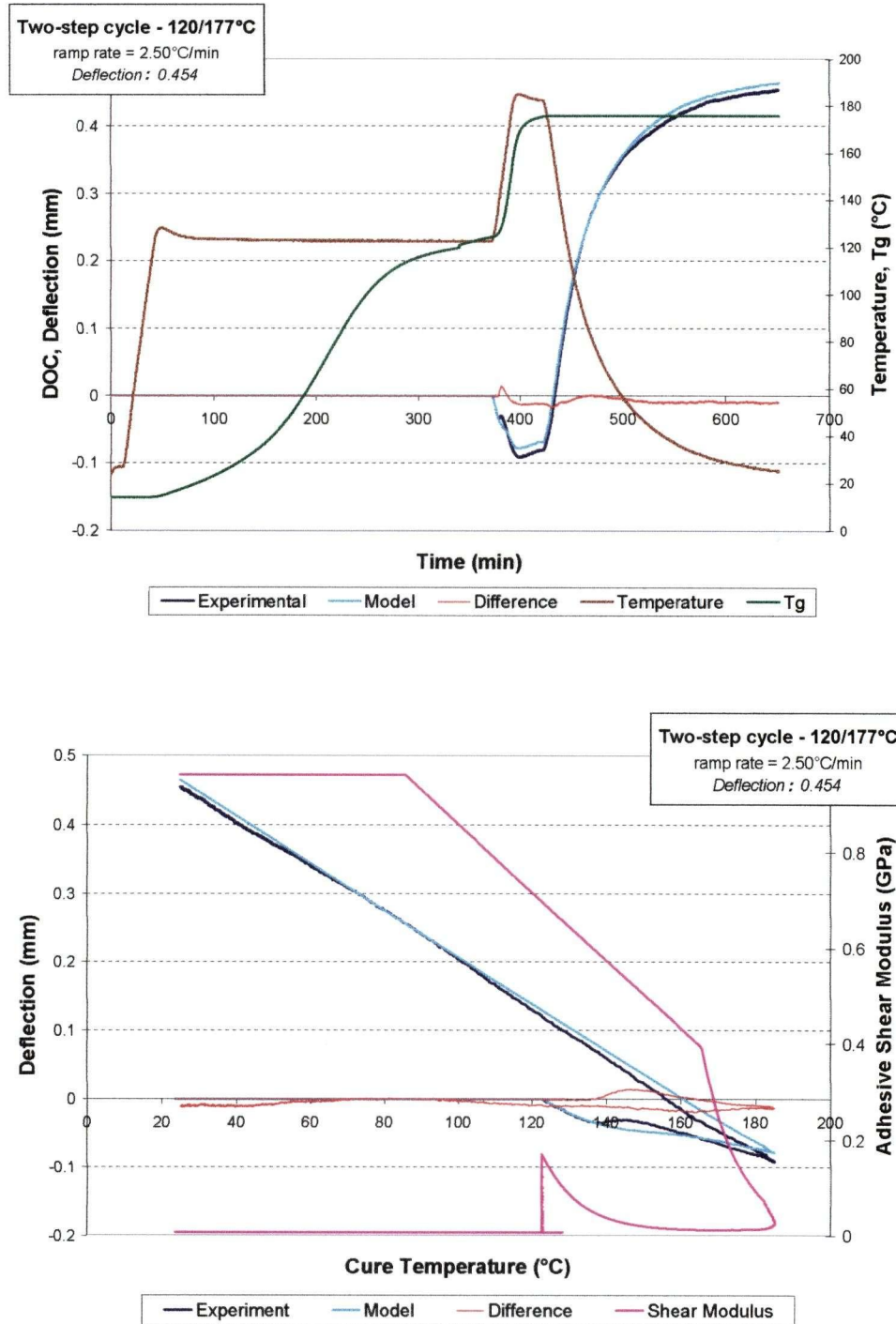
Figure A.16 - Two-step cycle – 120/177°C, 2.5°C/min - Specimen 8(b)

Experimental and model results in the time and temperature domains

Figure A.17 - Two-step cycle – 120/177°C, 2.5°C/min - Specimen 8(c)

Experimental and model results in the time and temperature domains

Figure A.18 - Two-step cycle 155/177°C, 1.0°C/min - Specimen 9(a)

Experimental and model results in the time and temperature domains

Figure A.19 - Two-step cycle 120/177°C, 1.0°C/min - Specimen 10(a)

Experimental and model results in the time and temperature domains

Figure A.20 - Two-step cycle 120/177°C, 1.0°C/min - Specimen 10(b)

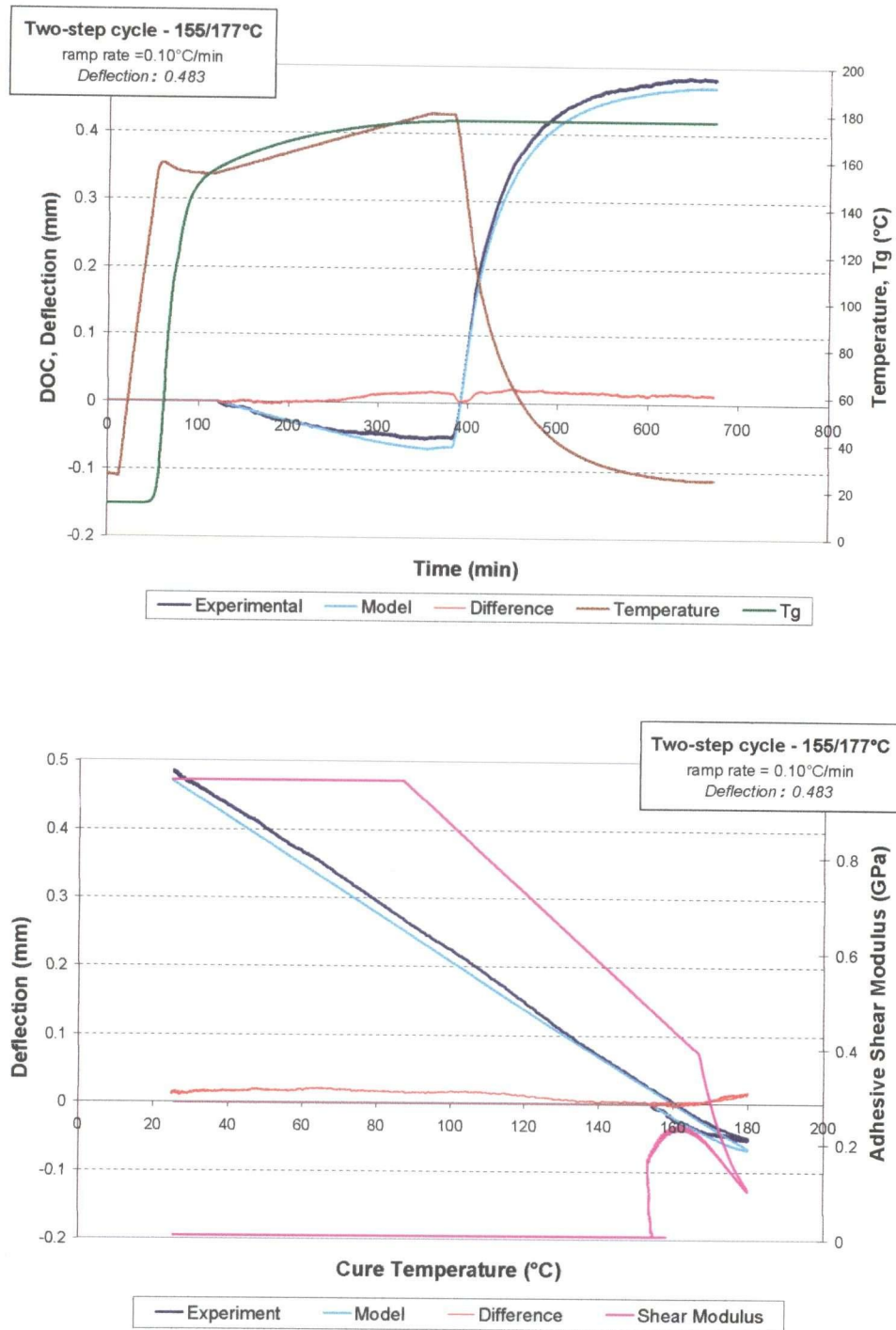**Experimental and model results in the time and temperature domains**

Figure A.21 - Two-step cycle – 155/177°C, 0.1°C/min - Specimen 11(a)

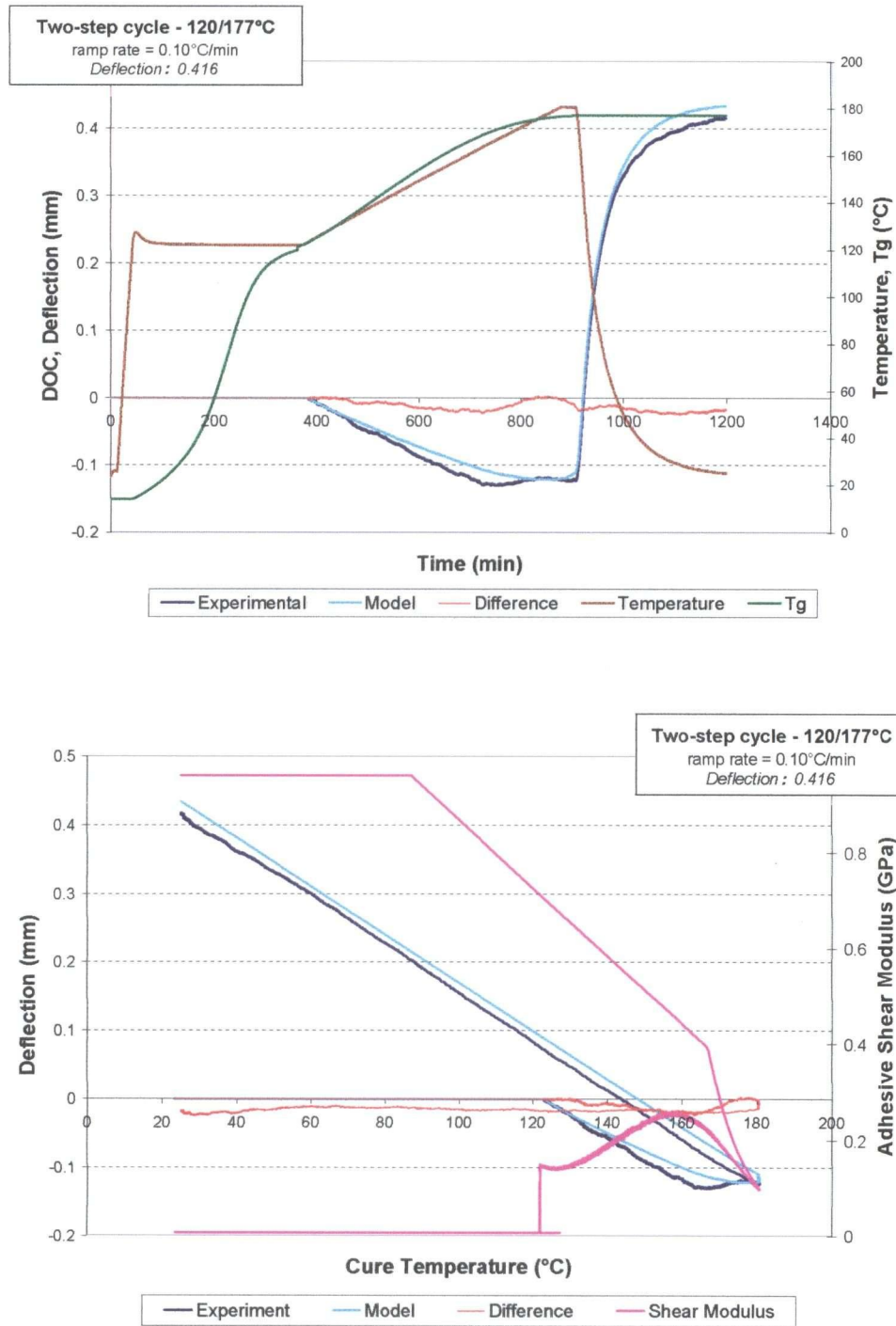**Experimental and model results in the time and temperature domains**

Figure A.22 - Two-step cycle – 120/177°C, 0.1°C/min - Specimen 12(a)

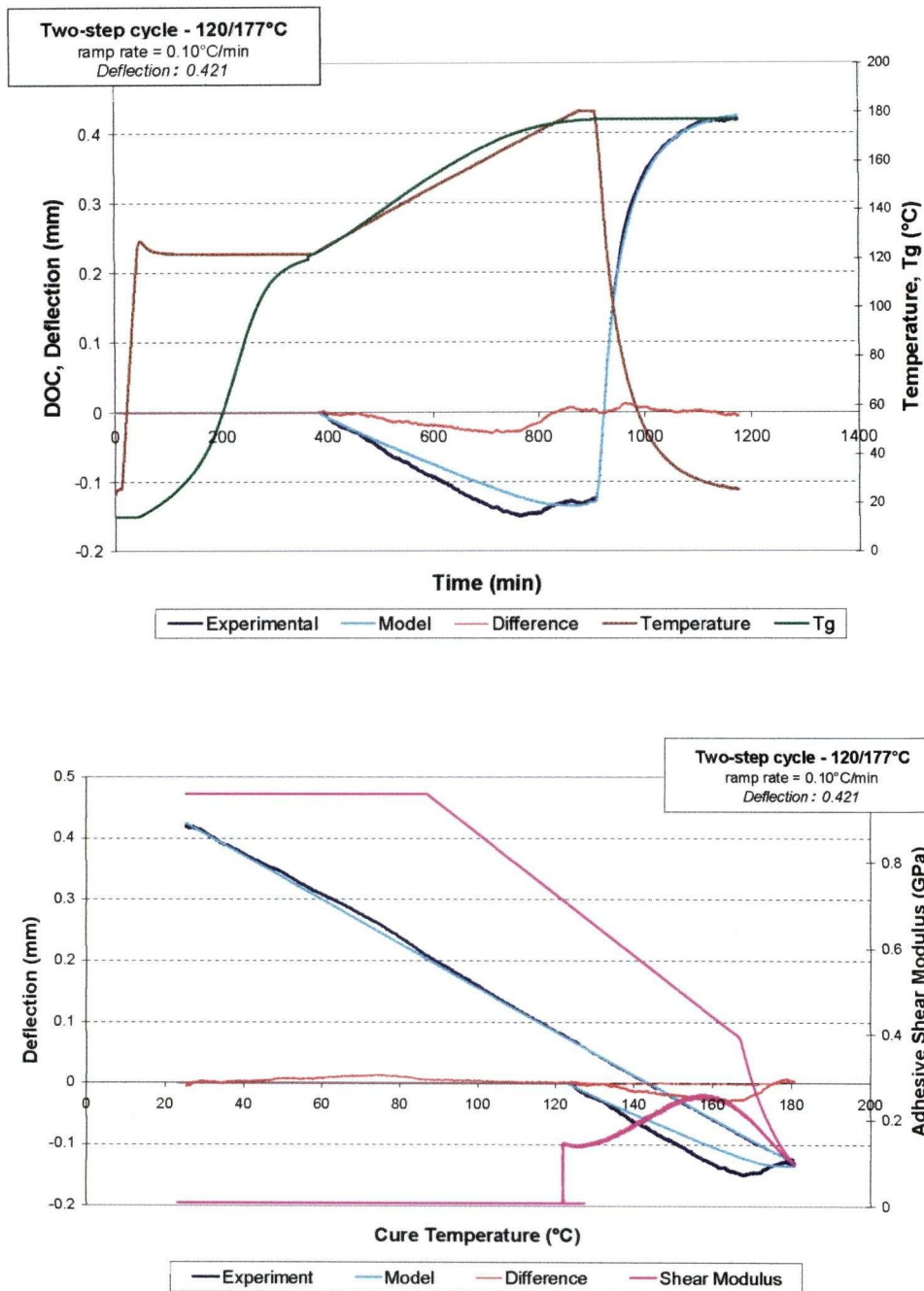**Experimental and model results in the time and temperature domains**

Figure A.23 - Two-step cycle – 120/177°C, 0.1°C/min - Specimen 12(b)

Experimental and model results in the time and temperature domains
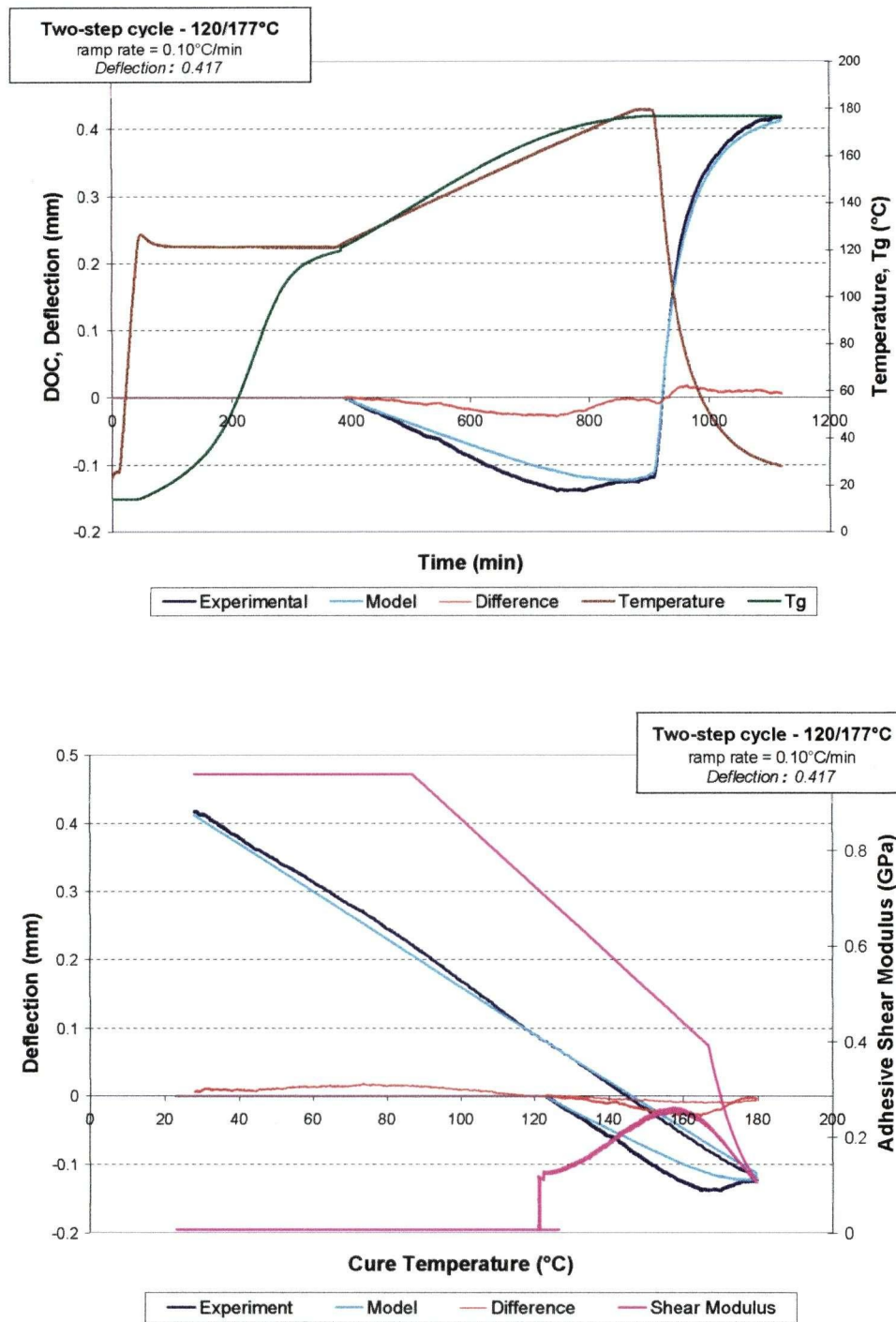
Figure A.24 - Two-step cycle – 120/177°C, 0.1°C/min - Specimen 12(c)

Experimental and model results in the time and temperature domains